REMOTE SENSING-BASED MONITORING OF LANDSCAPE CHANGES IN COASTAL SYSTEMS

by

DAVID FOREST RICHARDS IV

(Under the Direction of ADAM M. MILEWSKI)

ABSTRACT

Coastal landscapes provide significant natural resources and environmental sustainability. Due to the effects of sea level rise, increased storm frequency, climatic changes, rapid population growth, and anthropogenic activity, coastal landscapes have become increasingly vulnerable. To better understand the extent of changes occurring along the coast, this research is performed 3-fold in the southeastern United States (US) and in the Souss Massa Basin of Morocco. (1) The Southeast Coastal Network (SECN) of the National Park Service (NPS) has exhibited evidence of fluctuations in sea level which causes coastal erosion. Airborne LiDAR acquired from NOAA was analyzed to identify changes in both elevation and the spatial volume of unconsolidated sedimentary material in the coastal southeast from 2006 to 2018. Results indicate a quasi-cyclic process where unconsolidated sediment distribution and the morphodynamic equilibrium changes with time. (2) In the SECN of the NPS, salt marshes are representative of some of the most impacted vegetation type in these sites. Sentinel-2 data acquired from the USGS EarthExplorer database was used to identify the temporal and spatial changes in salt marsh presence from 2016 to 2020. ENVI-derived unsupervised and supervised classification algorithms were applied to determine the most appropriate procedure to measure distant areas of salt marsh increases and

decreases. The results from this approach indicate that the ENVI-derived maximum likelihood classification provides a statistical distribution and calculation of the probability (>90%) that the given pixels represented both water and salt marsh environments. (3) The Souss Massa Basin in Morocco has experienced extensive groundwater abstraction causing accelerated subsidence rates. The Souss-Massa Basin was analyzed using Interferometric Synthetic Aperture Radar (InSAR) techniques to identify land deformation and Gravity Recovery and Climate Experiment (GRACE) was used to approximate the amount of water stored in this region. Results suggest there is a correlation between groundwater storage changes and land deformation in the Souss Massa basin. Total water storage and groundwater storage decreased to (-10cm) between 2016-2021, while the InSAR analysis displayed land deformation of (-2cm) from 2016-2021. This analysis displays how the over-exploitation of groundwater resources influence landscape changes that impact groundwater dynamics.

INDEX WORDS: HYDROGEOLOGY, EROSION, LIDAR, ELEVATION, VOLUMETRIC CHANGE, SEA LEVEL, REMOTE SENSING, SALT MARSH, HYDROLOGY, COASTAL, SENTINEL-2, INSAR, GRACE, SUBSIDENCE, GROUNDWATER STORAGE

REMOTE SENSING-BASED MONITORING OF LANDSCAPE CHANGES IN COASTAL SYSTEMS

by

DAVID FOREST RICHARDS IV

AS, SAVANNAH STATE UNIVERSITY, 2015

BS, UNIVERSITY OF GEORGIA, 2017

A Dissertation Submitted to the Graduate Faculty of The University of Georgia in Partial Fulfillment of the Requirements for the Degree

DOCTOR OF PHILOSOPHY

ATHENS, GEORGIA

2024

REMOTE SENSING-BASED MONITORING OF LANDSCAPE CHANGES IN COASTAL SYSTEMS

by

DAVID FOREST RICHARDS IV

Major Professor: ADAM M. MILEWSKI

Committee: PAUL A. SCHROEDER
ROBERT A. CRADDOCK
TODD C. RASMUSSEN

Electronic Version Approved:

Ron Walcott
Vice Provost for Graduate Education and Dean of the Graduate School
The University of Georgia
May 2024

DEDICATION

I dedicate this work to my parents – Rev. David F. Richards, III, and Linda S. Richards, as well as my late grandparents – David F. Richards, Jr., and Swannie M. Richards. Through your continued love and support, the fruits of your labor have manifested this blessing. It is because of the love of God that resides in you this has become a reality. *"God's grace is sufficient."*

ACKNOWLEDGEMENTS

I give all honor and glory to my Lord and Savior, Jesus Christ. Through His grace the completion of this dissertation research has been made possible. He has surrounded me with a village that I wish to acknowledge. To my advisor, Dr. Adam M. Milewski, thank you for crafting me into the scientist I am today. Over the years we have completed numerous research-based projects around the world. Through these experiences you have trained me to complete sound research with a high degree of scientific merit. Your commitment to my success has positioned me with the knowledge and skills needed to be successful, and for that I am truly thankful. As I am thankful for the scholastic advisement you have given me, I am also thankful for our friendship that has developed along this journey. Our relationship extends beyond the bounds of academia, and for that I am grateful.

To my dissertation committee, your support and commitment to my success has been a blessing. Dr. Paul A. Schroeder, thank you for introducing me to the field of geology. You served as my undergraduate research advisor and continued to be a devoted member of my committee throughout my academic journey. Dr. Robert A. Craddock, thank you for expanding my knowledge and introducing me to different fields of geology. Through your advisement, the exposure gained has been monumental in my development as a scientist. Traveling the world with you on various research-based projects has molded me to be a well-trained scientist with a diverse skillset. Dr. Todd C. Rasmussen, thank you for providing me with a strong hydrogeological and groundwater interpretative background. The depth gained is tremendously valued. To my mentors, Dr. Douglas E. Crowe and Dean Ron R. Walcott, thank you for supporting and encouraging me

over the years. Your mentorship has been influential in this process. To each of my committee members and mentors, each of you have served in various capacities in my development over the years. Words cannot express my sincere level of appreciation for your mentorship, advisement, and friendship. It is through our unprecedented friendship; this great achievement is attained.

To my family and friends, thank you for your prayers, love, and support. This has been a journey, and you are just as part of this as me. To my brothers – Micah, Aaron, and Joshua, thank you for always being present and supportive. To my relatives – Richards family, Anthony family, and Spence family, I praise God for the love that is expressed in our family. To my church family – thank you for your prayers and words of encouragement. To my friends – thank you for being by my side for the entire journey. To the Water Resources and Remote Sensing lab – current and past members thank you for the friendships that have developed over the years. To the University of Georgia Geology Department – thank you for your help and support along the way. To my community – thank you for your support and serving as a beacon of motivation to keep pressing forward.

As acknowledged, it is from my spiritual, family, formal, and social education that I am able to produce this work. The qualities instilled in me have been exhibited throughout and now it is presented in this dissertation, thank you. *"To God be the glory for the great things He has done."*

ABBREVIATIONS

US – United States

SECN – Southeast Coastal Network

NPS – National Park Service

LiDAR – Light Detection and Ranging

NOAA – National Oceanic Atmospheric Administration

DEM – Digital Elevation Model

GIS – Geographic Information System

ENVI – Environment for Visualizing Images

NM- National Monument

NS – National Seashore

NHS – National Historic Site

ENSO – El Niño Southern Oscillation

IMU – Inertia Measurement Unit

RMSE – Root Mean Square Error

ASPRS – American Society for Photogrammetry and Remote Sensing

DTM – Digital Terrain Models

3D – Three Dimension

NDVI – Normalized Difference Vegetation Index

SC – South Carolina

NC – North Carolina

GA – Georgia

FL – Florida

ha – hectares

UAVs – Unmanned Aerial Vehicles

ROI – Regions of Interest

TOA – Top of Atmosphere

GPS – Global Positioning System

NIR – Near-Infrared

cm – centimeters

m – meters

MENA – Middle East and North Africa

MCM – Thousands of Cubic Meters

SAR – Synthetic Aperture Radar

InSAR – Interferometric Synthetic Aperture Radar

GRACE – Gravity Recovery and Climate Experiment

SWAT – Soil Water Assessment Tool

km – kilometers

SLC – Single Look Complex

USGS – United States Geological Survey

ESA – European Space Agency

SNAP – Sentinel Application Platform

DInSAR – Differential Interferometric Synthetic Aperture Radar

ERS-1 – European Remote Sensing Satellite 1

ERS-2 – European Remote Sensing Satellite 2

ENVISAT – Environmental Satellite

ALOS – Advanced Land Observing Satellite

PALSAR – Phased Array L-band Synthetic Aperture Radar

COSMO-SkyMed – Constellation of Small Satellites for the Mediterranean Basin Observation

IW – Interferometric Wide Swath

VV – Vertical Transmit-Vertical Receive

NASA – National Aeronautics and Space Administration

GLDAS – Global Land Data Assimilation System

TWSa – Total Water Storage Anomaly

GWSa – Groundwater Storage Anomaly

CANa – Canopy Storage Dataset Anomaly

SWEa – Snow Water Equivalent Anomaly

SMa – Soil Moisture Anomaly

SRTM – Shuttle Radar Topography Mission

ESD – Enhance Spectral Diversity

SNAPHU – Statistical-Cost, Network-FLOW Algorithm for Phase Unwrapping

Mgal/d – millions of gallons per day

TRMM – Tropical Rainfall Measurement Mission

TABLE OF CONTENTS

Page

LIST OF TABLES

Page

LIST OF FIGURES

Page

CHAPTER 1

INTRODUCTION

1.1. Background

Groundwater resources are essential for life. This resource provides sustainability in human, economic, environmental, and social productivity. The impact of the role groundwater plays on continental to global scales is unprecedented. Through its functionality, groundwater provides further understanding of the multiplicities of the hydrologic cycle in earth's system, water governance and management in groundwater systems, and the opportunity to view its widespread distribution both regionally and globally [*Gleeson et al., 2019; Wada and Heinrich, 2013; Dalin et al., 2017; Gleeson et al., 2020*].

Groundwater is distributed and stored as the largest unfrozen freshwater resource on earth. A report suggests the volume of modern groundwater is equivalent to a body of water with a depth of about 3m spread over the continents [*Gleeson et al., 2015*]. As this estimate is representative of a global perspective, Africa is estimated to have between 0.36-1.75 million km^3 of total groundwater present [*MacDonald et al., 2012*]. This range is indicative of the unevenly distributed groundwater resources throughout the continent of Africa, as not all groundwater present is available for extraction. Comparatively, in 2015, about 84,600 million gallons per day (Mgal/d) of groundwater was withdrawn in the United States (US) [*Lovelace, 2020*]. Of this total, about 94 percent was withdrawn from US principal aquifers [*Lovelace, 2020*]. The US principal aquifers represent five major lithologic groups contributing to public supply, domestic use, industrial, mining, thermoelectric power, livestock, and irrigation.

Groundwater is a major source of water across many regions of Africa and the US [*MacDonald and Calow, 2009; Lovelace et al., 2020; Maupin et al., 2010; JMP, 2010*]. Africa has a vast reservoir of groundwater supply, in fact, according to a study by the British Geological Survey, fossil groundwater resources in Africa have an estimated volume of more than a hundred times the estimate of surface freshwater resources. The largest groundwater aquifers are found in large sedimentary lithologies in the North African countries of- Libya, Algeria, Egypt, Chad and Sudan [*MacDonald et al., 2012*]. These North African sedimentary aquifers contain the largest groundwater reserves displaying the spatial extent where aquifer productivity is functional. Given the increased demand of groundwater resources, its functionality is a result of the aquifer hydraulic properties, changes in climate regimes, and the geomorphology present [*Gleeson et al., 2012; Kumar, 2012; Teixeira et al., 2010; Teixeira et al., 2013; Jaiswal et al., 2003; Surrette et al., 2008*].

Groundwater resources are impacted by various erosional, vegetative, and anthropogenic processes. Each of these processes are representative of variables that play a role in the geomorphological and hydrological response. These variables are connected, defining the interaction and link of hydrologic and geomorphic processes in both temporal and spatial dimensions [*Leatherman, 1984; Nicholls et al., 2007*]. The geomorphological features across regions of Africa and the coastal US all vary, but one component they each have in common is the interplay of landscape changes on groundwater resources. In the Souss-Massa Basin of Morocco and the southeast region of the US, soil moisture, evaporation, erosion, evapotranspiration, groundwater recharge, perched groundwater bodies and fluvial processes are fundamentally important in understanding these coastal systems. Each of these processes occur analogous to the geomorphological state of each region. Meaning, how these geomorphological features respond to

landscape changes (i.e., weathering, aeolian/fluvial processes, sediment supply, and surface subsidence) offer better understanding of how groundwater resources are impacted.

The Souss-Massa basin, located in south-western Morocco, and select sites of the Southeast Coastal Network (SECN) of the National Park Service (NPS), located in the coastal southeastern US, represent a comparison of regions to better understand the influence of landscape change on the geomorphologic-hydrogeologic interface. The Souss-Massa basin represents an over-populated region where there are limited water resources and extensive groundwater abstraction [*Bouchaou et al., 2008; Bouchaou et al., 2011; Sowers et al., 2011; d'Oleire-Oltmanns et al., 2011*]. The SECN of the NPS representing the coastal southeastern US, including Florida (FL), Georgia (GA), South Carolina (SC), and North Carolina (NC) is home to coastal regions that are highly susceptible to erosional activity and salt marsh density changes contributing to the geomorphological and hydrogeological interface [*Gornitz et al., 1994; Wu et al., 2002; Church et al., 2006; McInnes et al., 2003; Nicholls et al., 2007; Leatherman et al., 1984*]. In response to increased storm intensities and series of subsequent storms, accelerated erosion rates and changes in deposited sediment have occurred in these coastal areas [*Markewich et al., 1990; Gilluly, 1994; Leece et al., 2006; Philips et al., 1993; Sheridan et al., 1982; Slattery et al., 2002*]. Additionally, as coastal salt marshes experience effects of climate change, hydrological processes are altered, impacting the hydrogeological framework [*Stagg et al., 2021; Alber et al., 2008; Orson et al., 1985; Schwarz et al., 2022; Mariotti and Canestrelli, 2022; Guimond and Tamborski, 2021; Byrd and Kelly, 2006*]. Each of these sites are distinguished by their independent locations, where the Souss-Massa basin is located in the North African region and the coastal southeastern US is located along the Atlantic coast. These locations represent multiple coastal environments on a range of scales. Understanding the impact of coastal landscape changes on coastal systems at various sites

across a range of scales in different regions explores the multiplicities and how complex these processes are. Furthermore, these studies offer insight into how the implementation of known and new remote sensing-based techniques can be used to provide further understanding of how dynamic these processes are.

1.2. Purpose

Coastal environments are steadily being altered which is contributing to changes in groundwater dynamics. The opportunity to better understand the impacts of landscape changes on coastal systems provides insight to the impacts of coastal geomorphology changes on a range of scales. In identifying how these landscape changes impact coastal systems, the overall hypothesis is that coastal landscape changes influence hydrogeological resources along coastal systems.

The coastal southeast US is highly susceptible to geomorphological and hydrogeological changes in response to relative sea level rise. Sea level rise is a result of changes in climate, in which storm intensities have increased and series of subsequent storms have occurred [*Gornitz et al., 1994; Wu et al., 2002; Church et al., 2006; McInnes et al., 2003; Nicholls et al., 2007; Leatherman et al., 2000*]. Many variables play a role in the geomorphological and hydrological response, however, these processes are intrinsically connected, defining the interaction and linkage of hydrologic processes with geomorphic processes in temporal and spatial dimensions [*Leatherman, 1984; Davidson-Arnott and Bauer, 2010; Masselink et al., 2013*]. The Atlantic Coastal Plain is extremely sensitive to sea level rise, causing accelerated erosion rates and changes of the amount of sediment deposited in coastal areas [*Markewich et al., 1990; Gilluly, 1964; Leece et al., 2006; Philips et al., 1993; Sheridan et al., 1982; Slattery et al., 2002*]. As this is representative of the hydrogeological impact, the economic impacts are analogous to the direct damages of sea level rise [*Hauer et al., 2016; Tol et al., 1996; Klein and Nicholls, 1999*].

Global mean sea level rise has risen about 8-9 inches (21-24 centimeters) since 1880, with about a third of that coming in just the last two and a half decades [*Lindsey et al., 2019*]. By 2100, research suggests that sea level rise could exceed 6.6 feet (2 m) given the climate regimes continue at its current rate [*Bamber, 2019*]. Along the southeastern US coastline, approximately 43% (~2,000 km) of the area is projected to have an increase in coastal erosion vulnerability by the 2030s, with respect to its present vulnerability [*Von Holle et al., 2019*]. Studies have shown that the coastal sediment budget, representing the sediment supply, is extremely vulnerable [*Morton, 2003; Morton, 2005; Gutierrez et al., 2011; Schwartz and Musialowski, 1977; Valverde et al., 1999; Leonard et al., 1995*]. The effects of coastal erosion are continuously altering the environment and mitigating its effect has become increasingly important. To meet the increasing demand of coastal resource management, remote sensing techniques are being used to provide rapid data acquisition of large areas that would normally require extensive and lengthy field surveys. Furthermore, the ability to use light detection and ranging (LiDAR) in both natural resource management and economic sustainability creates the opportunity to distinctively characterize the coastal dynamic response at high spatial resolutions.

Typically, LiDAR is used in forest management to understand forest biomass dynamics as it was historically believed to show the greatest promise over forested areas. However, the use of LiDAR in coastal applications has become a pivotal tool in coastal change detection [*Carson et al., 2004; Brock and Purkis, 2009*]. The ability of LiDAR has garnered efficient, productive, and accurate measurements of topographical mapping [*Woolard and Colby, 2002; Danchenkov et al., 2019; Danchenkov and Belov, 2019; White and Wang, 2003; Sallenger et al., 2003; Young and Ashford, 2006*]. LiDAR's application enables rapid elevation data collected through repeated measurements of the observed topographic region [*O'Dea et al., 2019*]. The high spatial resolution

data retrieved produces digital elevation models (DEMs) indicative of current and historical coastal geomorphological changes. The results have become an asset in improving the knowledge of complex coastal geomorphological processes creating better preventative and mitigating initiatives [*Gesch, 2009; Elaksher, 2008; Titus and Richmond, 2001; Rumson et al., 2019; Anderson et al., 2017*].

In recognition of the coastal changes occurring along the coastal southeast US, the sediment budget has displayed both aggraded and degraded material [*Barnhardt et al., 2007; Warner et al., 2012; Denny et al., 2013*]. The presented LiDAR analysis offers the use of LiDAR in characterizing the spatial and temporal changes of the coastal southeast US, and quantification of changes at select National Park sites. More specifically, this study identifies the temporal changes in elevation and quantification of the spatial volumetric changes of unconsolidated sedimentary material in the SECN of the NPS.

Globally, salt marshes are decreasing with a loss of approximately 25% to 50% of their vegetative cover [*Crooks et al., 2011; Duarte et al., 2008; Mcowen et al., 2017*]. Over the past 300 years, global salt marshes have declined in area by 87%, and they have declined 54% since 1900 [*IPBES, 2018*]. A recent study suggested that approximately 561 square miles (1453 square kilometers) of salt marshes have been removed over the past 20 years worldwide [*Campbell et al., 2022*]. By 2060, the National Oceanic and Atmospheric Administration (NOAA) estimates that 14% to 34% of existing South Atlantic salt marshes could be lost [*Fretwell et al., 2021*]. Spanning the coasts of North Carolina (NC), South Carolina (SC), Georgia (GA), and Florida (FL), approximately 1 million acres (404,686 hectares (ha)) of salt marshes are threatened by climate change and the human-induced impacts that degrades salt marsh environments [*South Atlantic Salt Marsh Initiative, 2023*].These studies have shown how vital Spartina salt marshes are, and due to

their increased vulnerability, proper mitigation is imperative to provide natural coastal resource management. Traditionally, salt marshes have been analyzed through field-based techniques, however, due to limited access to some areas, the use of remote sensing has been implemented [*Campbell and Wang, 2019; DiGiacomo et al., 2020*]. Remote sensing techniques offer the opportunity to monitor short- and long-term landscape changes under high spatial resolutions to provide mapping accuracy. Salt marsh environments have been analyzed using data collected from various satellites to distinctively characterize how they have changed over time [*Roughgarden et al., 1991; Belluco et al., 2006; Silvestri et al., 2003; Farris et al., 2019; Zhang et al., 1997*].

The development of salt marsh monitoring has evolved due to the increase in changes to the ecomorphodynamic response due to climate change [*Fagherazzi et al., 2004; Silvestri and Marani, 2004; Day et al., 2008*]. Coastal salt marshes are experiencing extreme temperatures, changes in storm frequency and intensity, sediment redistribution, changes in nutrient inputs, and the oscillation of high and low tides [*Scavia et al., 2002; Kirwan and Mudd, 2012; Schuerch et al., 2013; Mwamba and Torres, 2002; Valiela et al., 1978; Sanderson et al., 2000*]. These processes consequently impact salt marsh growth and resilience as well as the ability to provide the necessary barrier for aquatic life and resources. When this occurs, the geomorphic characterization of these regions is altered, causing changes to the hydrologic/hydrogeologic interface [*Sanderson et al., 2000; Tempest et al., 2015; Hughes et al., 2012; Wilson et al., 2015*]. Modeling and field-based techniques have been used and shown to be useful in understanding vegetative changes [*Byrd and Kelly, 2006; Giri et al., 2011; Vo et al., 2013*]. Even as current research and monitoring of salt marshes continue to progress, challenges remain. Can coupled-based classification schemes identify small-scale changes? Can validation techniques be implemented to increase accuracy? How can coupled-based classification scheme approaches improve accuracy? As these questions

persist, the instituted approach aims to provide solutions to these questions. The ability to use field-based data and manually selected ROIs under supervised classification schemes provides a nuanced approach to better interpret salt marsh changes, therefore, the improvement of classification techniques is still needed [*Yeo et al., 2020*]. Here, we explored methods to identify and quantify how salt marshes are changing along the southeastern coast of the US and how they can provide valuable data for coastal natural resource management.

In the North African region water is scarce. Population growth and water usage, particularly for irrigation, have contributed to water stress through withdrawals of more than annual renewable supplies [*Milewski et al., 2019*]. Though all North African countries experienced declines in groundwater storage except for Morocco, the Souss Massa Basin in Morocco has experienced the effects of anthropogenic demand and groundwater depletion [*Hssaisoune et al., 2016; Lezzaik and Milewski, 2017*]. The lack of data availability and limited research on these topics has presented the opportunity for this study. Understanding the available groundwater resources and how they are impacted from over-abstraction will not only better characterize this coastal system, but also provide informed decisions in meeting the water resource demand.

The water balance and water levels of the Souss-Mass Basin indicate an overall decrease in water resources due to the combination of the natural decreased recharge and extent of abstraction. From 1972 to 2007, the water balance of shallow aquifers displayed a decreasing trend of infiltration from rain and surface runoff in the Souss and Massa-Chtouka aquifer system, except for a spike in 1996. The reduction of the water table of the Souss and Massa-Chtouka aquifer is due to the decrease of infiltration, less/variable rainfall, and over-abstraction of groundwater resources. The decreasing water deficit varies between both shallow aquifer systems which are variable in time and space, quantity of recharge and inflow to groundwater systems, the amount of

groundwater abstraction, and the distribution and intensity of the selected pumping wells. The demand for water in the Souss Massa basin exceeds the sustainable supply, but what is important to note is the effect the climate regimes have on recharge in this region. It is evident recurring droughts will further deplete the available water resources [*Hssaisoune et al., 2016*].

Climate change along with groundwater abstractions has impacted the groundwater in the region. Monitoring water resources in an arid region is difficult, as available and reliable datasets are not common [*Milewski et al., 2009; Ritzema et al., 2010; Milewski et al., 2009; Ireson et al., 2006; Lezzaik et al., 2018; Milewski et al., 2015*]. Numerous studies on precipitation and temperature have characterized this basin to represent climate variables for temporal and spatial scales [*Tramblay et al., 2013; Bouchaou et al., 2011; N'da et al., 2016; Filahi et al., 2016; Hssaisoune et al., 2016*]. To understand the hydrogeological impacts on groundwater resources climate and hydrogeological data must be interpreted. Milewski et al recognized the lack of available datasets to characterize this region and developed an integrated model of satellite remote sensing utilizing Gravity Recovery and Climate Experiment (GRACE), Tropical Rainfall Measurement Mission (TRMM) and Soil Water Assessment Tool (SWAT). The climate projections IPCCAR5 model was created [*Milewski et al., 2020*] to evaluate the regional scale of Morocco and the Souss Massa Basin.

The climate change projections show that precipitation will most likely begin to decrease. Groundwater recharge rates will be impacted, thus magnifying the current decreasing groundwater trends [*Milewski et al., 2020*]. Through remote sensing techniques, the determination of climate change in precipitation and total water storage was identified, examination of current and projected impacts on surface/groundwater resources was assessed, and the relation on climate regime effects on groundwater resources was investigated.

This study was not only critical in understanding the effects of climate regimes in the Souss Massa Basin hydrogeological system, but it also created a streamline to better understand groundwater resources in coastal systems. Due to the climate regime effects occurring in the Souss Massa Basin, resulting in the decrease of groundwater resources, surface subsidence can take place. The over-abstraction of groundwater resources will cause groundwater levels to decline and aquifer compaction [*Ingebritsen and Galloway, 2014; Galloway and Sneed, 2013; Tolman and Poland, 1940; Poland and Davis, 1969; Poland, 1984; Sneed, 2008; Sneed and Galloway, 2000; Pavelko, 2003; Holzer, 1981*]. In this examination, surface subsidence was assessed though Interferometric Synthetic Aperture Radar (InSAR) to identify the land displacement occurring in this region. Additionally, GRACE datasets (i.e., groundwater storage anomalies (GWSa) and total water storage anomalies (TWSa)) were correlated to displacement changes in order to identify how increased anthropogenic activity contributes to surface subsidence and its impacts on groundwater resources.

1.3. Research Objective

The overall objective of this research is to use remote sensing-based monitoring to better understand how landscape changes impact coastal systems at various sites across a range of scales. Coastal systems are continuously being altered by landscape changes which are impacting groundwater resources. The use of remote sensing-based techniques will identify how landscape changes influence groundwater resources from erosional activity, changes in vegetation density, and increased anthropogenic activity. Specific objectives include:

1. Using LiDAR to identify temporal changes in elevation and quantifying the spatial volumetric changes of unconsolidated sedimentary material to demonstrate the erosional activity occurring in the southeast US.

2. Outline classification algorithms that are most appropriate for salt marsh monitoring by evaluating the usefulness of each classification scheme and determining the most appropriate classifications representative of the southeast US.
3. Perform an examination of InSAR techniques to determine relative subsidence in the Souss Massa basin due to over abstraction of groundwater resources.

This research highlights the complex nature of coastal systems and how landscapes are steadily evolving from numerous processes. Understanding how coastal systems are altered from vegetation density, erosional activity, and anthropogenic processes provides insight on the hydrogeological impact. Groundwater and surface water is impacted by these landscape changes which warrants these nuanced approaches. Through each of these studies, remote sensing-based techniques were used to identify the role geomorphology plays in landscape changes, while also contributing to the enhancement of natural resource management and improved water resource monitorization.

References

Alber, M.; Swenson, E.M.; Adamowicz, S.C.; Mendelssohn, I.A. Salt marsh dieback: An overview of recent events in the US. Estuar. Coast. Shelf Sci. 2008, 80, 1–11.

Andersen, M.S., Gergely, Á., Al-Hamdani, Z., Steinbacher, F., Larsen, L.R. and Ernstsen, V.B., 2017. Processing and performance of topobathymetric lidar data for geomorphometric and morphological classification in a high-energy tidal environment. *Hydrology and Earth System Sciences*, *21*(1), pp.43-63.

Bamber, J.L., Oppenheimer, M., Kopp, R.E., et al., 2019. Ice sheet contributions to future sea-level rise from structured expert judgment. Proceedings of the National Academy of Sciences. 116(23), 11195- 11200. DOI: https://doi.org/10.1073/pnas.1817205116

Barbier, E.B.; Hacker, S.D.; Kennedy, C.; Koch, E.W.; Stier, A.C.; Silliman, B.R.2011. The value of estuarine and coastal ecosystem services. Ecol. Monogr. 2011, 81, 169–193.

Barnhardt, W., Denny, J., Baldwin, W., et al., 2007. Geologic framework of the Long Bay inner shelf: implications for coastal evolution in South Carolina. Coastal Sediments. 2151-2160. DOI: https://doi.org/10.1061/40926(239)169

Belluco, E.; Camuffo, M.; Ferrari, S.; Modenese, L.; Silvestri, S.; Marani, A.; Marani, M. Mapping salt-marsh vegetation by multispectral and hyperspectral remote sensing. Remote Sens. Environ. 2006, 105, 54–67.

Bouchaou, L; Michelot, J; Vengosh, A; Hsissou, Y, Qurtobi, M; Gaye, C; Bullen, T; Zuppi, G. 2008. Application of multiple isotopic and geochemical tracers for investigation of recharge, salinization, and residence time of water in the Souss-Massa aquifer, southwest of Morocco. *J. Hydrol.* 352, 267-287.

Bouchaou, L; Tagma, T; Boutaleb, S; Hssaisoune, M and El Morjani, ZEA. 2011. Climate

change and its impacts on groundwater resources in Morocco: The case of the Souss-Massa basin. In *Climate Change Effects on Groundwater Resources: A Global Synthesis of Findings and Recommendations*; Taylor & Francis Group: Albingdon, UK

Brock, J.C., Purkis, S.J., 2009. The emerging role of lidar remote sensing in coastal research and resource management. Journal of Coastal Research. (10053), 1-5. DOI: https://doi.org/10.2112/SI53-001.1

Byrd, K.B.; Kelly, M. Salt marsh vegetation response to edaphic and topographic changes from upland sedimentation in a Pacific estuary. Wetlands 2006, 26, 813–829.

Campbell, A.D.; Fatoyinbo, L.; Goldberg, L.; Lagomasino, D. Global hotspots of salt marsh change and carbon emissions. Nature 2022, 612, 701–706.

Campbell, A.; Wang, Y. High spatial resolution remote sensing for salt marsh mapping and change analysis at Fire Island National Seashore. Remote Sens. 2019, 11, 1107. Remote Sens. 2024, 16, 2 18 of 19

Carson, W.W., Anderson, H.E., Reutebuch, S.E., et al., 2004. May. LiDAR applications in forestry – An overview. Proceedings of the American Society of Photogrammetry and Remote Sensing Annual Conference (pp. 1-9) 04-1-2-02_04_1_2_02_deliverable_06.pdf (firescience.gov).

Church, JA; Hunter, JR; McInnes, KL and White, NJ. 2006. Sea-level rise around the Australian coastline and the changing frequency of extreme sea-level events. *Aust. Meteorol. Mag.* 55, 253-260.

Crooks, S.; Herr, D.; Tamelander, J.; Laffoley, D.; Vandever, J. 2011. Mitigating Climate

Change through Restoration and Management of Coastal Wetlands and Near-Shore Marine Ecosystems: Challenges and Opportunities; The World Bank: Washington, DC, USA, 2011.

Crosby, S.C.; Sax, D.F.; Palmer, M.E.; Booth, H.S.; Deegan, L.A.; Bertness, M.D.; Leslie, H.M. 2016. Salt marsh persistence is threatened by predicted sea-level rise. Estuar. Coast. Shelf Sci., 181, 93–99.

Dalin, C; Wada, Y; Kastner, T and Puma, MJ. 2017. Groundwater depletion embedded in international food trade. Nature 543(7647):700-4.

Danchenkov, A.R. and Belov, N.S., 2019. Morphological changes in the beach-foredune system caused by a series of storms. Terrestrial laser scanning evaluation. Russian Journal of Earth Sciences, 19(4), p.4.

Danchenkov, A., Belov, N. and Stont, Z., 2019. Using the terrestrial laser scanning technique for aeolian sediment transport assessment in the coastal zone in seasonal scale. Estuarine, Coastal and Shelf Science, 223, pp.105-114.

Davidson-Arnott, R., Bauer, B. and Houser, C., 2019. Introduction to coastal processes and geomorphology. Cambridge university press.

Day, J.W.; Christian, R.R.; Boesch, D.M.; Yáñez-Arancibia, A.; Morris, J.; Twilley, R.R.; Naylor, L.; Schaffner, L.; Stevenson, C. Consequences of climate change on the ecogeomorphology of coastal wetlands. Estuaries Coasts 2008, 31, 477–491.

Denny, J.F., Schwab, W.C., Baldwin, W.E., Barnhardt, W.A., Gayes, P.T., Morton, R.A., Warner, J.C., Driscoll, N.W. and Voulgaris, G., 2013. Holocene sediment distribution on the inner continental shelf of northeastern South Carolina: implications for the regional

sediment budget and long-term shoreline response. Continental Shelf Research, 56, pp.56-70.

DiGiacomo, A.E.; Bird, C.N.; Pan, V.G.; Dobroski, K.; Atkins-Davis, C.; Johnston, D.W.; Ridge, J.T. Modeling salt marsh vegetation height using unoccupied aircraft systems and structure from motion. Remote Sens. 2020, 12, 2333.

D'Oleire-Oltmanns, S; Marzolff, I; Peter, KD; Ries, JB and Ait Hssaine, A. 2011. Monitoring soil erosion in the Souss Basin, Morocco, with a multiscale object-based remote sensing approach using UAV and satellite data. In *Proceedings of the 1st World Sustainability Forum*; Sciforum Electronic Conference Series; MDPI: Basel, Switzerland.

Duarte, C.M.; Dennison, W.C.; Orth, R.J.; Carruthers, T.J. 2008. The charisma of coastal ecosystems: Addressing the imbalance. Estuaries Coasts, 31, 233–238.

Fagherazzi, S.; Marani, M.; Blum, L.K. The Ecogeomorphology of Tidal Marshes; American Geophysical Union: Washington, DC, USA, 2004.

Farris, A.S.; Defne, Z.; Ganju, N.K. Identifying salt marsh shorelines from remotely-sensed elevation data and imagery. Remote Sens. 2019, 11, 1795.

Elaksher, A., 2008. Fusion of hyperspectral images and lidar-based dems for coastal mapping. Optics and Lasers in Engineering. 46(7), 493-498. DOI: https://doi.org/10.1016/j.optlaseng.2008.01.012

Filahi, S; Tanarhte, M; Mouhir, L; El Morhit, M and Tramblay, Y. 2016. Trends in indices of daily temperature and precipitations extremes in Morocco. *Theor. Appl. Climatol.* 124, 959-972.

Fretwell, S.; Wagner, A.; Lee, A. "A Million Acres of 'Priceless' Marshes Protect NC, SC,

GA. Will They Perish in Rising Tides?" The News and Observer. 2021. Available online: https://pulitzercenter.org/stories/million-acres-priceless-marshes-protect-ncsc-ga-will-they-perish-rising-tides (accessed on 18 June 2023).

Galloway, DL and Sneed, M. 2013. Analysis and simulation of regional subsidence accompanying groundwater abstraction and compaction of susceptible aquifer systems in the USA. Boletin de la Sociedad Geologica Mexicana, Vol. 65, No. 1, Numero especial Geoquimica Ambiental, pp. 123-136.

Gesch, D.B., 2009. Analysis of lidar elevation data for improved identification and delineation of lands vulnerable to sea-level rise. Journal of Coastal Research. 53, 49-58. DOI: https://doi.org/10.2112/SI53-006.1

Gilluly, J. 1964. Atlantic sediments, erosion rates, and the evolution of the continental shelf; some speculations, *Geol. Soc. Am Bull.* 75, 483-492.

Giri, C.; Ochieng, E.; Tieszen, L.L.; Zhu, Z.; Singh, A.; Loveland, T.; Masek, J.; Duke, N. Status and distribution of mangrove forests of the world using earth observation satellite data. Glob. Ecol. Biogeogr. 2011, 20, 154–159.

Gleeson, T; Befus, K; Jasechko, S; Luijendijk, E and Cardenas, MB. 2015. The global volume and distribution of modern groundwater. Nature Geosci.http://dx.doi.org/10.1038/ngeo2590.

Gleeson, T; Cuthbert, M; Ferguson, G and Perrone, D. 2020. Global groundwater sustainability, resources, and systems in the Anthropocene. Annu. Rev. Earth Planet. Sci. 48 431-63.

Gleeson, T; Wada, Y; Bierkens, M and Van Beek, L. 2012. Water balance of global aquifers revealed by groundwater footprint. *Nature* 488, 197-200.

Gleeson, T; Wegener, T; Cuthbert, M; Rahman, S; Bierkens, M; Doll, P; Rosolem, R; Zipper, S; Bresciani, E; Ducharne, A; Taylor, R; Hill, M; Wada, Y; Lo, M; Luijendijk, E; Maxwell, R; Hartmann, A; de Graaf, I; Oshinlaja, N; West, C; Famiglietti, J; Kollet, S; Condon, L; Scanlon, B and Kim, H. 2019. Groundwater representation in continental to global hydrologic models: A call for open and holistic evaluation, conceptualization, and classification. *EarthArXiv*. https://doi.org/10.31223/osf.io/zxyku.

Gornitz, VM; Daniels, RC; White, TW and Birdwell, KR. 1994. The development of a coastal risk assessment database: vulnerability to sea level rise in the U.S. Southwest. *J. Coast. Res. Special Issue.* 12, 327-338.

Guimond, J.; Tamborski, J. Salt marsh hydrogeology: A review. Water 2021, 13, 543.

Gutierrez, B.T., Plant, N.G., Thieler, E.R., 2011. A Bayesian network to predict coastal vulnerability to sea level rise. Journal of Geophysical Research: Earth Surface. 116(F2). DOI: https://doi.org/10.1029/2010JF001891

Hauer, F.R., Locke, H., Dreitz, V.J., Hebblewhite, M., Lowe, W.H., Muhlfeld, C.C., Nelson, C.R., Proctor, M.F. and Rood, S.B., 2016. Gravel-bed river floodplains are the ecological nexus of glaciated mountain landscapes. *Science Advances*, *2*(6), p.e1600026.

Holzer, T.L., 1981. Preconsolidation stress of aquifer systems in areas of induced land subsidence. *Water Resources Research, 17*(3), pp.693-703.

Hssaissoune, M; Boutaleb, S; Benssaou, M and Bouchaou, L. 2016. Physical geography, geology, and water resource availability of the Souss-Massa River Basin. In: Choukr-Allah, R; Ragab, r; Bouchaou, L; Barcelo, D (eds) The Souss-Massa River Basin, Morocco. Springer, Switzerland, pp 27-56.

Hughes, A.L.; Wilson, A.M.; Morris, J.T. Hydrologic variability in a salt marsh: Assessing

the links between drought and acute marsh dieback. Estuar. Coast. Shelf Sci. 2012, 111, 95–106.

Ingebritsen, SE and Galloway, DL. 2014. Coastal subsidence and relative sea level rise. *Environ. Res. Lett.* 9, 091002, 4pp.

IPBES (Intergov. Sci. Policy Platf. Biodivers. Ecosyst. Serv.). The Assessment Report on Land Degradation and Restoration. Rep., IPBES, Bonn, Ger, 2018. Available online: http://www.ipbes.net (accessed on 18 June 2023).

Ireson, A; Makropoulos, C and Maksimovic, C. 2006. Water resources modelling under data scarcity: coupling: Mike Basin and ASM groundwater model. *Water Resour.Manag.* 20, 567-590.

Jaiswal, R; Mukherjee, S; Krishnamurthy, J and Saxena, R. 2003. Role of remote sensing and GIS techniques for generation of groundwater prospect zones towards rural development: an approach. *International Journal of Remote Sensing* 24(50, 993-1008. Doi:10.1080/01431160210144543

JMP. 2010. Progress on sanitation and drinking-water, 2010 update. WHO/UNICEF, Geneva and New York, ISBN 978-92-806-4313-8.

Kirwan, M.L.; Mudd, S.M. Response of salt-marsh carbon accumulation to climate change. Nature 2012, 489, 550–553.

Klein, R.J. and Nicholls, R.J., 1999. Assessment of coastal vulnerability to climate change. Ambio, pp.182-187.

Kumar, CP. 2012. Climate change and its impact on groundwater resources. International Journal of Engineering and Science 1:43-60.

Leatherman, S.P., 1984. Coastal geomorphic response to sea level rise: Galveston Bay,

Texas. Barth and Titus (eds). Coastal Zone. 151-178.

Leatherman, SP; Zhang, K and Douglas, BC. 2000. Sea level rise shown to drive coastal erosion. *EOS Trans. Am. Geophys. Union.* 81, 55-56.

Leece, SA; Pease, PP; Gares, PA; Wang, JY. 2006. Seasonal controls on sediment delivery in a small coastal plain watershed, North Carolina, USA. *Geomorphology*. 73 (3-4), 246-260.

Leonard, L.A., Hine, A.C., Luther, M.E., Stumpf, R.P. and Wright, E.E., 1995. Sediment transport processes in a west-central Florida open marine marsh tidal creek; the role of tides and extra-tropical storms. Estuarine, Coastal and Shelf Science, 41(2), pp.225-248.

Lezzaik, K and Milewski, A. 2017. A quantitative assessment of groundwater resources in the Middle East and North Africa region. *Hydrogeol. J.* 26, p. 251.

Lezzaik, K; Milewski, A and Mullen, J. 2018. The groundwater risk index: development and application in the Middle East and North Africa region. *Sci Total Environ* 628-629:1149-1164.

Lindsey, R., 2019. Climate Change: Global Sea Level. National oceanic and atmospheric administration (NOAA), National Ocean Service, Silver Spring. https://www.climate.gov/news-features/understanding-climate/climate-change-global-sea-level (Accessed on 18 January 2020).

Lovelace, JK; Nielsen, MG; Read, AL; Murphy, CJ. 2020. Estimated groundwater withdrawals from principal aquifers in the United States, 2015 (ver. 1.2, October 2020): U.S. Geological Survey Circular 1464, 70 p.,

MacDonald, A; Bonsor, H; Dochartaigh, B and Taylor, R. 2012. Quantitative maps of groundwater resources in Africa. Environ. Res. Lett. 7, 024009.

MacDonald, A and Calow, R. 2009. Developing groundwater for secure water supplies in Africa. Desalination 248; 546-556.

Mariotti, G.; Canestrelli, A. Long-term morphodynamics of muddy backbarrier basins: Fill in or empty out? Water Resour. Res. 2017, 53, 7029–7054.

Markewich, HW; Pavich, MJ and Buell, GR. 1990. Contrasting soils and landscapes of the Piedmont and Coastal Plain, eastern United States. *Geomorphology*. 3, 417-447.

Masselink, G. and Russell, P., 2013. Impacts of climate change on coastal erosion. MCCIP Science Review, 2013, pp.71-86.

Maupin, MA; Kenny, JF; Hutson, SS; Lovelace, JK; Barber, NL and Linsey, KS. 2014. Estimated use of water in the United States in 2010: U.S. Geological survey Circular 1405, 56 p.

McInnes, KL; Walsh, KJE; Hubbert, GD and Beer, T. 2003. Impact of sea-level rise and storm surges on a coastal community. *Nat. Hazards.* 30, 187-207.

Mcowen, C.J.; Weatherdon, L.V.; Van Bochove, J.W.; Sullivan, E.; Blyth, S.; Zockler, C.; Stanwell-Smith, D.; Kingston, N.; Martin, C.S.; Spalding, M.; et al. 2017. A global map of salt marshes. Biodivers. Data J, 5, e11764

Milewski, A; Lezzaik, K and Rotz, R. 2020. Sensitivity analysis of the groundwater risk index in the Middle East and North Africa region. *Environ Process* 7:53-71. Doi:10.1007/s40710-019-00421-7.

Milewski, A; Seyoum, WM; Elkadiri, R and Durham, M. 2020. Multi-scale hydrologic sensitivity to climatic and anthropogenic changes in Northern Morocco. *Geosciences* 10 (1), 13. Doi:10.3390/geosciences10010013.

Milewski, A; Elkadiri, R and Durham, M. 2015. Assessment and comparison of TMPA

Satellite Precipitation Products in Varying Climatic and Topographic Regimes in Morocco. *Remote Sens.*7, 5697-5717.

Milewski, A; Sultan, M; Jayapraksh, SM; Balekai, R and Becker, R. 2009. RESDEM, a tool for integrating temporal remote sensing data for use in hydrogeologic investigations. *Comput. Geosci.* 35, 2001-2010.

Milewski, A; Sultan, M; Yan, E; Becker, R; Abdeldayem, A; Soliman, F and Gelil, KA. 2009. A remote sensing solution for estimating runoff and recharge in arid environments. *J. Hydrogeol.* 373, pp. 1-14.

Morton, R.A., 2003. An overview of coastal land loss: With emphasis on the southeastern United States. United States (p. 28). US Geological Survey, Center for Coastal and Watershed Studies. https://citeseerx.ist.psu.edu/viewdoc/download?-doi=10.1.1.730.5008&rep=rep1&type=pdf.

Morton, R.A., Miller, T.L., 2005. National assessment of shoreline change: Part 2, Historical shoreline change and associated land loss along the U.S. Southeast Atlantic coast. U.S. Geological Survey. Open-File Report. 1401, 1-40. DOI: https://doi.org/10.3133/ofr20051401

Mwamba, M.J.; Torres, R. Rainfall effects on marsh sediment redistribution, North Inlet, South Carolina, USA. Mar. Geol. 2002, 189, 267–287.

N'da, AB; Bouchaou, L; Reichert, B; Hanich, L; Brahim, YA; Chehbouni, A; Beraaouz, EH and Michelot, JL. 2016. Isotopic signatures for the assessment of snow water resources in the Moroccan high Atlas Mountains: Contribution to surface and groundwater recharge. *Environ. Earth Sci.* 75, 755.

Nicholls, R.J., Wong, P.P., Burkett, V., et al., 2007. Coastal systems and low-lying areas.

https://ro.uow. edu.au/scipapers/. 164, 315-356.

O'Dea, A., Brodie, K.L., Hartzell, P., 2019. Continuous coastal monitoring with an automated terrestrial lidar scanner. Journal of Marine Science and Engineering. 7(2), 37. DOI: https://doi.org/10.3390/jmse7020037

Orson, R.; Panageotou, W.; Leatherman, S.P. Response of tidal salt marshes of the US Atlantic and Gulf coasts to rising sea levels. J. Coast. Res. 1985, 1, 29–37.

Pavelko, MT. 2003. Estimates of hydraulic properties from a one-dimensional numerical model of vertical aquifer-system deformation, Lorenzi Site, Las Vegas, Nevada: Carson City, Nevada, U.S. United States Geological Survey, Water-Resources InvestigationsReport03-4083, 36 p.http://pubs.usgs.gov/wri/wri034083/index.html

Phillips, JD; Wyrick, M; Robbins, JG and Flynn, M. 1993. Accelerated erosion on the North Carolina coastal plain. *Phys. Georgr.* 14, 114-130.

Poland, JF. 1984. Guidebook to the studies of land subsidence due to groundwater withdrawal: Paris, UNESCO, Studies and reports in hydrology 40, http://wwwrcamnl.wr.usgs.gov/ rgws/Unesco/,

Poland, JF and Davis, GH. 1969. Land subsidence due to withdrawal of fluids, in Varnes, DJ, Kiersch, G. (eds.): Reviews in Engineering Geology, 2, 187-269.

Ritzema, H; Froebrich, J; Raju, R; Sreenivas, C and Kselik, R. 2010. Using participatory modeling to compensate for data scarcity in environmental planning: A case study from India. *Environ. Model. Softw.* 25, 1450-1458.

Roughgarden, J.; Running, S.W.; Matson, P.A. What does remote sensing do for ecology? Ecology 1991, 72, 1918–1922.

Rumson, A.G., Hallett, S.H. and Brewer, T.R., 2019. The application of data innovations

to geomorphological impact analyses in coastal areas: An East Anglia, UK, case study. Ocean & Coastal Management, 181, p.104875.

Sallenger, A.H., Jr., Krabill, W.B., Swift, R.N., et al., 2003. Evaluation of airborne topographic lidar for quantifying beach changes. Journal of Coastal Research. 125-133. https://www.jstor.org/stable/4299152.

Sanderson, E.W.; Ustin, S.L.; Foin, T.C. The influence of tidal channels on the distribution of salt marsh plant species in Petaluma Marsh, CA, USA. Plant Ecol. 2000, 146, 29–41.

Scavia, D.; Field, J.C.; Boesch, D.F.; Buddemeier, R.W.; Burkett, V.; Cayan, D.R.; Fogarty, M.; Harwell, M.A.; Howarth, R.W.; Mason, C.; et al. Climate change impacts on US coastal and marine ecosystems. Estuaries 2002, 25, 149–164.

Schuerch, M.; Vafeidis, A.; Slawig, T.; Temmerman, S. Modeling the influence of changing storm patterns on the ability of a salt marsh to keep pace with sea level rise. J. Geophys. Res. Earth Surf. 2013, 118, 84–96.

Schwarz, C.; van Rees, F.; Xie, D.; Kleinhans, M.G.; van Maanen, B. Salt marshes create more extensive channel networks than mangroves. Nat. Commun. 2022, 13, 2017.

Schwartz, R.K. and Musialowski, F.R., 1977. Nearshore disposal: onshore sediment transport. Coastal Engineering Research Center.

Sheridan, JM; Booram, CV and Asmussen, LE. 1982. Sediment delivery ratios for a small coastal plain agricultural watershed. *Trans. Am. Soc. Agric. Eng.* 25, 610-615.

Silvestri, S.; Marani, M.; Marani, A. Hyperspectral remote sensing of salt marsh vegetation, morphology and soil topography. Phys. Chem. Earth Parts A/B/C 2003, 28, 15–25.

Silvestri, S.; Marani, M. Salt-marsh vegetation and morphology: Basic physiology,

modelling and remote sensing observations. Ecogeomorphology Tidal Marshes 2004, 59, 5–25.

Simas, T.; Nunes, J.P.; Ferreira, J.G. 2001. Effects of global climate change on coastal salt marshes. Ecol. Model, 139, 1–15.

Slattery, MC; Gares, PA and Phillips, JD. 2002. Slope-channel linkage and sediment delivery on North Carolina coastal plain cropland. *Earth Surface Processes and Landforms.* 27, 1377-1387.

Sneed, M. 2008. Aquifer-system compaction and land subsidence data and simulations, the Holly Site, Edwards Air Force Base, California: sacramento, California, California State University-Sacramento, M.S. thesis, 40 p.

Sneed, M. and Galloway, D.L., 2000. Aquifer-system compaction and land subsidence: measurements, analyses, and simulations: the Holly site, Edwards Air Force Base, Antelope Valley, California (No. 4015). US Department of the Interior, US Geological Survey.

Sowers, J; Vengosh, A and Weinthal. 2011. Climate change, water resources, and the politics of adaptation the Middle East and North Africa. *Clim Chang.* 104, 599-627.

Stagg, C.L.; Osland, M.J.; Moon, J.A.; Feher, L.C.; Laurenzano, C.; Lane, T.C.; Jones, W.R; Hartley, S.B. Extreme precipitation and flooding contribute to sudden vegetation dieback in a coastal salt marsh. Plants 2021, 10, 1841.

Surrette, M; Allen, D and Journeay, M. 2008. Regional evaluation of hydraulic properties in variably fractured rock using a hydrostructural domain approach. Hydrogeology Journal 16(1), 11-30. Doi: 10.1007/s10040-007-0206-9.

Teixeira, J; Chamine, H; Carvalho, J; Perez-Alberti, A and Rocha, F. 2013.

Hydrogeomorphological mapping as a tool in groundwater exploration. Journal of Maps. 9:2, 263-273, DOI: 10.1080/17445647.2013.776506.

Teixeira, J; Chamine, H; Espinha Marques, J; Gomes, A; Carvalho, J; Perez-Alberti, A and Rocha, F. 2010. Integrated approach of hydrogeomorphology and GIS mapping to the evaluation of groundwater resources: An example from the hydromineral system of Caldas da Cavaca, NW Portugal. In Global groundwater resources and management, selected papers from the 33rd international geological congress, general symposium: Hydrogeology, Edited by: Paliwal, B.S. 227-249. Oslo (Norway): Scientific Publishers (India), Jodhpur.

Tempest, J.A.; Harvey, G.L.; Spencer, K.L. Modified sediments and subsurface hydrology in natural and recreated salt marshes and implications for delivery of ecosystem services. Hydrol. Process. 2015, 29, 2346–2357.

Titus, J.G., Richmond, C., 2001. Maps of lands vulnerable to sea level rise: modeled elevations along the US Atlantic and Gulf coasts. Climate Research. 18(3), 1-24. DOI: https://doi.org/10.3354/cr018205

Tolman, CF and Poland JF. 1940. Groundwater, saltwater infiltration, and ground surface recession in Santa Clara Valley, Santa Clara County, California: *Transactions, American Geophysical Union,* 1, 23-35.

Tol, R.s..J., Klein, R.J.T., Jansen, H.M.A. and Verbruggen, H. 1996. Some economic considerations on the importance of proactive integrated coastal zone management. Ocean Coast. Mgmt 32, 39-55.

Tramblay, Y; Ruelland, D; Somot, S; Bouaicha, R and Servat, E. 2013. High-resolution

Med-CORDEX regional climate model simulations for hydrological impact studies: A first evaluation of the ALADIN-Climate model in Morocco. *Hydrol. Earth Syst. Sci*. 17, 3721-3739.

Valiela, I.; Teal, J.M.; Volkmann, S.; Shafer, D.; Carpenter, E.J. Nutrient and particulate fluxes in a salt marsh ecosystem: Tidal exchanges and inputs by precipitation and groundwater 1. Limnol. Oceanogr. 1978, 23, 798–812.

Valverde, H.R., Trembanis, A.C. and Pilkey, O.H., 1999. Summary of beach nourishment episodes on the US east coast barrier islands. Journal of Coastal Research, pp.1100-1118.

Von Holle, B., Irish, J.L., Spivy, A., et al., 2019. Effects of future sea level rise on coastal habitat. Journal of Wildlife Management. 83(3), 694-704. DOI: https://doi.org/10.1002/jwmg.21633

Vo, Q.T.; Oppelt, N.; Leinenkugel, P.; Kuenzer, C. Remote sensing in mapping mangrove ecosystems—An object-based approach. Remote Sens. 2013, 5, 183–201.

Wada, Y and Heinrich, L. 2013. Assessment of transboundary aquifers of the world vulnerability arising from human water use. Environ. Res. Lett. 8(2):024003.

Warner, J.C., Armstrong, B., Sylvester, C.S., et al., 2012. Storm-induced inner-continental shelf circulation and sediment transport: Long Bay, South Carolina. Continental Shelf Research. 42, 51-63. DOI: https://doi.org/10.1016/j.csr.2012.05.001

White, S.A. and Wang, Y., 2003. Utilizing DEMs derived from LIDAR data to analyze morphologic change in the North Carolina coastline. Remote sensing of environment, 85(1), pp.39-47.

Wilson, A.M.; Evans, T.; Moore, W.; Schutte, C.A.; Joye, S.B.; Hughes, A.H.; Anderson,

J.L. Groundwater controls ecological zonation of salt marsh macrophytes. Ecology 2015, 96, 840–849.

Woolard, J.W., Colby, J.D., 2002. Spatial characterization, resolution, and volumetric change of coastal dunes using airborne LIDAR: Cape Hatteras, North Carolina. Geomorphology. 48(1-3), 269-287. DOI: https://doi.org/10.1016/S0169-555X(02)00185-X

Wu, SY; Yarnal, B and Fisher, A. 2002. Vulnerability of coastal communities to sea-level rise: A case study of Cape May county, New Jersy, USA. *Climate Research.* 22, 255-270.

Yeo, S.; Lafon, V.; Alard, D.; Curti, C.; Dehouck, A.; Benot, M.L. Classification and mapping of saltmarsh vegetation combining multispectral images with field data. Estuar. Coast. Shelf Sci. 2020, 236, 106643.

Young, A.P. and Ashford, S.A., 2006. Application of airborne LIDAR for sea cliff volumetric change and beach-sediment budget contributions. Journal of Coastal Research, 22(2), pp.307-318.

Zhang, M.; Ustin, S.L.; Rejmankova, E.; Sanderson, E.W. Monitoring Pacific coast salt marshes using remote sensing. Ecol. Appl. 1997, 7, 1039–1053.

CHAPTER 2

THE USE OF AIRBORNE LIDAR IN ASSESSING COASTAL EROSION IN THE SOUTHEASTERN USA[1]

[1] Richards, David F., IV, Milewski, Adam M., and Gregory, Brian. 2022. *Journal of Geographical Research*, 5(3), 22-40, DOI: https://doi.org/10.30564/jgr.v5i3.4762. Reprinted here with permission of the publisher.

Abstract

Changes in sea level along the coastal southeastern United States (U.S.) influence the dynamic coastal response. In particular, the Southeast Coastal Network (SECN) of the National Park Service (NPS) has exhibited evidence of fluctuations in sea level which caused coastal erosion. Airborne LiDAR acquired from NOAA for Fort Matanzas National Monument, Fort Pulaski National Monument, Charles Pinckney National Historic Site, and Cape Lookout National Seashore were analyzed to identify changes in both elevation and the spatial volume of unconsolidated sedimentary material in the coastal southeast over time. Areas that exhibited an increase (deposited material) or decrease (eroded material) in elevation were mapped across the study area from 2006 to 2018. Results indicate a quasi-cyclic process where unconsolidated sediment distribution and the morphodynamic equilibrium changes with time. The coastal zones are steadily oscillating between the process of erosion and deposition affecting the coastal geomorphological dynamic. The use of LiDAR for evaluating coastal sustainability and resiliency due to this environmental phenomenon is clear.

2.1. Introduction

The coastal southeast United States (U.S.) is highly susceptible to geomorphological and hydrogeological changes in response to relative sea level rise. Climate change increases both the quantity and intensity of storms which results in subsequent sea level rise [*Gornitz et al., 1994; Wu et al., 2002; Church et al., 2006*]. Many variables play a role in the geomorphological and hydrological response to this shift. These variables are intrinsically connected, defining the interaction and link of hydrologic and geomorphic processes in both temporal and spatial dimensions [*Leatherman, 1984; Nicholls et al., 2007*]. The Atlantic Coastal Plain is extremely sensitive to sea level rise, causing accelerated erosion rates and changes in the amount of sediment deposited in coastal areas [*Markewich et al., 1990; Leece et al., 2006; Philips et al., 1993*]. As this is representative of the hydrogeological impact, the economic impacts are analogous to the direct damages of sea level rise [*Hauer et al., 2016; Desmet et al., 2018; Klein and Nicholls 1999*].

Global mean sea level rise has risen about 21 centimeters ~ 24 centimeters (0.21 meters ~ 0.24 meters) since 1880, with about a third of that coming in just the last two and a half decades [*Lindsey, 2019*]. By 2100, research suggests that sea level rise could exceed 2 meters, given the climate regimes continue at their current rates [*Bamber et al., 2019*]. Along the southeastern US coastline, approximately 43% (~2,000 km) of the area is projected to have an increase in coastal erosion vulnerability by the 2030s, with respect to its present vulnerability [*Von Holle et al., 2019*]. Studies have shown that the coastal sediment budget, representing the sediment supply, is extremely vulnerable [*Morton, 2003; Morton and Miller, 2005; Gutierrez et al., 2011*]. Coastal erosion is continuously altering the environment and mitigating its effects has become increasingly important. To meet the increasing demand for coastal resource management, remote sensing techniques are being used to provide rapid data acquisition of large areas that would normally

require extensive and lengthy field surveys. Furthermore, the ability to use light detection and ranging (LiDAR) in both natural resource management and economic sustainability, creates the opportunity to distinctively characterize the coastal dynamic response at high spatial resolutions.

Typically, LiDAR is used in forest management to understand biomass dynamics as it was historically believed to show the greatest promise over these areas, however, its use in coastal applications has become a pivotal tool in coastal change detection [*Brock and Purkis, 2009; Carson et al., 2004*]. The ability of LiDAR has garnered efficient, productive, and accurate measurements of topographical mapping [*Sallenger et al., 2003; Woolard and Colby, 2002; Young and Ashford, 2006*]. LiDAR's application enables rapid elevation data collection through repeated measurements of the observed topographic region [*O'Dea et al., 2019*]. The high spatial resolution data retrieved produce digital elevation models (DEMs) indicative of current and historical coastal geomorphological changes. The results have become an asset in improving the knowledge of complex coastal geomorphological processes creating better preventative and mitigating initiatives [*Gesch, 2009; Elaksher, 2008; Titus and Richmond, 2001*].

In recognition of the changes occurring along the coastal southeast US, the sediment budget has displayed both aggraded and degraded material [*Barnhardt et al., 2007; Warner et al., 2012*]. In this paper, we present the use of LiDAR in characterizing the spatial and temporal changes of the coastal southeast US, and quantify these changes at select National Park sites. More specifically to identify the temporal changes in elevation and quantify the spatial volumetric changes of unconsolidated sedimentary material in the Southeastern Coastal Network (SECN) of the National Park Service (NPS).

In the acquisition of temporal LiDAR of SECN NPS sites, land cover data is used to represent the topographic features of the coastal southeast US through ArcGIS and ENVI LiDAR. The final outputs are presented in a GIS framework, providing a volumetric spatial change analysis detailing the specific areas where the erosional activity occurred (net loss) and where unconsolidated material was returned to the environment (net gain). This high-resolution LiDAR data not only exhibits the advantages of LiDAR to improve coastal water resources and the understanding of the coastal geomorphologic dynamic, but also its applicability in providing sustainability and resiliency of environmental change.

2.2. Study Area

The SECN of the NPS monitors seventeen national parks extending along the Atlantic coast from the North Carolina-Virginia border to Cape Canaveral, Florida providing natural resource management. The areas used in this study are Fort Matanzas National Monument (NM) in St. Augustine, Florida, Fort Pulaski National Monument (NM) in Savannah, Georgia, Charles Pinckney National Historic Site (NHS) in Sullivan's Island, South Carolina, and Cape Lookout National Seashore (NS) in Harkers Island, North Carolina. The areas used for Fort Matanzas NM and Cape Lookout NS are within the SECN site boundaries, while the areas used for Fort Pulaski NM and Charles Pinckney NHS are in the vicinity of the SECN site boundary. These sites were selected as each is representative of the states in a longitudinal context along the southeastern US coastline covering 959 km (959,000 m). The distance between each site location is as follows: Fort Matanzas NM to Fort Pulaski NM is 312 km (312,000 m), Fort Pulaski NM to Charles Pinckney NHS is 189 km (189,000 m) and Charles Pinckney NHS to Cape Lookout NS is 468 km (468,000

m). The climate within this region can be categorized as humid subtropical where a wide range of extreme weather and climate events persist [*Ingram et al., 2013; Davey et al., 2007*]. The El Niño Southern Oscillation (ENSO) is key to understanding the interannual variations of the climate of the SECN. El Niño will usually have lower temperatures in winter and spring, increased winter precipitation, and fewer tropical systems [*Davey et al., 2007*]. Mean annual precipitation in the SECN is mostly consistent, however, precipitation increases towards the Atlantic coast. In each of the SECN NPS sites the mean annual precipitation is between 1,001- 1,400 millimeters (mm)/year [*Davey et al., 2007*]. Along the Atlantic coastline precipitation is more present during the summer months. Temperatures in the SECN vary largely as a function of latitude and proximity to the coast. Mean annual temperatures are between 14.1 °C to 24 °C [*Davey et al., 2007*]. The temperatures are higher in the southern states and lower in the northern states. Winter temperatures show a strong latitudinal gradient, while summer temperatures are moderate along the coast but warmer inland. Although the proximity of oceans generally moderates extreme temperature conditions with average summertime maximum temperatures around 30 °C, daytime temperatures can occasionally reach 40 °C [*Davey et al., 2007*].

Each of the sites is in the Atlantic Coastal Plain geological province, where geomorphologic changes have occurred [*Phillips, 1997*]. Fort Matanzas NM is located in the Southeastern Coastal Plain geologic province, specifically in the east central Floridan aquifer system (Figure 2-1). Within the site are saltwater marshes and freshwater wetlands underlain by a surficial aquifer, confining unit and the upper Floridan aquifer [*Campbell et al., 2001; Faulkner, 1970*]. The surficial aquifer varies seasonally while containing sands, marl, peats, mud, and alluvium [*Faulkner, 1970; Graham, 2009*]. The upper Floridan aquifer contains materials from the Eocene to Miocene, where the Hawthorn, Suwanee limestone and Ocala limestone formations are

present [*Faulkner, 1970*]. Separating the surficial aquifer from the upper Floridan aquifer unit is an unconformity where the Hawthorne formation is above the Suwannee limestone [*Tibbals, 1990*]. The Hawthorn formation contains interbedded sand, phosphatic clay, dolomite, and limestone [*Faulkner, 1970*]. Within the Suwannee limestone, silt and clay are present [*Faulkner, 1970*]. The Ocala limestone is separated by an upper and lower lithological unit. The upper member is a marine limestone with coquina and chert, whereas the lower member is a marine limestone with dolomite [*Faulkner, 1970*].

Fort Pulaski NM is located within the Atlantic Coastal Plain geologic province lying at the bottom most region of the Savannah River, which consist of salt marshes and hummocks (Figures 2-1 and 2-2). This site is composed of sand, peat, alluvium, unconsolidated material, clay, and beach sand [*Clarke et al., 1990*]. Most of the material is of carbonates, while the younger rocks are clastic with limestone present near the surface and traces of glauconite underneath the limestone [*Clarke et al., 1990*]. These materials are of the Late Cretaceous to Holocene with rocks of early Eocene to Oligocene [*Clarke et al., 1990*]. The sands are of the Satilla, Coosawhatchie, and Marks Head formations [*Weems and Edwards, 2001*]. The Satilla Formation immediately underlies the land surface where it is composed of sand, clay, and silt deposited in shallow marine environments [*Veatch and Stephenson, 1911; Huddleston, 1988*]. The Coosawhatchie Formation is mostly comprised of silty clay, clay diatomite and phosphate sands [*Weems and Edwards, 2001; Heron et al., 1965*]. These materials persist heavily, thus, they are divided into individual sedimentary units. The five-unit members are Tybee Phosphorite, Meigs, Berryville Clay (upper) Berryville Clay (lower) and Ebenezer formations [*Huddleston, 1988*]. In the Marks Head formation is predominantly of medium to coarse phosphate-calcareous sands [*Huddleston, 1988; Sloan, 1979]*. These formations are in the Upper and Lower Floridan carbonate aquifer system

where the layers are of limestone and dolomite [*Weems and Edwards, 2001*]. The Upper and Lower Brunswick aquifers are present in this region [*Clarke et al., 1990*]. The upper Brunswick aquifer is home to the Marks Head and members of Coosawhatchie formations. The confining unit with the surficial aquifer above contains other members of the Coosawhatchie formation except for the Ebenezer formation [*Weems and Edwards, 2001*].

Charles Pinckney NHS is in the Atlantic Coastal Plain geologic province of South Carolina (Figure 2-2). In this region there are layers of surficial aquifer systems that are separated by an unconfined upper surficial aquifer composed of artificial till and a partially to fully confined lower surficial aquifer composed of sands [*Campbell, 1996*]. Specifically, this site is underlain by confining units, Black Creek, Middendorf, and Cape Fear aquifer systems [*Aucott et al., 1987*]. The confining unit between the Black Creek aquifer and Middendorf aquifer consists of sandy clay material [*Aucott, 1996*]. This lithology is similar in the confining unit between the Middendorf and Cape Fear aquifers. Black Creek's aquifer unit is composed of fine to medium sand where the aquifer's thickness remains constant [*Aucott, 1988*]. The Middendorf aquifer consists of thin, laminated layers of fine to medium sand and clayey material [*Aucott, 1996*]. The layers of clayey material persist in Cape Fear's aquifer unit, but it is separated by sand, silt, and gravel [*Aucott, 1996*].

Cape Lookout NS is a member of the North Carolina Outer Banks, a barrier island within the Atlantic Coastal Plain geologic province (Figure 2-2). This site is underlain by surficial aquifers with confining units. Yorktown, Castle Hayne, Beaufort, Peedee, Black Creek, Upper and Lower Cape Dear aquifer systems are composed of marine sediments [*Lautier, 2001*]. The upper confined aquifer is part of the early Pliocene Yorktown Formation which is comprised of sand, partially consolidated shell beds and sandy limestone. Some of these sand and shell beds near the

surface of the aquifer are of the Quaternary age [*Winner, 1978*]. The lower confined aquifer, Castle Hayne, is composed of medium to coarse grained limestone [*Winner, 1978*]. This aquifer is confined by the Pungo River formation of the early and middle Miocene age, where layers of clay, silty clay, and clayey sand persist [*Lautier, 2001*]. The Pungo River Formation is the highest yielding aquifer in the North Carolina coastal plain [*Lautier, 2009*].

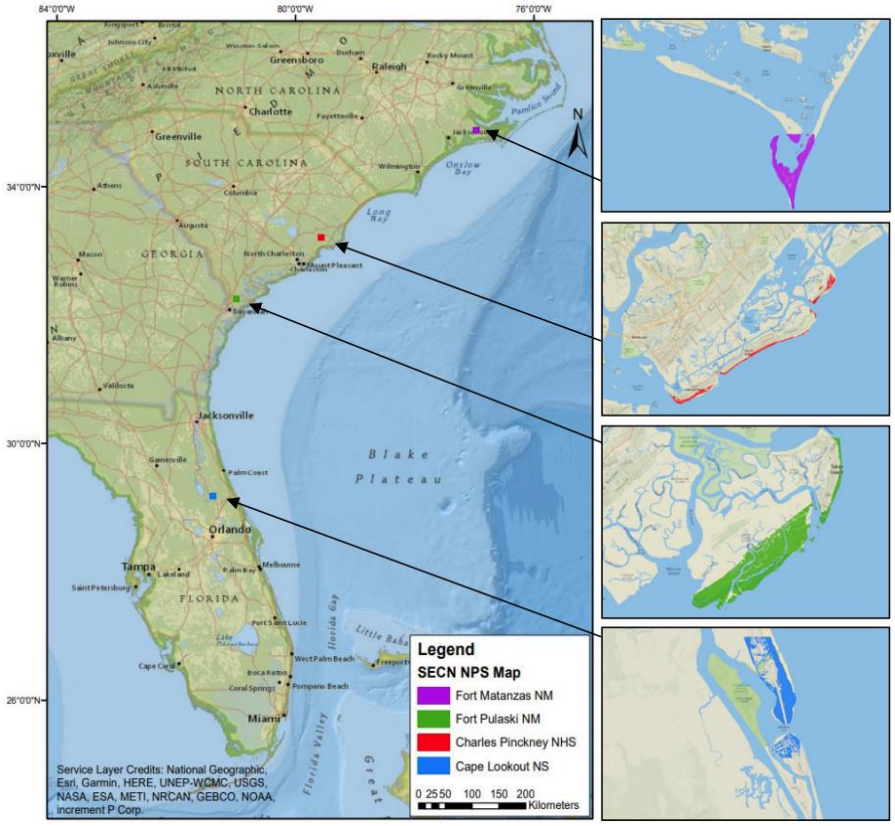

Figure 2-1. GIS-derived map of Fort Matanzas NM, Fort Pulaski NM, Charles Pinckney NHS, and Cape Lookout NS locations.

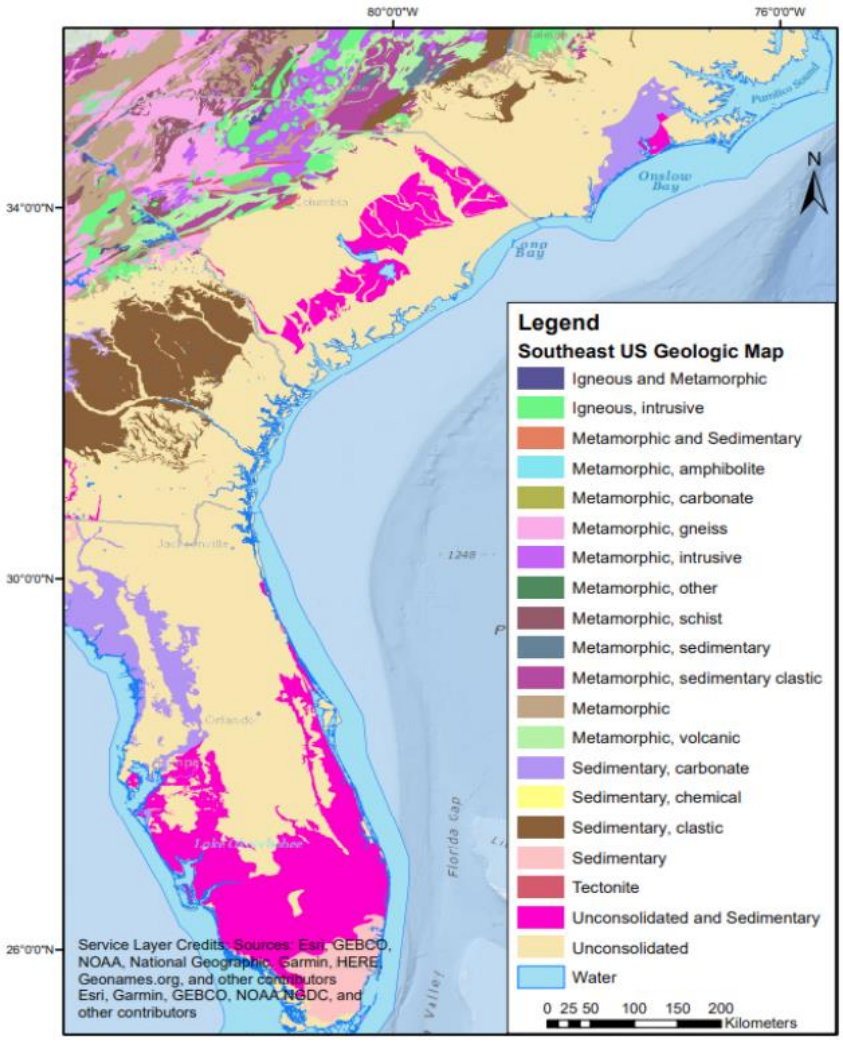

Figure 2-2. Geologic map of southeast US. Data retrieved from the USGS State Geologic Map Compilation geodatabase of the conterminous United States.

2.3. Methodology

The methodology implemented in this study incorporates a series of steps designed to synthesize volumetric, spatial, and temporal changes using LiDAR (Figure 2-3). The LiDAR data acquired were retrieved from the National Oceanic and Atmospheric Administration (NOAA), (https://coast.noaa.gov/dataviewer/#/lidar/search/), in LAS format. The data were collected, categorized, and processed individually for each of the four respective SECN NPS sites. The

processed data was used to create a change analysis both spatially and temporally. Using ENVI LiDAR 5.5, each acquired LiDAR dataset generated point clouds, orthophotos and DEMs (horizontal accuracy: 1-meter, vertical accuracy: 0.196 meters) to produce the base maps. From the production of the temporal LiDAR base maps detailing changes in elevation, the data were then used to provide a volumetric spatial change analysis. The volumetric spatial change analysis was used to detail specific areas where the erosional activity occurred (net loss) and where unconsolidated material was returned to the environment (net gain). Using the spatial analyst tool, the raster calculator calculated the difference from each year to generate a difference map. The difference maps were then edited by the Cut Fill tool to display the volumetric changes that were quantified and measured to visually represent the net gain/net loss of unconsolidated material.

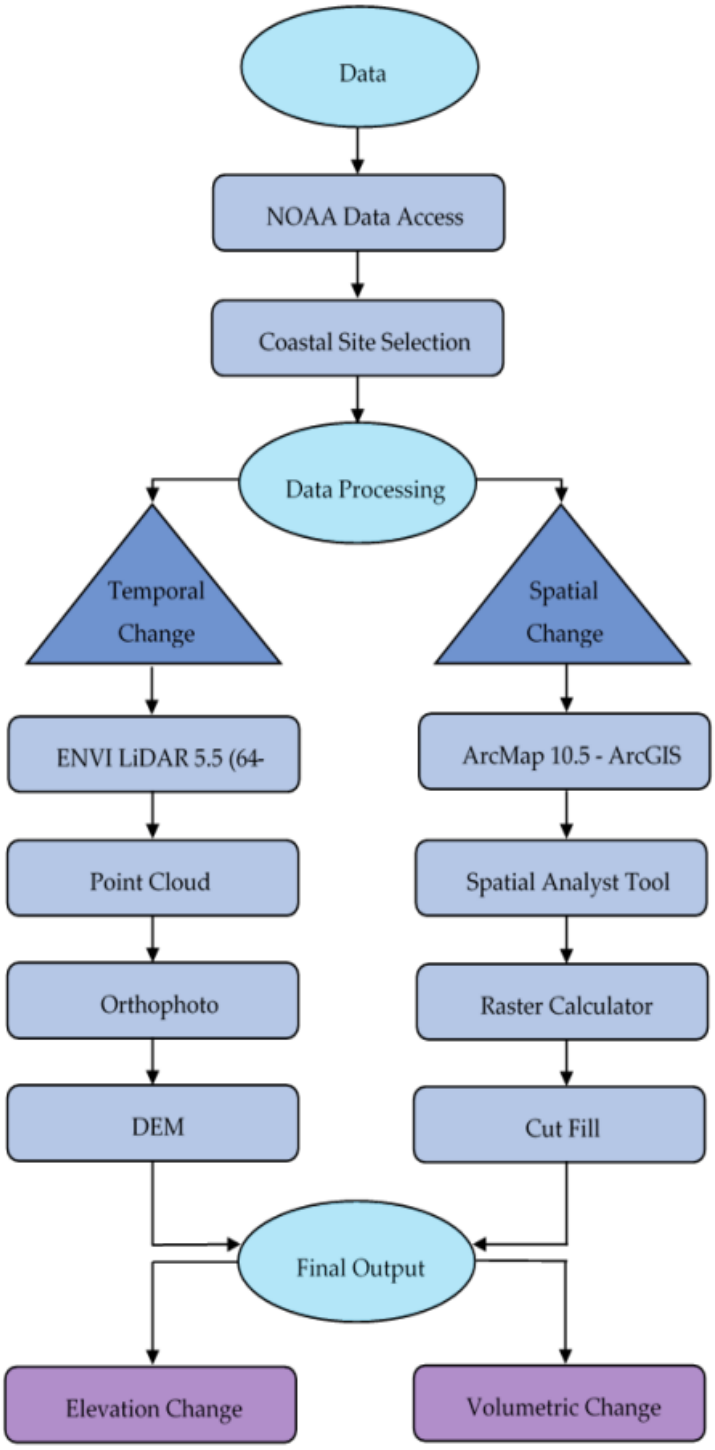

Figure 2-3. Processing flow chart representing data acquisition, processing procedure, and final output of the LiDAR dataset. Each step in this series was used to display the temporal changes over the specified period and the spatiotemporal volumetric changes.

Data Acquisition

Before the LiDAR acquisition, the LiDAR system underwent calibration to verify the operational accuracy and misalignment angles. Boresight calibrations were performed for the LiDAR system at the beginning and end of each flight mission. LiDAR data was processed immediately after the acquisition to verify the coverage had no voids. The GPS/Inertia Measurement Unit (IMU) data was post processed using differential and Kalman filter algorithms to produce the best estimates of unknown variables [*NOAA, 2018*].

The vertical and horizontal accuracy was performed using a standard method to compute the root mean square error (RMSE) based on comparing ground control points and filtered LiDAR data points. Each compiled vertical and horizontal accuracy value met the 95th percentile confidence level requirements recommended by the American Society for Photogrammetry and Remote Sensing (ASPRS) when analyzing elevation generated by LiDAR. The horizontal accuracy quantitative value is 1 meter, and the vertical accuracy quantitative value is 0.196 meters (19.6 cm). The ASPRS guidelines follow the National Digital Elevation Program sections on vertical accuracy testing that follows the Federal Geographic Data Committee and the National Standard for Spatial Data Accuracy [*NOAA, 2018*]. The filtered LiDAR data represented the bare earth elevations from 2006 to 2018 for each NPS site (Table 2-1). The bare earth elevations collected multiple returns x, y, and z data as well as intensity data. This data was then compressed in a LAS binary file format containing the information specific to the LiDAR data (number of returns, intensity value, x, y, z, etc.). The LAS data was projected to input datum NAD83, the projection system was geographic longitude/latitude, and the input units were converted to meters [*NOAA, 2018*]. As a result, the data acquired from NOAA are as follows:

LiDAR-based DEM Temporal Changes

In the acquisition of temporal LiDAR at each of the SECN NPS sites, land cover data were used to represent the topographic features of the coastal southeast US using ArcGIS and ENVI LiDAR. The topographic features detailed the elevation changes that have occurred at each of the sites.

ENVI LiDAR was used to process the geo-referenced LiDAR point cloud data into geographical information system layers that were then produced in output formats for a 3D visual database. ENVI LiDAR created Digital Elevation Models (DEMs) from the Digital Terrain Models (DTMs) to characterize the elevation of the site's topography. Geospatial measurements of the point cloud data were used to provide accuracy of the existing topographic cover. Each point is classified by a value of elevation height to determine its class feature.

ENVI LiDAR used the DTM to create the DEM by including vector data of the natural terrain and linear features. The vector data are composed of regularly spaced raw points and natural features of the observed area. The linear features used are representative of the shape of the bare-earth terrain. The regularly spaced raw points, vector data and linear features are used to augment a DEM providing its distinctive terrain features. To ensure DEM extraction from LiDAR data based on DTMs was accurate, a density map was generated to check the raw point density and coverage of the LiDAR data. Each of the LiDAR datasets had more than the recommended minimum of 5 to 6 points per square meter by L3 Harris Geospatial. Due to the dense raw dataset, ENVI LiDAR identified features for extraction and avoided false readings including overestimations of topographical features. Usage of Variable Sensitivity Algorithm for low density datasets was not performed.

ArcGIS was used to provide the final output of the processed LiDAR point cloud data in a GIS produced map. The base maps were used to create the different maps, which display the differences in elevation over a specified year. These maps detailed the elevation values of the processed LiDAR points acquired from NOAA. The maps provide a geographical representation of the temporal changes that have occurred over time.

Table 2-1. LiDAR data details for each NPS site.

Sites											
Fort Matanzas NM			Fort Pulaski NM			Charles Pinckney NHS			Cape Lookout NS		
Value	**Season**	**Year**	**Value**	**Season**	**Year**	**Value**	**Season**	**Year**	**Value**	**Season**	**Year**
0.30m	Fall	2006	0.30m	Winter	2006	0.20m	Winter	2007	0.30m	Fall	2012
0.20m	Fall	2010	0.24m	Winter	2009	0.20m	Fall	2010	0.10m	Fall	2014
0.22m	Winter	2013	0.20m	Fall	2010	0.23m	Winter	2016	0.23m	Winter	2017
0.20m	Fall	2016	0.23m	Winter	2016	0.20m	Fall	2018	0.20m	Fall	2018
0.20m	Fall	2017	0.10m	Winter	2017	N/A	N/A	N/A	N/A	N/A	N/A

Spatial Change Analysis

The temporal LiDAR base maps provided a volumetric spatial change analysis detailing erosional activity (net loss) and deposition (net gain). To identify the changes occurring spatially, the ArcGIS Cut Fill tool was applied. This tool analyzed topographic features at two different periods to identify the volumetric change by (1) identifying regions of erosional activity and deposition, (2) calculating the volume of sedimentary material, and (3) identifying inundated regions.

The Cut Fill tool displays regions of net loss and net gain from the attribute table of the output raster. Each raster represents a region's volume, which is calculated for each cell, and the area, calculated by the number of cells in each region by the cell size. The volume is greater than zero in regions where the unconsolidated sedimentary material was cut, and less than zero where it was filled. This repeated spatial change analysis identified the erosional and depositional activity that has occurred.

2.4. Results

Each site analyzed in this study displays the temporal changes in elevation and the quantification of spatial volumetric changes of unconsolidated sedimentary material presented in a GIS framework. The LiDAR-based DEM temporal changes display the highest and lowest elevation for each year at each site. Of the temporal change analysis, the spatial changes occurring were displayed volumetrically to identify the deposited material and erosional activity occurring during specific years at each site.

Fort Matanzas NM, Fort Pulaski NM, Charles Pinckney NHS, and Cape Lookout NS are all depicted to display how each site individually changed temporally and spatially during the specified period time (Figures 2-4, 2-5, 2-6, 2-7, 2-8, 2-9, 2-10, 2-11, Tables 2-2, 2-3, 2-4, 2-5). Tables 2-2, 2-3, 2-4, 2-5 present the net loss and net gain of the given total area for each output raster's attribute table of the specified year. These tables detail the percentages of erosional and depositional activity that occurred spatially. The temporal changes were characterized by the acquisition of LiDAR derived DEMs for each location (Figures 2-4, 2-6, 2-8, 2-10). The earliest acquired DEM was selected as the base map to display how elevation changed from the base map's year to each specified year. The spatial change maps were derived from the temporal change maps

to represent the volumetric distribution of erosional activity and deposited unconsolidated sedimentary material (Figures 2-5, 2-7, 2-9, 2-11). These maps display the extent and location of where changes have occurred over the study period. Results show instances of elevation and volumetric changes of sediment though no consistent trend was found.

Fort Matanzas National Monument

LiDAR derived DEMs of Fort Matanzas NM display the elevation changes that have occurred from 2006 to 2017. From 2006 to 2010 the elevation dropped a meter and there was a majority net loss of material occurring (Table 2-2) (Figure 2-4).

From 2006 to 2017, the elevation drops considerably within the middle of Fort Matanzas NM (Figure 2-4). During 2010 to 2017, the areas of the highest elevations, labeled in red, include the areas around the coastline and some of the inner portions of this coastal environment (Figure 2-4). As depicted in the images, the coastline is continuously altered as the elevation changes from year to year. From 2010 to 2013 the coastline is at its highest elevation, while from 2016 to 2017 the coastline continues to decrease. Near the Matanzas Inlet you see a consistent decline in elevation from 2010 to 2017. The eastern coastline displays higher elevation values in comparison to the inlet near Rattlesnake Island.

Table 2-2. Fort Matanzas NM spatial change extent of sedimentary material deposited (net gain) and areas where erosional activity occurred (net loss).

FORT MATANZAS NATIONAL MONUMENT SPATIAL CHANGE ANALYSIS		
	2010	
Total Area (m^2)	59,729	100%
Net Loss	48,497	81%
Net Gain	11,231	19%
	2013	
Total Area (m^2)	104,255	100%
Net Loss	91,590	88%
Net Gain	12,664	12%
	2016	
Total Area (m^2)	102,385	100%
Net Loss	90,863	89%
Net Gain	11,521	11%
	2017	
Total Area (m^2)	100,803	100%
Net Loss	90,279	90%
Net Gain	10,523	10%

The volumetric change of unconsolidated sedimentary material at Fort Matanzas NM displays a net loss from 2010 to 2017. During this time period, the spatial extent of where the erosional activity occurred increased (Table 2-2). In 2010, there was a net loss of 81%, while in 2017, the net loss increased to 90% over the given area. Though much of the material displayed is a net loss, there is also a net gain. Outlined by the red color on the volumetric change maps, the eastern coastline shows where much of the sedimentary material was deposited back into the environment representing a net gain (Figure 2-5). Additionally, there is a net gain of material where tidal inlets are present. According to the spatial change analysis, from 2010 to 2017, there is a decrease in sedimentary material being deposited back into this environment (Table 2-2).

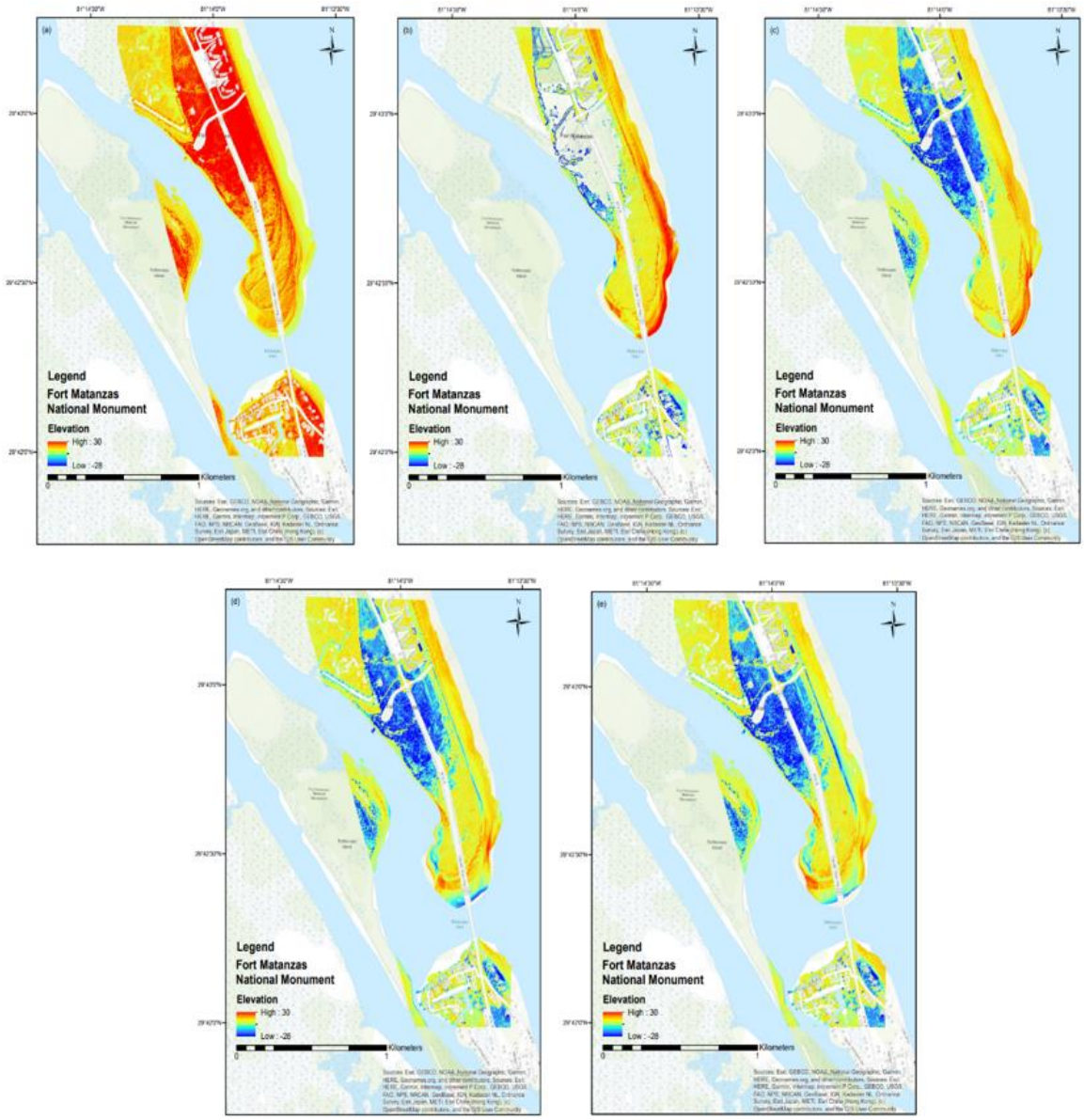

Figure 2-4. LiDAR derived DEM difference maps generating three-dimensional elevation changes of Fort Matanzas NM from 2006 to 2017. Each panel corresponds to the specified year: (a) 2006, (b) 2010, (c) 2013, (d) 2016, and (e) 2017.

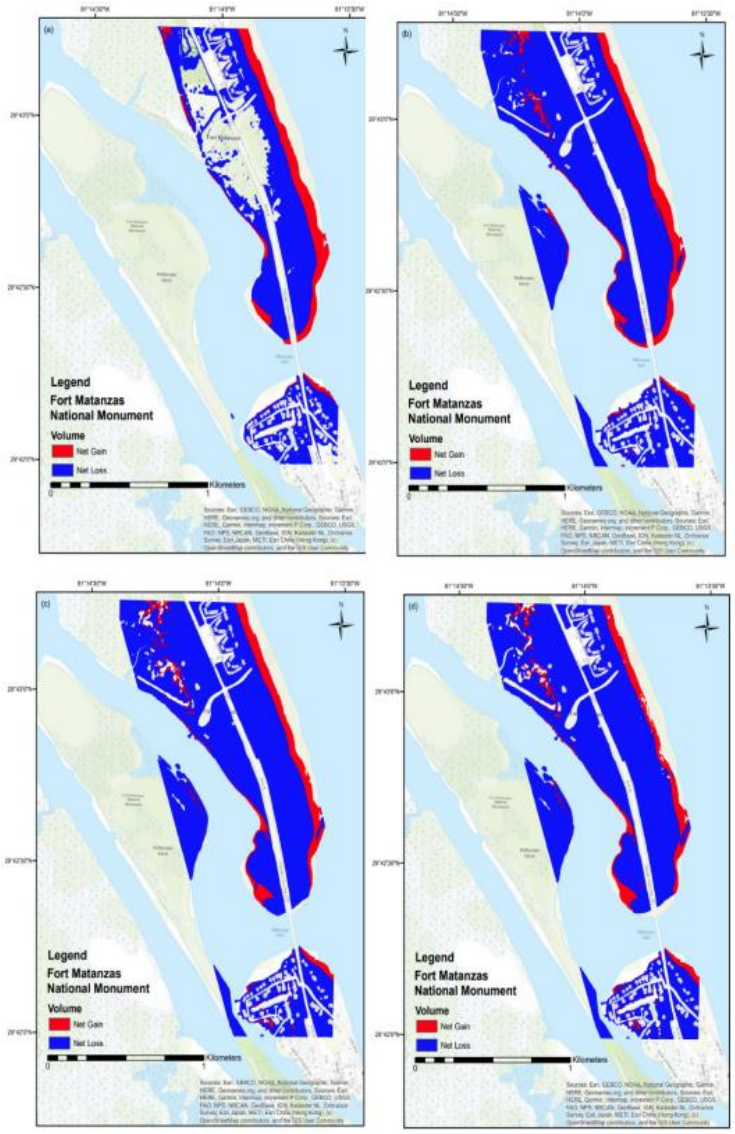

Figure 2-5. Spatial change maps detailing the volumetric distribution changes of both deposited (net gain) and erosional activity (net loss) of unconsolidated sedimentary material at Fort Matanzas NM from 2010 to 2017. Each panel corresponds to the specified year: (a) 2010, (b) 2013, (c) 2016, and (d) 2017.

Fort Pulaski National Monument

From 2006 to 2017, the area near Fort Pulaski NM exhibited varied changes in elevation. The LiDAR derived DEMs of this coastal environment display how the elevation

is fluctuating over a given period of time. From 2009 to 2010, elevation values display an increase towards to southern most region of the site and towards the northeast. In 2016, there is a decrease in elevation in pockets near the southern most region and along the eastern coastline. In 2017, the elevation remains constant (Figure 2-6). The northernmost and southernmost regions exhibited the highest elevation values in Tybee Island and Little Tybee Island, while the center most regions recorded the lowest elevation values (Figure 2-6).

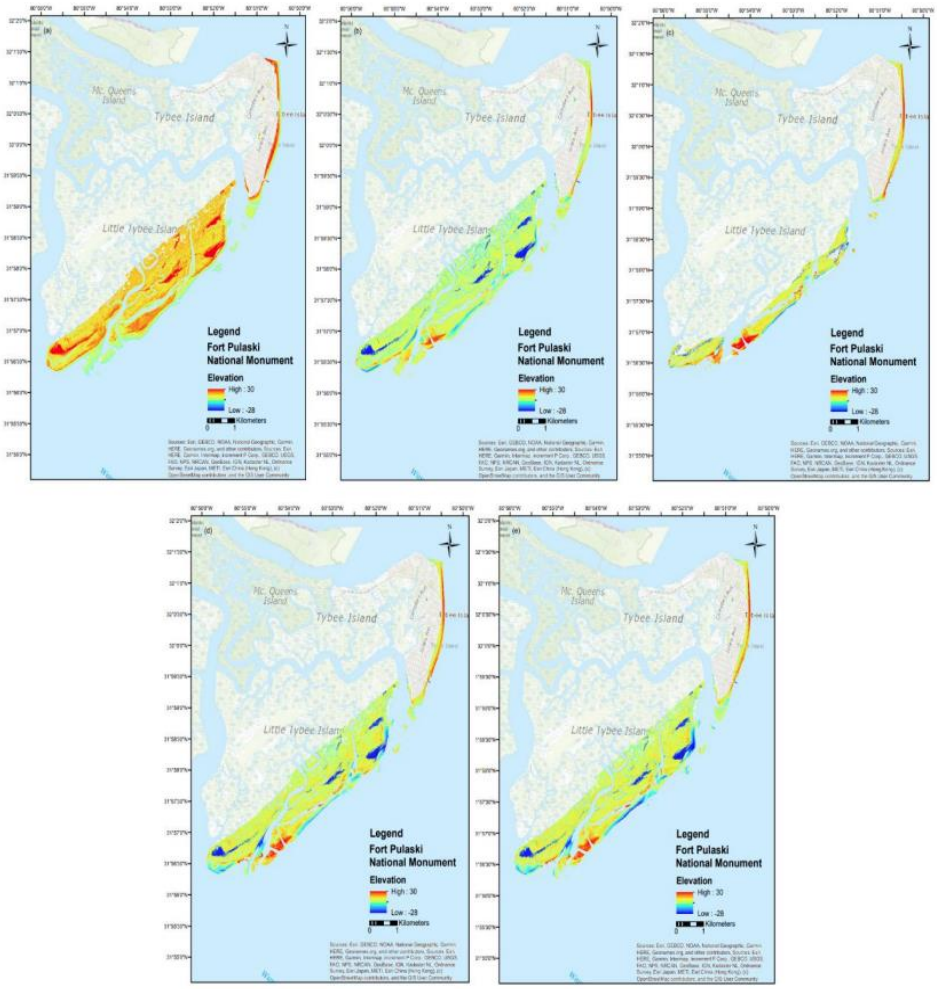

Figure 2-6. LiDAR derived DEM difference maps generating three-dimensional elevation changes of the area near Fort Pulaski NM from 2006 to 2017. Each panel corresponds to the specified year: (a) 2006, (b) 2009, (c) 2010, (d) 2016, and (e) 2017.

The volumetric change maps of this area show an overall net loss of unconsolidated sedimentary material from 2009 to 2017 (Table 2-3). In 2009, there was a net loss of 85% but the erosional activity that occurred from 2009 to 2010 decreased to 75% over the given area (Figure 2-6). In 2016 and 2017, there is an increase in unconsolidated sedimentary material with a net loss of 84% (Figure 2-7). The locations where there is a net gain are similar during this temporal data collection. Material has been deposited back into this environment along the eastern coastline displaying a net gain of material in the tidal inlet between Little Tybee and Tybee Island. The southern region along the coastline displays regions of a net gain where the majority of the unconsolidated sedimentary material is a net loss. The southern region displays a large portion of the material being deposited back into this region (Figure 2-7).

Table 2-3. Spatial change extent of sedimentary material deposited (net gain) and areas where erosional activity occurred (net loss).

SAVANNAH COAST SPATIAL CHANGE ANALYSIS		
	2009	
Total Area (m^2)	1,018,432	100%
Net Loss	870,192	85%
Net Gain	148240	15%
	2010	
Total Area (m^2)	377,555	100%
Net Loss	284,050	75%
Net Gain	93,504	25%
	2016	
Total Area (m^2)	931,287	100%
Net Loss	785,213	84%
Net Gain	146,074	16%
	2017	
Total Area (m^2)	964,442	100%
Net Loss	812,018	84%
Net Gain	152,423	16%

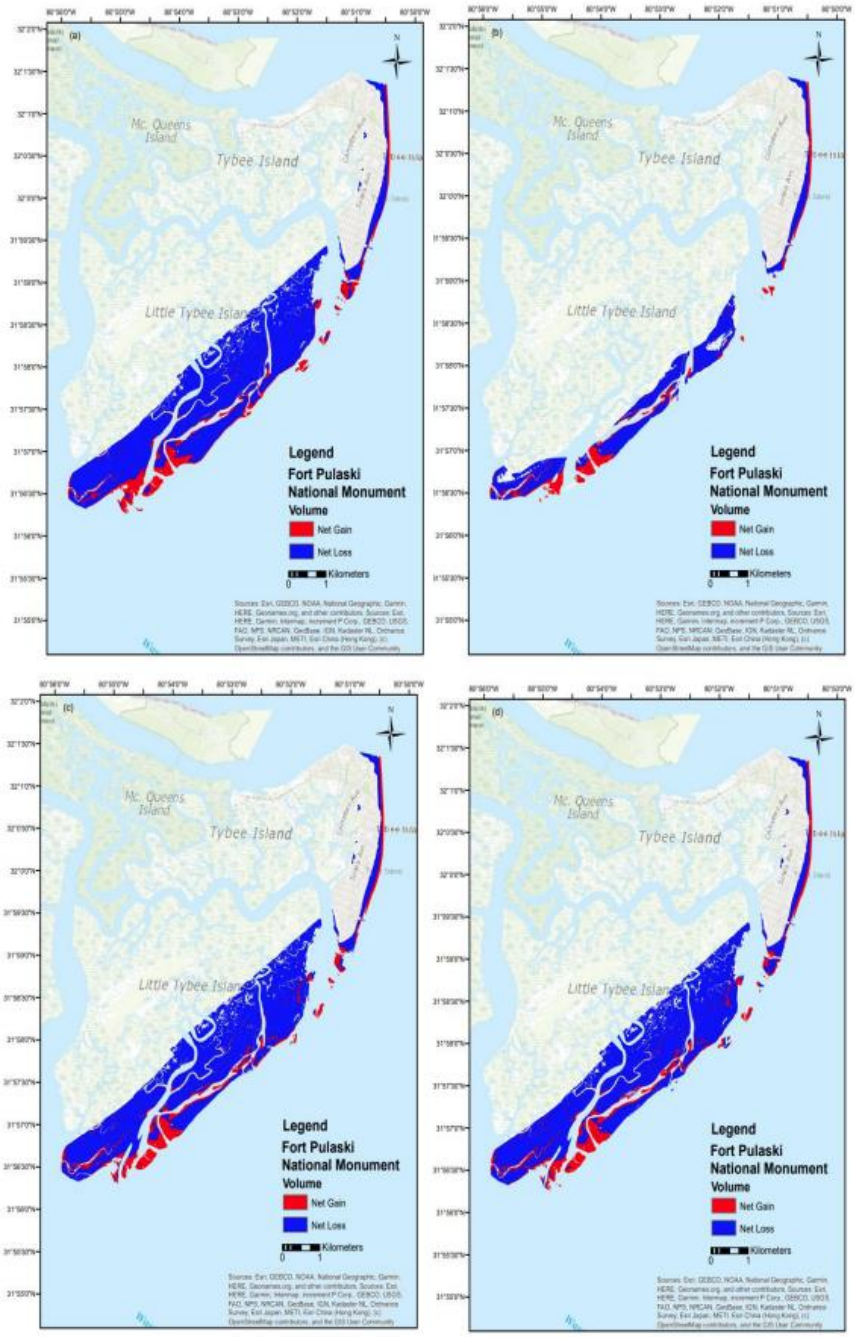

Figure 2-7. Spatial change maps detailing the volumetric distribution changes of both deposited (net gain) and erosional activity (net loss) of unconsolidated sedimentary material at Fort Pulaski NM from 2009 to 2017. Each panel corresponds to the specified year: (a) 2009, (b) 2010, (c) 2016, and (d) 2017.

Charles Pinckney National Historic Site

Areas near Charles Pinckney NHS experienced fluctuating elevations from 2007 to 2016. From 2010 to 2016, the elevation increased along the coastline and within the inter-coastal waterway, while from 2016 to 2018 the elevation decreased along the coastline (Figure 2-8). Along this coastline the elevation changes that occurred were in many of the same areas. From 2010 to 2018 the areas representing the highest elevation remained constant as well as the areas with the lowest elevation. Though much of the area remained constant, the data represent areas that both decreased and increased in elevation along the coastline (Figure 2-8).

The volumetric change maps inform us that even though there is an overall net loss of unconsolidated sedimentary material, the volume fluctuated between 2010 to 2018 (Table 2-4). In 2010, erosional activity occurred at approximately 89%, decreased to 87% in 2016, and then increased to 89% in 2018. This suggests the unconsolidated sedimentary material fluctuated between a net gain and loss (Figure 2-9). The net gain is mostly in the southernmost region, while also visible in the tidal inlets near the Isle of Palms (Figure 2-9).

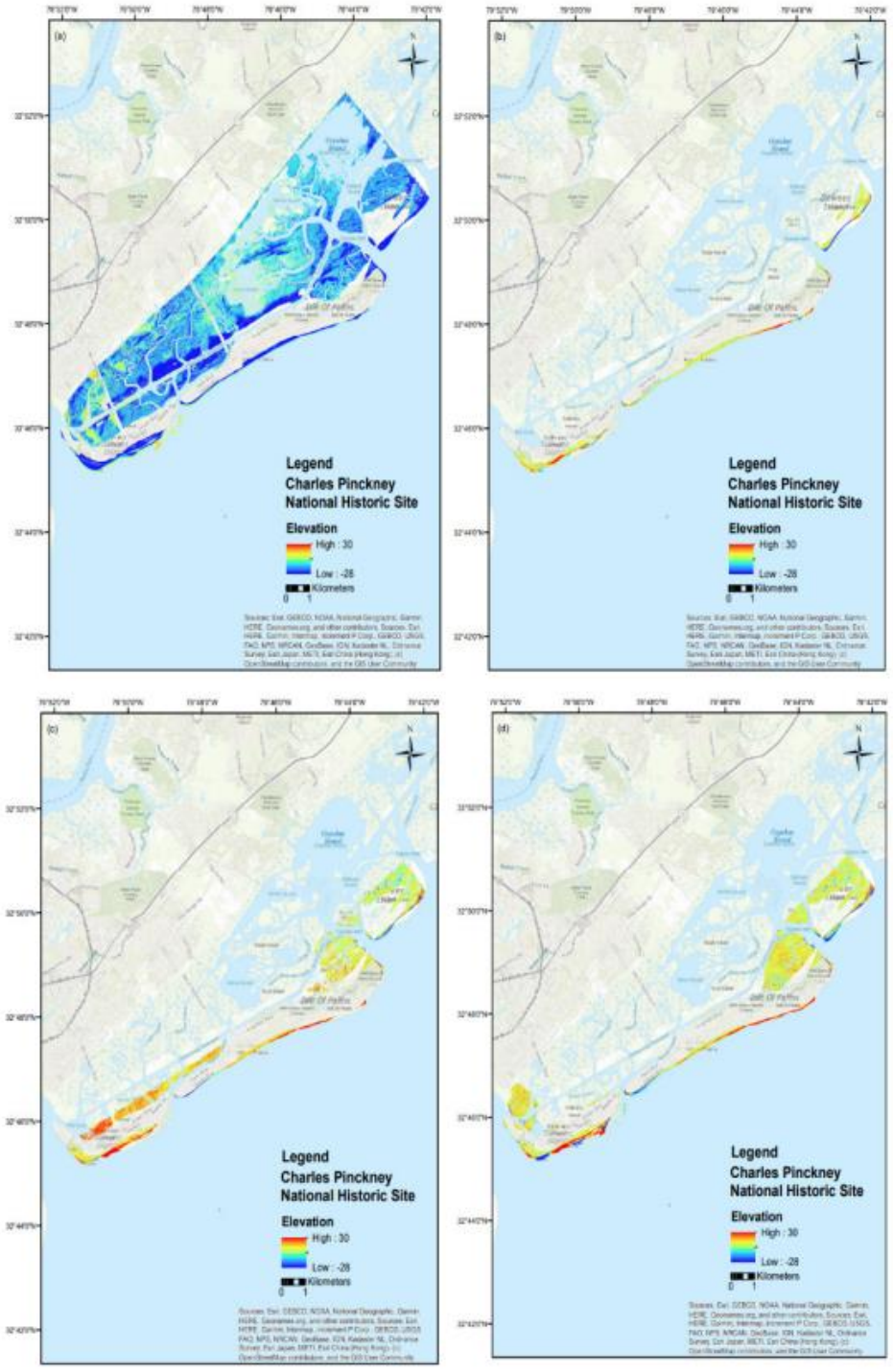

Figure 2-8. LiDAR derived DEM difference maps generating three-dimensional elevation changes of the area near Charles Pinckney NHS from 2007 to 2018. Each panel corresponds to the specified year: (a) 2007, (b) 2010, (c) 2016, and (d) 2018.

Table 2-4. Spatial change extent of sedimentary material deposited (net gain) and areas where erosional activity occurred (net loss).

SULLIVAN'S ISLAND COAST SPATIAL CHANGE ANALYSIS		
	2010	
Total Area (m^2)	242,790	100%
Net Loss	217,203	89%
Net Gain	25,587	11%
	2016	
Total Area (m^2)	672,972	100%
Net Loss	587,863	87%
Net Gain	85,109	13%
	2018	
Total Area (m^2)	846,323	100%
Net Loss	755,791	89%
Net Gain	90,532	11%

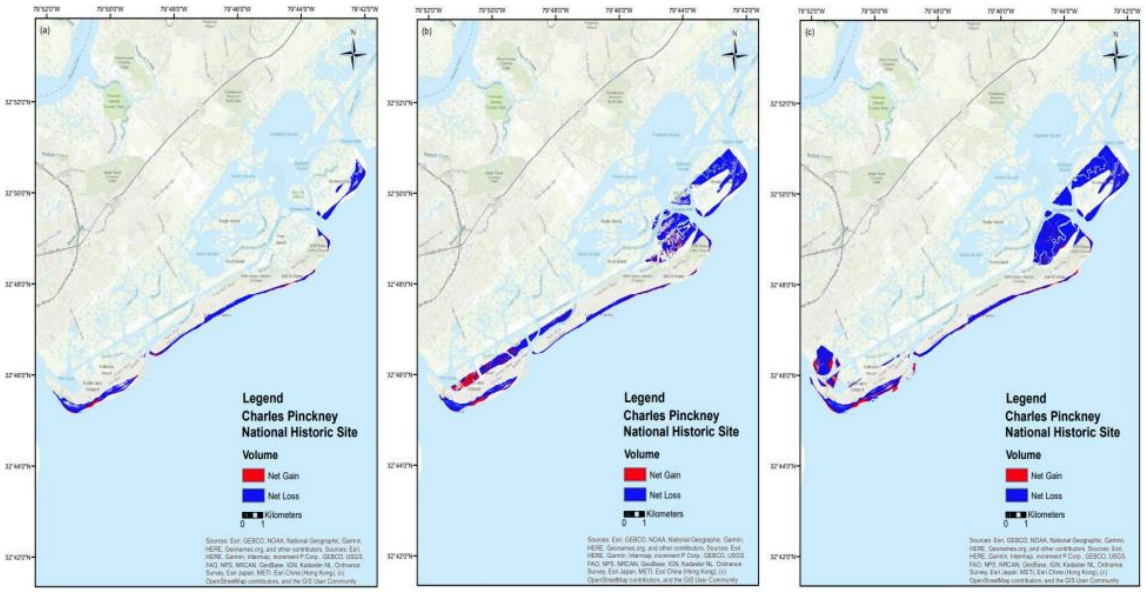

Figure 2-9. Spatial change maps detailing the volumetric distribution changes of both deposited (net gain) and erosional activity (net loss) of unconsolidated sedimentary material at Charles Pinckney NHS from 2010 to 2018. Each panel corresponds to the specified year: (a) 2010, (b) 2016, and (c) 2018.

Cape Lookout National Seashore

The LiDAR derived DEMs of Cape Lookout NS depict a coastal environment that has continuously changed from 2012 to 2018. Elevations decreased from 2012 to 2014, increased from 2014 to 2016, and decreased from 2016 to 2018 (Figure 2-10). The difference maps also display areas along the coastline where the lowest elevation (western coastline) values remain constant along with the areas of higher elevation (eastern coastline) (Figure 2-10). The center of this coastal environment displayed topography that remained nearly consistent.

The volumetric change maps of Cape Lookout NS display a majority net loss of unconsolidated sedimentary material. The spatial change analysis shows how erosional activity decreased from 2014 to 2016, but then increased in 2018 (Table 2-5). This coastal environment displays that most of the erosional activity occurring is around the coastline, while the unconsolidated sedimentary material being deposited back into this environment is more inland (Figure 2-11). Noticeably, there is a drastic change from 2014 to 2016, where the inland portions of this region shifted from a net loss to a net gain (Figure 2-11). This depiction indicates how coastal environments can change over time. The volumetric distribution along the coastline shows a net gain, while the majority is a net loss. Identification of differences in the unconsolidated sedimentary material of this coastline is evident from 2014 to 2018. The inland portions of this region experienced the most change spatially. From 2014 to 2016, there was an increase of 47%

of unconsolidated sedimentary material deposited back into this region, but in 2018 the volumetric distribution changed, resulting in a net loss of 60% (Table 2-5).

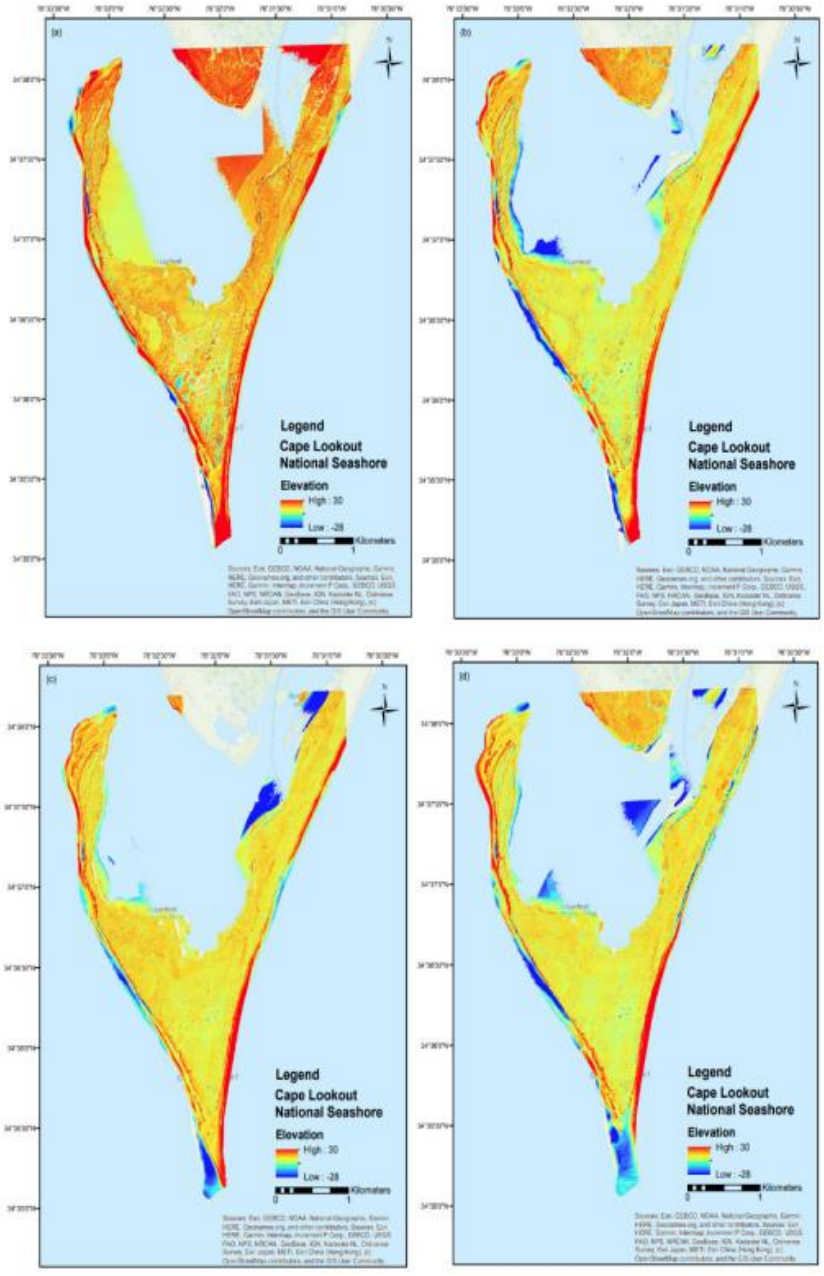

Figure 2-10. LiDAR derived DEM difference maps generating three-dimensional elevation changes of Cape Lookout NS from 2012 to 2018. Each panel corresponds to the specified year: (a) 2012, (b) 2014, (c) 2016, and (d) 2018.

Table 2-5. Cape Lookout NS spatial change extent of sedimentary material deposited (net gain) and areas where erosional activity occurred (net loss).

CAPE LOOKOUT NATIONAL SEASHORE SPATIAL CHANGE ANALYSIS		
	2014	
Total Area (m^2)	594,181	100%
Net Loss	449,294	76%
Net Gain	144,886	24%
	2016	
Total Area (m^2)	638,251	100%
Net Loss	337,810	53%
Net Gain	300,440	47%
	2018	
Total Area (m^2)	605,340	100%
Net Loss	363,235	60%
Net Gain	242,105	40%

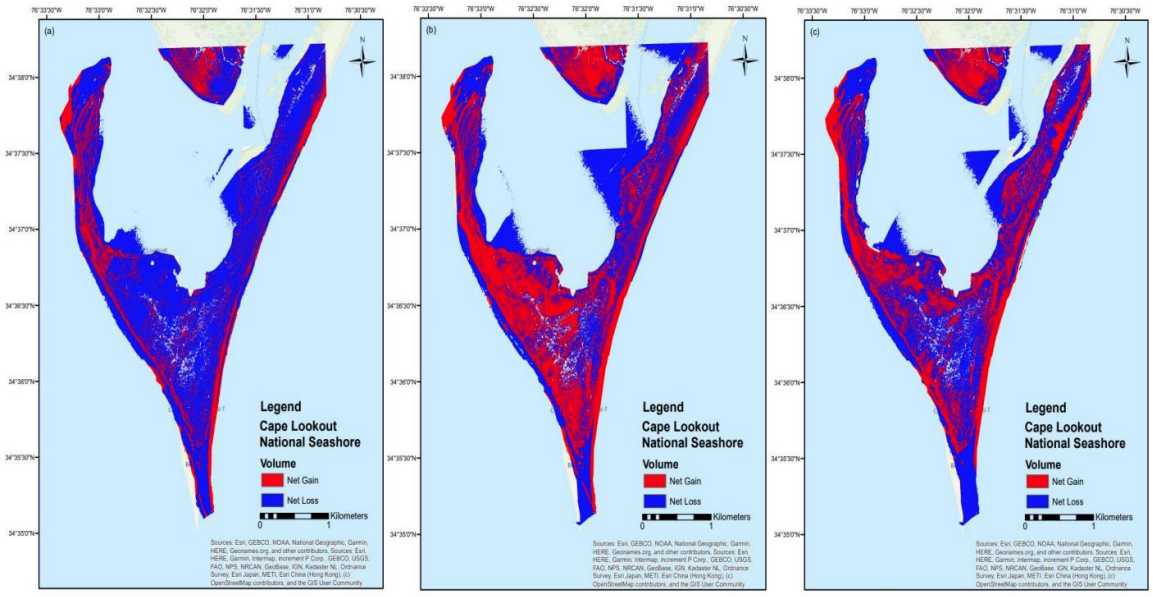

Figure 2-11. Spatial change maps detailing the volumetric changes of both deposited (net gain) and erosional activity (net loss) of unconsolidated sedimentary material at Cape Lookout NS from 2014 to 2018. Each panel corresponds to the specified year: (a) 2014, (b) 2016, and (c) 2018.

2.5 Discussion

The coastal southeastern US has experienced the effects of sea level rise, storm frequency, and changes in climatic regimes that have caused this coastal region to be unstable. The steadily climbing sea level and increases in storm activity and intensity, threaten these coastal zones by making them susceptible to extreme flooding events, inundation, and erosion. These changes were demonstrated in this study using LiDAR at selected SECN NPS sites along the southeastern USA (Figures 2-4, 2-5, 2-6, 2-7, 2-8, 2-9, 2-10, 2-11). Results indicated that though erosional activity was present, there was a net gain of sedimentary material returned within the sites (Figures 2-5, 2-7, 2-9, 2-11). Temporal erosion and longshore transport of sediment are results of the ever-changing climate producing storm surges and relative sea level rise.

Spatially distributed erosion occurred from 2006-2018 at each of the sites. In the data presented, Fort Matanzas NM displayed a steady decline in net gain of unconsolidated sedimentary material, while the areas near Fort Pulaski NM, Charles Pinckney NHS and Cape Lookout NS display how the geomorphology is steadily oscillating between erosional and depositional processes (Tables 2-2, 2-3, 2-4, 2-5). It is clear the sediment budget of each of these coastal sites can change in response to fluctuations of coastal depositional and erosional processes. The erosion that is occurring is in response to relative sea level and changes in climatic regimes, but what is most important is that these causes represent the quasi-cyclic phenomena [*Ranasinghe, 2016; Clarke and Eliot, 1987*]. This phenomenon represents how the unconsolidated sediment distribution and morphodynamic equilibrium change from the influence of fluctuating climatic regimes. These processes are not just exclusive to the coastal southeastern US but are found in other regions as well [*Aubrey, 1983; Vousdoukas et al., 2020*]. As the variability and frequency of these events continue, the impact of longshore transport on these coastal zones is unforeseen.

Throughout the study period, unconsolidated sedimentary material was either eroded or deposited at these SECN NPS sites, however there was an overall net gain. This is most notable along the coastlines (Figures 2-5, 2-7, 2-9, 2-11) where eroded areas had new material deposited causing the overall net gain. There are multiple processes that can cause this coastal morphodynamics, however, longshore sediment transport is evident. Longshore sediment transport depends on many factors, but the direction and speed of the longshore current primarily depend on the direction and height of the wave energy. Though these are highly variably, and the wave energy is dependent on the transport gradient under varying wave conditions, the sites indicate this process is plausible (Figures 2-5, 2-7, 2-9). For example, Cape Lookout NS shows longshore currents have caused repeated oscillation of eroded and deposited sediments under various conditions [*Park and Wells, 2005*]. Previous studies at Cape Lookout NS have shown evidence of longshore sediment transport just as the findings of this study [*Park and Wells, 2005*].

Along the coastal southeastern US, storm surges pose an imminent threat to coastal geomorphology. In 2016 a Category 5 hurricane, Hurricane Matthew, occurred in the coastal southeastern US causing inundation from precipitation in a geologically unstable coastal zone [*Leung and Prasad, 2019*]. Post-Hurricane Matthew LiDAR datasets from this study show the impact of such hurricanes (Figures 2-5, 2-9, 2-11). The amplitude of the storm surge created the abnormal rise of sea level by wind energy. The wind energy produced strong tides and currents causing coastal erosion to increase. Erosional activity and longshore sediment transport events changed the volumetric distribution of unconsolidated sedimentary material of the coastal zone.

These elevation changes demonstrate how change in the land surface can impact the coastal hydrogeologic framework. Coastal recharge and discharge drainage networks can be altered with changes in sedimentary material [*Leung and Prasad, 2019*]. Within this coastal zone there are both

shallow and deep aquifers, thus, each respond differently [*Faulkner, 1970; Clarke et al., 1990; Weems and Edwards, 2001; Campbell, 1996; Aucott, 1996; Aucott, 1988; Lautier, 2001; Winner, 1978; Hoover et al., 2017*]. The shallow aquifers are more responsive to the immediate climatic regimes, while the deeper aquifers have a delayed reaction. However, each aquifer is important as they each contribute to the coastal groundwater system of the coastal southeastern US.

Efficacy of Airborne LiDAR

LiDAR serves as a critical tool in understanding temporal and spatial topographic changes in the coastal southeastern US. LiDAR offers capabilities that allow researchers the opportunity to acquire large-scale elevation and derived topographic data for interpretation. The performance of the 3D laser scanners has advanced the speed and accuracy of assessing geomorphological changes within these coastal zones (Figures 2-4, 2-5, 2-6, 2-7, 2-8, 2-9, 2-10, 2-11). The 3D lasers can take millions of precise measurements by examining the earth's topographical features through volume and elevation [*Woolard and Colby, 2002; Deronde et al., 2008*]. This ability highlights the success and scientific merit of observing the elevation and volumetric changes occurring in this study. The high accuracy and relative surface reflectance to define the topographic features are key in understanding erosional activity and where unconsolidated sediment is being deposited.

The defined topographic features are in part due to LiDAR's capabilities, while also using an appropriate ground truth validation technique to identify coastal changes. Through ENVI LiDAR, point cloud classification was applied to identify each class feature determined by the value of elevation height. These class features provide the capability to extract the necessary data related to various features on the surface. Point cloud classification displays the ability to be an appropriate approach to ground truth validation for the extraction of ground features representative

of the earth's surface. This capability removed all roads, bridges, and buildings to accurately represent each region's surface. This technique will assist in providing accurate resource management to future studies on coastal environments [*Sallenger et al., 2003; Woolard and Colby, 2002; Young and Ashford, 2006; O'Dea et al., 2019; Titus and Richmond, 2001; Hoover et al., 2017; Deronde et al., 2008*].

Although more investigations are needed to understand the geomorphological changes that are occurring temporally and spatially, the remote sensing techniques used are advantageous. (1) Observations and investigations were performed remotely using available public domain datasets. (2) Surface data represented high sample density while not being affected by extreme weather conditions. (3) Data were acquired inaccessible areas with no geometric distortions. (4) The vast datasets provide the opportunity to identify relationships and new insights to better understand these coastal zones. The remote sensing techniques used through the acquisition of temporal LiDAR provided an appropriate representation of the geomorphological changes occurring [*Sallenger et al., 2003; Woolard and Colby, 2002; Young and Ashford, 2006; O'Dea et al., 2019; Gesch, 2009; Elaksher, 2008; Titus and Richmond, 2001*].

Limitations and Applicability

This study provides sound results in distinctively describing the geomorphology of the coastal southeast US, along with some limitations that provide an opportunity for further research. First, the temporal LiDAR datasets aren't collected at the same time. This is important because the time in which the climatic regimes persist per unit area must be accounted for to characterize and understand which processes are occurring in an entire coastal zone. Second, under certain conditions elevation errors can occur while on water surfaces. This can produce a return value that

is unreliable due to the height of the water depth affecting the reflection of the pulses. These errors are corrected by vertical and horizontal accuracy when using a standard method to compute the root mean square error (RMSE). Vertical accuracy is assessed by the fundamental accuracy value calculated at the 95th percentile confidence level as a function of the RMSE. The 95th percentile indicates that 95 percent of the errors in the dataset have absolute values of equal or lesser value, while 5 percent of the errors will be of larger value. Thus, there is approximately a 5 percent error. In suspected inundated areas where there was no return signal, no interpolation was applied. ENVI will interpolate the elevation data for missing data, however, this interpolation can result in false readings. Lastly, access to LiDAR data is limited. The temporal LiDAR data acquired for Fort Matanzas NM and Cape Lookout NS were in the SECN site boundaries, however, data acquired for Fort Pulaski NM and Charles Pinckney NHS were not in the SECN site boundary. The LiDAR data presented represented an area in the vicinity of the Fort Pulaski NM and Charles Pinckney NHS SECN site boundaries. The quality of this study is not only relevant to the advancement of understanding the coastal dynamic response, but it also presents efficient results with limited LiDAR derived datasets over the selected sites [*Woolard and Colby, 2002; Hoover et al., 2017; Deronde et al., 2008*].

2.6. Conclusions

The southeast of the US is composed of numerous SECN NPS sites and each has experienced coastal changes. Outlined in this paper, Fort Matanzas NM, the area near Fort Pulaski NM, the area near Charles Pinckney NHS, and Cape Lookout NS, were analyzed to understand the geomorphologic changes occurring through the acquisition of temporal LiDAR derived datasets. These sites represented a portion of the coastal southeastern US to display the usefulness and versatility of processed LiDAR. Identifying the temporal changes in elevation and quantifying

the spatial volumetric changes of unconsolidated sedimentary material allows for further understanding of the coastal dynamic response of the coastal southeast. This temporal and spatial change analysis displayed the vulnerability of these coastal zones due to elevation changes. In some cases, the elevation changes occur rapidly, but in other cases they occur over extended periods. Fort Matanzas NM displayed a 1-meter decrease in elevation from 2006 to 2017. Also, these elevation changes fluctuate causing these coastal zones to be unstable, presenting the opportunity for continuous change. Fort Matanzas NM elevation increased from 2010 to 2013 but decreased from 2016 to 2017 along the coastline. Fort Pulaski NM elevation increased from 2009 to 2010 and decreased in 2016. Charles Pinckney NHS elevation increased by 1-meter from 2010 to 2016 and decreased by 1-meter between 2016 to 2018. Cape Lookout NS elevation increased from 2012 to 2014, decreased from 2014 to 2016 and decreased from 2016 to 2018 on a magnitude of 2-3 meters. With respect to the coastal sediment budget, the volumetric spatial change of sedimentary material responded in conjunction with the elevation changes, however, the changes were not consistent. In areas in which there was a net gain/net loss of returned sedimentary material, the elevation increased and in areas where there was a net loss/net gain displaying erosional activity, the elevation decreased. Fort Matanzas NM displayed a 7% increase in erosional activity from 2010 to 2013, 1% increase from 2013 to 2016, and a 1% increase from 2016 to 2017. From 2009 to 2010 erosional activity in Fort Pulaski NM decreased by 10% but increased by 9% in 2016. Charles Pinckney NHS erosional activity decreased by 2% from 2010 to 2016 but increased in 2018 by 2%. Cape Lookout NS erosional activity decreased by 23% from 2014 to 2016 but increased in 2018 to 60%. These volumetric changes infer the climatic regimes that are persisting in the southeast US expose these coastal zones to instability. The quasi-cyclic phenomena that are occurring are due to these coastal zones being exposed to fluctuating climate

regimes. As a result, there are different erosional processes and longshore sediment transport affecting the coastal hydrogeological and geomorphological dynamic.

The use of processed LiDAR derived data has furthered the understanding of coastal environments. The ability to use remote sensing techniques has offered the opportunity to identify the changes in geomorphology and its relationship with the climatic regime effects. As technology advances, new tools emerge, and more datasets are produced, the high-resolution data will improve coastal water resources and their applicability in providing sustainability and resiliency of coastal geomorphological change.

References

Aubrey, D.G., 1983. Beach changes on costs with different wave climates. Sandy beaches as ecosystems. pp. 63-85.

Aucott, W.R., Davis, M.E., Speiran, G.K., 1987. Geohydrologic framework for the Coastal Plain aquifers of South Carolina (No. 85-4271).

Aucott, W.R., 1996. Hydrology of the Southeastern Coastal Plain aquifer system in South Carolina and parts of Georgia and North Carolina (No. 1410-E). U.S. Geological Survey. DOI: https://doi.org/10.3133/pp1410E

Aucott, W.R., 1988. The predevelopment groundwater flow system and hydrologic characteristics of the Coastal Plain aquifers of South Carolina (Vol. 86, No. 4347). US Department of the Interior, U.S. Geological Survey.

Bamber, J.L., Oppenheimer, M., Kopp, R.E., et al., 2019. Ice sheet contributions to future sea-level rise from structured expert judgment. Proceedings of the National Academy of Sciences. 116(23), 11195- 11200. DOI: https://doi.org/10.1073/pnas.1817205116

Barnhardt, W., Denny, J., Baldwin, W., et al., 2007. Geologic framework of the Long Bay inner shelf: implications for coastal evolution in South Carolina. Coastal Sediments. 2151-2160. DOI: https://doi.org/10.1061/40926(239)169

Brock, J.C., Purkis, S.J., 2009. The emerging role of lidar remote sensing in coastal research and resource management. Journal of Coastal Research. (10053), 1-5. DOI: https://doi.org/10.2112/SI53-001.1

Campbell, B.G., 1996. Geology, hydrogeology, and potential of intrinsic bioremediation at the National Park Service Dockside II site and adjacent areas, Charleston, South Carolina, 1993-94 (Vol. 96, No. 4170). US Geological Survey.

Campbell, K.M., Rupert, F.R., Arthur, J.D., et al., 2001. Geologic map of the state of Florida. Tallahassee, FL: Florida Geological Survey.

Carson, W.W., Anderson, H.E., Reutebuch, S.E., et al., 2004. May. LiDAR applications in forestry – An overview. Proceedings of the American Society of Photogrammetry and Remote Sensing Annual Conference (pp. 1-9) 04-1-2-02_04_1_2_02_deliverable_06.pdf (firescience.gov).

Church, J.A., Hunter, J.R., McInnes, K.L., et al., 2006. Sea-level rise around the Australian coastline and the changing frequency of extreme sea-level events. Australian Meteorological Magazine. 55(4), 253-260.

Clarke, D.J., Eliot, I.G., 1987. Groundwater level changes in a coastal dune, sea-level fluctuations and shoreline movement on a sandy beach. Marine Geology. 77(3-4), 319-326. DOI: https://doi.org/10.1016/0025-3227(87)90120-4

Clarke, D.J., Eliot, I.G., 1987. Groundwater level changes in a coastal dune, sea-level fluctuations and shoreline movement on a sandy beach. Marine Geology. 77(3-4), 319-326.

Clarke, J.S., Hacke, C.M., Peck, M.F., 1990. Geology and ground water resources of the coastal area of Georgia. Bulletin (USA).

Davey, C.A., Redmond, K.T., Simeral, D.B., 2007. Weather and Climate Inventory, National Park Service, Southeast Coast Network. Natural Resource Technical Report NPS/SECN/NRTR- 2007/010. National Park Service, Fort Collins, Colorado.

Deronde, B., Houthuys, R., Henriet, J.P., et al., 2008. Monitoring of the sediment dynamics along a sandy shoreline by means of airborne hyperspectral remote sensing and LiDAR: a case study in Belgium. Earth Surface Processes and Landforms: The Journal of the British Geomorphological Research Group. 33(2), 280-294. DOI: https://doi.org/10.1002/esp.154

Desmet, K., Kopp, R.E., Kulp, S.A., et al., 2018. Evaluating the economic cost of coastal flooding (No. w24918). National Bureau of Economic Research. DOI: https://doi.org/10.3386/w24918

Elaksher, A., 2008. Fusion of hyperspectral images and lidar-based dems for coastal mapping. Optics and Lasers in Engineering. 46(7), 493-498. DOI: https://doi.org/10.1016/j.optlaseng.2008.01.012

Faulkner, G.L., 1970. Geohydrology of the Cross-Florida Barge Canal area with special reference to the Ocala vicinity. Diane Publishing.

Gesch, D.B., 2009. Analysis of lidar elevation data for improved identification and delineation of lands vulnerable to sea-level rise. Journal of Coastal Research. 53, 49-58. DOI: https://doi.org/10.2112/SI53-006.1

Gornitz, V.M., Daniels, R.C., White, T.W., et al., 1994. The development of a coastal risk assessment database: vulnerability to sea level rise in the U.S. Southwest. Journal of Coastal Research Special Issue. 12, 327-338. http://www.jstor.org/stable/25735608.

Graham, J., 2009. Geologic resources inventory scoping summary Fort Matanzas National Monument, Florida. Geologic resources Division National Park Service U.S. Department of the Interior. 1-9.

Gutierrez, B.T., Plant, N.G., Thieler, E.R., 2011. A Bayesian network to predict coastal vulnerability to sea level rise. Journal of Geophysical Research: Earth Surface. 116(F2). DOI: https://doi.org/10.1029/2010JF001891

Hauer, M.E., Evans, J.M., Mishra, D.R., 2016. Millions projected to be at risk from sea-level rise in the continental United States. Nature Climate Change. 6(7), 691-695. DOI: https://doi.org/10.1038/nclimate2961

Heron, S.D., Robinson, G.D., Johnson, H.S., Jr., 1965. Clays and opal-bearing claystones of the South Carolina Coastal Plain (No. 31). State Department Board.

Hoover, D.J., Odigie, K.O., Swarzenski, P.W., et al., 2017. Sea-level rise and coastal groundwater inundation and shoaling at select sites in California, USA. Journal of Hydrology: Regional Studies. 11, 234- 249. DOI: https://doi.org/10.1016/j.ejrh.2015.12.055

Huddleston, P.F., 1988. A revision of the lithostratigraphic units of the Coastal Plain of Georgia: The Miocene through Holocene. Georgia Geological Survey, Bulletin. 105, 1-152. B-104.pdf (georgia.gov).

Ingram, K., Dow, K., Carter, L., et al., 2013. Climate of the southeast United States: Variability, change, impacts, and vulnerability. Washington DC; Island Press/Center for Resource Economics.

Klein, R.J.T., Nicholls, R.J., 1999. Assessment of coastal vulnerability to climate change. Ambio. pp. 182-187. https://www.jstor.org/stable/4314873.

Lautier, J.C., 2001. Hydrogeologic framework and groundwater conditions in the North Carolina Central Coastal Plain. North Carolina Department of Environment and Natural Resources Division of Water Resources.

Lautier, J.C., 2009. Hydrogeologic framework and groundwater conditions in the North Carolina East Central Coastal Plain. North Carolina Department of Environment and Natural Resources Division of Water Resources.

Leatherman, S.P., 1984. Coastal geomorphic response to sea level rise: Galveston Bay, Texas. Barth and Titus (eds). Coastal Zone. 151-178.

Leece, S.A., Pease, P.P., Gares, P.A., et al., 2006. Seasonal controls on sediment delivery

in a small coastal plain watershed, North Carolina, USA. Geomorphology. 73 (3-4), 246-260. DOI: https://doi.org/10.1016/j.geomorph.2005.05.017

Leung, L.R., Prasad, R. 2019. Potential impacts of accelerated climate change: Third Annual Report of Work (No. PNNL-27452-Rev. 1). Pacific Northwest National Lab. (PNNL), Richland, WA United States. DOI: https://doi.org/10.2172/1524249

Lindsey, R., 2019. Climate Change: Global Sea Level. National oceanic and atmospheric administration (NOAA), National Ocean Service, Silver Spring. https://www.climate.gov/news-features/understanding-climate/climate-change-global-sea-level (Accessed on 18 January 2020).

Markewich, H.W., Pavich, M.J., Buell, G.R., 1990. Contrasting soils and landscapes of the Piedmont and Coastal Plain, eastern United States. Geomorphology. 3(3-4), 417-447. DOI: https://doi.org/10.1016/0169-555X(90)90015-I

Morton, R.A., 2003. An overview of coastal land loss: With emphasis on the southeastern United States. United States (p. 28). US Geological Survey, Center for Coastal and Watershed Studies. https://citeseerx.ist.psu.edu/viewdoc/download?-doi=10.1.1.730.5008&rep=rep1&type=pdf.

Morton, R.A., Miller, T.L., 2005. National assessment of shoreline change: Part 2, Historical shoreline change and associated land loss along the U.S. Southeast Atlantic coast. U.S. Geological Survey. Open-File Report. 1401, 1-40. DOI: https://doi.org/10.3133/ofr20051401

Nicholls, R.J., Wong, P.P., Burkett, V., et al., 2007. Coastal systems and low-lying areas. https://ro.uow. edu.au/scipapers/. 164, 315-356.

NOAA: Data Access Viewer. n.d. National Oceanic and Atmospheric Administration

(NOAA), NOAA Office of Coastal Management. https://coast.noaa.gov/dataviewer/#/lidar/search/ (Accessed on 3 May 2018).

O'Dea, A., Brodie, K.L., Hartzell, P., 2019. Continuous coastal monitoring with an automated terrestrial lidar scanner. Journal of Marine Science and Engineering. 7(2), 37. DOI: https://doi.org/10.3390/jmse7020037

Park, J.Y., Wells, J.T., 2005. Longshore transport at Cape Lookout, North Carolina: shoal evolution and the regional sediment budget. Journal of Coastal Research. 21(1), 1-17. DOI: https://doi.org/10.2112/02051.1

Philips, J.D., Wyrick, M., Robbins, J.G., et al., 1993. Accelerated erosion on the North Carolina coastal plain. Physical Geography. 14(2), 114-130. DOI: https://doi.org/10.1080/02723646.1993.10642471

Phillips, J.D., 1997. A short history of a flat place, three centuries of geomorphic change in the Croatan. Annals of the Association of American Geographers. 87(2), 197-216. DOI: https://doi.org/10.1111/0004-5608.872050

Ranasinghe, R., 2016. Assessing climate change impacts on open sandy coasts: A review. EarthScience Reviews.160, 320-332. DOI: https://doi.org/10.1016/j.earscirev.2016.07.011

Sallenger, A.H., Jr., Krabill, W.B., Swift, R.N., et al., 2003. Evaluation of airborne topographic lidar for quantifying beach changes. Journal of Coastal Research. 125-133. https://www.jstor.org/stable/4299152.

Sloan, E., 1979. Catalogue of the mineral localities of South Carolina. South Carolina Geological Survey.

Tibbals, C.H., 1990. Hydrology of the Floridan aquifer system in east-central Florida. U.S. Geological Survey Professional Paper; (USA).

Titus, J.G., Richmond, C., 2001. Maps of lands vulnerable to sea level rise: modeled elevations along the US Atlantic and Gulf coasts. Climate Research. 18(3), 1-24. DOI: https://doi.org/10.3354/cr018205

Veatch, O., Stephenson, L.W., 1911. Preliminary report on the geology of the Coastal Plain of Georgia (No. 26). Foote & Davies Company.

Von Holle, B., Irish, J.L., Spivy, A., et al., 2019. Effects of future sea level rise on coastal habitat. Journal of Wildlife Management. 83(3), 694-704. DOI: https://doi.org/10.1002/jwmg.21633

Vousdoukas, M.I., Ranasinghe, R., Mentaschi, L., et al., 2020. Sandy coastlines under threat of erosion. Nature Climate Change. 10(3), 260-263. DOI: https://doi.org/10.1038/s41558-020-0697-0

Warner, J.C., Armstrong, B., Sylvester, C.S., et al., 2012. Storm-induced inner-continental shelf circulation and sediment transport: Long Bay, South Carolina. Continental Shelf Research. 42, 51-63. DOI: https://doi.org/10.1016/j.csr.2012.05.001

Winner, M.D., 1978. Ground-water resources of the Cape Lookout National Seashore, North Carolina (No. 78-52) U.S. Geological Survey, Raleigh, North Carolina. 78-52, 1-59.

Weems, R.E., Edwards, L.E., 2001. Geology of Oligocene, Miocene and Younger deposits in the coastal area of Georgia (Vol. 131). Department of Natural Resources, Environmental Protection Division, Georgia Geologic Survey.

Woolard, J.W., Colby, J.D., 2002. Spatial characterization, resolution, and volumetric change of coastal dunes using airborne LIDAR: Cape Hatteras, North Carolina. Geomorphology. 48(1-3), 269-287. DOI: https://doi.org/10.1016/S0169-555X(02)00185-X

Wu, S.Y., Yarnal, B., Fisher, A., 2002. Vulnerability of coastal communities to sea-level rise: A case study of Cape May county, New Jersey, USA. Climate Research. 22(3), 255-270.

Young, A.P., Ashford, S.A., 2006. Application of airborne lidar for seacliff volumetric change and beach-sediment budget contributions. Journal of Coastal Research. 22(2), 307-318. DOI: https://doi.org/10.2112/05-0548.1

CHAPTER 3

EVALUATION AND ANALYSIS OF REMOTE SENSING-BASED APPROACH FOR SALT MARSH MONITORING[2]

[2] Richards, D. F., IV; Milewski, A.M.; Becker, S.; Donaldson, Y.; Davidson, L.J.; Zowam, F.J.; Mrazek, J.; Durham, M. *Remote Sens.* 2024, 16, 2. https://doi.org/10.3390/rs16010002. Reprinted here with permission of the publisher.

Abstract

In the United States (US), salt marshes are especially vulnerable to the effects of projected sea level rise, increased storm frequency, and climatic changes. Sentinel-2 data offer the opportunity to observe the land surface at high spatial resolutions (10 m). The Sentinel-2 data, encompassing Cumberland Island National Seashore, Fort Pulaski National Monument, and Canaveral National Seashore, were analyzed to identify temporal changes in salt marsh presence from 2016 to 2020. ENVI-derived unsupervised and supervised classification algorithms were applied to determine the most appropriate procedure to measure distant areas of salt marsh increases and decreases. The Normalized Difference Vegetation Index (NDVI) was applied to describe the varied vegetation biomass spatially. The results from this approach indicate that the ENVI-derived maximum likelihood classification provides a statistical distribution and calculation of the probability (>90%) that the given pixels represented both water and salt marsh environments. The salt marshes captured by the maximum likelihood classification indicated an overall decrease in salt marsh area presence. The NDVI results displayed how the varied vegetation biomass was analogous to the occurrence of salt marsh changes. Areas representing the lowest NDVI values (−0.1 to 0.1) corresponded to bare soil areas where a salt marsh decrease was detected.

3.1. Introduction

Coastal salt marshes are some of the most vulnerable and threatened natural ecosystems [*Barbier et al., 2011; Crosby et al., 2016; Simas et al., 2001*]. These ecosystems serve as wetlands in the upper coastal intertidal zone between the upland coastal plain and aquatic brackish waters, helping to control ecosystem function and structure. In this transition zone, salt marshes experience the impacts of alternating high and low tides, causing salt marsh diebacks following extreme precipitation and flooding events [*Stagg et al., 2021; Alber et al., 2008; Orson et al., 1985*]. As these salt marshes evolve, changes in channelization occur, contributing to the hydrologic dynamic [*Schwarz et al., 2022; Mariotti and Canestrelli, 2017*]. Salt marsh migration alters hydrologic processes, which are part of a multidimensional hydrogeological framework [*Guimond and Tamborski, 2021]*. In addition, these events have made salt marshes highly susceptible to geomorphological changes that cause erosional effects and subsidence in response to an increased sea level rise [*Craft et al., 1993*]. As the climatic regime effects serve as a prominent factor in altering these ecosystems, increased anthropogenic activity impacts these systems tangentially [*Halpern et al., 2008; Hartig et al., 2002; Kennish, 2001*]. The South Atlantic salt marshes of the United States (US) are representative of some of the most vulnerable salt marshes globally. Spanning the coasts of North Carolina (NC), South Carolina (SC), Georgia (GA), and Florida (FL), approximately 1 million acres (404,686 hectares (ha)) of salt marshes are threatened by climate change and the human-induced impact that degrades salt marsh environments [*South Atlantic Salt Marsh Initiative, 2023*].

Globally, salt marshes are decreasing, with a loss of approximately 25% to 50% of their vegetative cover [*Crooks et al., 2011; Duarte et al., 2008; Mcowen et al., 2017*]. Over the past 300 years, global salt marshes have declined in area by 87%, and they have declined 54% since 1900

[*IPEBS, 2018*]. A recent study suggested that approximately 561 square miles (1453 square kilometers) of salt marshes have been removed over the past 20 years worldwide [*Campbell et al., 2022*]. By 2060, the National Oceanic and Atmospheric Administration (NOAA) estimates that 14% to 34% of existing South Atlantic salt marshes could be lost [*Fretwell et al., 2021*]. These studies have shown how vital Spartina salt marshes are, and due to their increased vulnerability, proper mitigation is imperative to provide natural coastal resource management. Traditionally, salt marshes have been analyzed through field-based techniques; however, due to limited access to some areas, the use of remote sensing has been implemented [*Campbell and Wang, 2019; DiGiacomo et al., 2020*]. Remote sensing techniques offer the opportunity to monitor short- and long-term landscape changes under high spatial resolutions to provide mapping accuracy. Specifically, salt marsh environments have been analyzed using data collected from various satellites to distinctively characterize how they have changed over time [*Roughgarden et al., 1991; Belluco et al., 2006; Silvestri et al., 2003; Farris et al., 2019; Zhang et al., 1997*].

The development of salt marsh monitoring has evolved due to the increase in changes to the ecomorphodynamic response due to climate change [*Fagherazzi et al., 2004; Silvestri and Marani, 2004; Day et al., 2008*]. Coastal salt marshes are experiencing extreme temperatures, changes in storm frequency and intensity, sediment redistribution, changes in nutrient inputs, and the oscillation of high and low tides [*Scavia et al., 2002; Kirwan and Mudd, 2012; Schuerch et al., 2013; Mwamba and Torres, 2002; Valiela et al., 1978; Sanderson et al., 2000*]. These processes consequently impact salt marsh growth and resilience as well as the ability to provide the necessary barrier for aquatic life and resources. When this occurs, the geomorphic characterization of these regions is altered, causing changes to the hydrologic/hydrogeologic interface [*Sanderson et al., 2000; Tempest et al., 2015; Hughes et al., 2012; Wilson et al., 2015*].

Modeling and field-based techniques have been used and have been shown to be useful in understanding vegetative changes [*Byrd and Kelly, 2006; Giri et al., 2011; Vo et al., 2013*]. Field-based techniques have provided valuable data; however, the collection of data has become more difficult in densely vegetated areas, and as such, the use of remote sensing based tools has been introduced [*Byrd and Kelly, 2006; Giri et al., 2011; Vo et al., 2013*]. Remote sensing-based salt marsh monitoring has become a catalyst in providing long-term datasets to assess the variability and trends occurring in salt marshes. Through satellite observations, imagery products provide multi-temporal datasets for salt marsh monitoring. Sentinel datasets provide high spatial resolutions with efficient temporal sampling to identify rapid changes [*Berger et al., 2012*]. Unmanned aerial vehicles (UAVs) have been used to measure the influence of morphological changes on salt marshes [Dale et al., 2020]. Furthermore, large-scale computing using Google Earth, a cloud-based platform, has made it easy to access large geospatial datasets in a suitable fashion [*Gorelick et al., 2017; Campbell and Wang, 2020*]. As current research and monitoring of salt marshes continue to progress, challenges remain. Can coupled-based classification schemes identify small-scale changes? Can validation techniques be implemented to increase accuracy? How can coupled-based classification scheme approaches improve accuracy? As these questions persist, the instituted approach aims to provide solutions to these questions. The ability to use field-based data and manually selected ROIs under supervised classification schemes provides a nuanced approach to better interpret salt marsh changes; thus, the improvement of classification techniques is still needed [*Yeo et al., 2020*]. Here, we explored methods to identify and quantify how salt marshes are changing along the southeastern coast of the US and how they can provide valuable data for coastal natural resource management.

Field-based and remote sensing techniques are often used, but not always in unison. The integration of both techniques allows for a better understanding of the changes occurring in these ecosystems. In this study, we evaluated and applied a remote sensing-based modeling approach in conjunction with field-based data to determine vegetative cover changes in salt marshes located in the National Park Service (NPS) areas along the US South Atlantic coastline. The vegetative cover changes detailed areas of salt marsh increase and/or decrease between two specified time periods. In addition, we spatially characterized the vegetative biomass by identifying the vegetation density and relative growth. From this analysis, this study outlined the classification algorithms that are most appropriate for mapping salt marshes. Thus, the purpose of this paper was to evaluate the usefulness of the classification schemes, determine the best classification method, and demonstrate classifications representative of the southeast US. This monitoring approach can be implemented to improve salt marsh management as well as inform natural resource conservation management on how to better protect them.

3.2. Study Area

The NPS areas along the South Atlantic coastline included in this study were Fort Pulaski National Monument (NM) in Savannah, GA; Cumberland Island National Seashore (NS) in Camden County, GA; and Canaveral National Seashore (NS) in Titusville, FL (Figure 3-1). Each of these sites was selected due to the high proportion of marsh land in the area. Cumberland Island NS is representative of the largest and southernmost barrier island along the South Atlantic, where the NPS estimates that there are 9341 acres (3780 ha) of salt marsh [*McManamay, 2017*]. At Fort Pulaski NM, the NPS estimates that approximately 90% of the monument is classified as a wetland, including over 4800 acres (1942 ha) of salt marsh [*McManamay et al., 2013*]. The NPS categorizes

Canaveral National Seashore as a barrier island where the salt marshes cover approximately 4400 acres (1781 ha) of the seashore [*Cotton et al., 2020*].

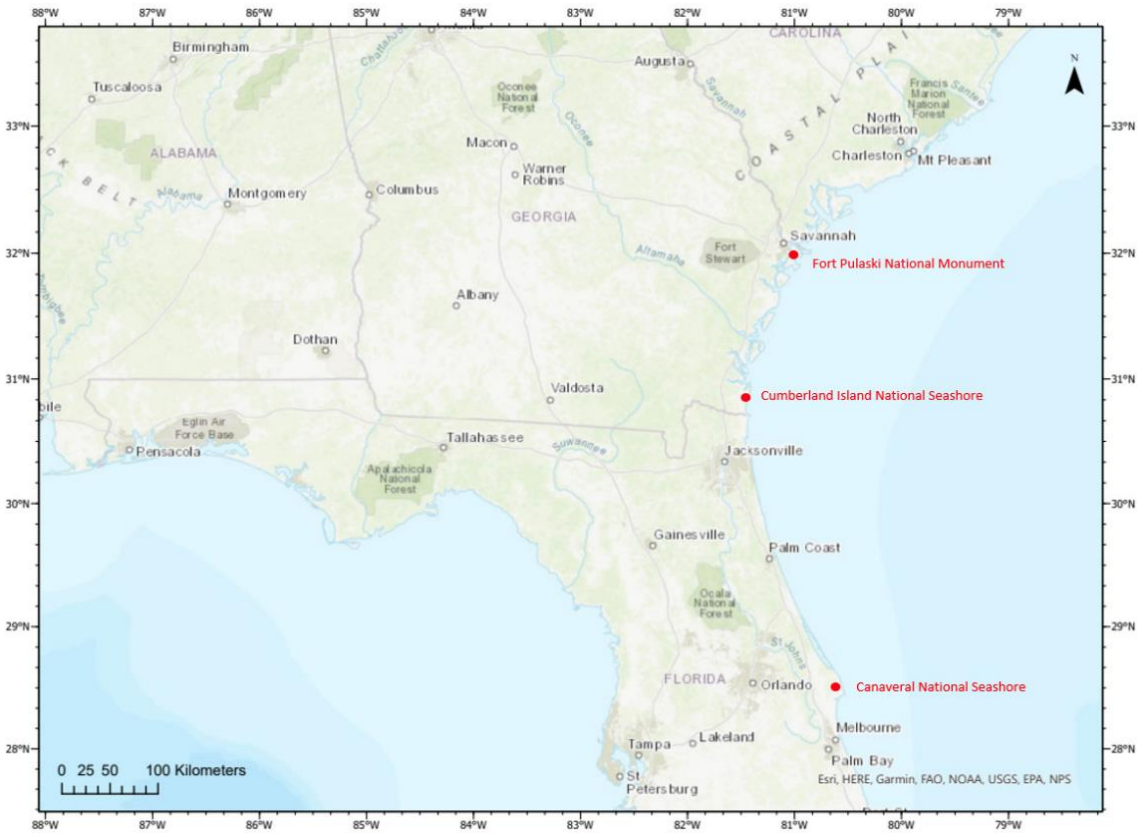

Figure 3-1. Cumberland Island National Seashore, Canaveral National Seashore, and Fort Pulaski National Monument site locations.

Cumberland Island NS is approximately 36,423 acres (13,526 ha). Of this area, salt marshes occupy approximately 9019 acres (3650 ha), and the dominant vegetative type is *Spartina alterniflora* (smooth cordgrass) [*McManamay, 2013*]. In the marsh areas, this region is mostly comprised of poorly drained soils in tidal marshes and poorly drained soils in shallow depressions [*McManamay, 2017*]. Since Cumberland Island NS is near Fort Pulaski NM, the site's climate and average precipitation are considered the same [*McManamay, 2013; McManamay, 2017; Davey et al., 2007*].

Fort Pulaski NM is approximately 90% wetland, and the majority of the vegetation is *Spartina alterniflora* (smoothgrass) [*McManamay, 2013*]. This marsh land represents areas of marshy soil and a black to bluish-gray heavy silt, and it contains large amounts of shells and decaying organic matter [*McManamay, 2013*]. The marsh land represents areas of marshy soil and a black to bluish-gray heavy silt, and it contains large amounts of shells and decaying organic matter [*McManamay et al., 2013*]. The climate at this site is hot to humid during the summer (88.0–89.6 ◦F, 31–32 ◦C), with mild, brief cold periods (39.3–42.8 ◦F, 4–6 ◦C) during the winter [*McManamay, 2013; Davey et al., 2007*]. Storm fronts of precipitation events usually occur during the winter and spring months, while tropical storms, hurricanes, and thunderstorms occur during the fall and summer months [*McManamay, 2013; Davey et al., 2007*]. This site receives approximately 1201–1400 mm/year (47.3–55.1 inches/year) of rain [*McManamay, 2013; Davey et al., 2007*].

Canaveral NS is approximately 58,807 acres (23,798 ha). The vegetative types present in the salt marshes are *Spartina* (*Juncus*), mangroves, and saltwort (saltgrass), representing approximately 13% of the area [*Cotton et al., 2020*]. The climate in this area is semi-tropical to temperate; the summer months are hot and humid (88.0–90.0 ◦F, 31–32.2 ◦C), and winter months range in temperature from 30.0 to 70.0 ◦F (−1 to 21.1 ◦C) [*Cotton et al., 2020; Davey et al., 2007*].

3.3. Methodology

The approach developed involved the classification of salt marsh presence with a data processing procedure, the calculation of vegetation biomass, and the determination of changes occurring within each site. Sentinel-2 data (2016–2020) were acquired from the United States Geological Survey (USGS) Earth Explorer (Figure 3-2). Two Sentinel-2 images were acquired for each site: Cumberland Island NS (6 September 2019 and 19 March 2020), Fort Pulaski NM (30

December 2016 and 21 October 2018), and Canaveral NS (20 November 2016 and 31 October 2017). The selected images were selected at different tidal stages. Fort Pulaski NM and Cumberland Island NS were in the tidal stage of 1.8–2.7 m (m), while the Canaveral NS tidal stage was 0.3–0.6 m. To identify the salt marshes present, unsupervised and supervised classification schemes were used to determine each class (Figure 3-3). The classes were then validated using manual pixel selection and field-based training data collection. To calculate the vegetation biomass, the Normalized Difference Vegetation Index (NDVI) was applied at each site. These results yielded a change analysis identifying the areas of salt marsh increase (%) and decrease (%).

Data Acquisition

Sentinel-2 data (10 m resolution) were collected from 2016 to 2020 at each NPS site. The Sentinel-2 data product was distributed as a Level-1C top-of-atmosphere (TOA) reflectance orthorectification to generate highly accurate geolocated products from the USGS Earth Explorer and the European Space Agency (ESA) [*Pieschke, 2017*]. Each Level-1C product is a 100 km × 100 km tile with a UTM/WGS84 (Universal Transverse Mercator/World Geodetic System 1984) projection and datum. The Level-1C product is the result of applying a Digital Elevation Model (DEM) to project the image in cartographic geometry [*European Space Agency-Sentinel, 2022*]. Radiometric measurements are taken from each pixel and projected in TOA reflectance along with the parameters to transform them into radiances (the formula is below) [*European Space Agency-Sentinel, 2022*]. Level-1C processing applies radiometric and geometric corrections (including orthorectification and spatial registration). The Level-1C dataset was processed from its true color image. Each data file can be accessed here: https://sentinels.copernicus.eu (accessed on 21 July 2023). The formula conversion for reflectance to radiance is as follows:

radiance = reflectance ∗ cos (radians (SunZenithAngle)) ∗ solar Irradiance ∗ U (thermal transmittance)/pi

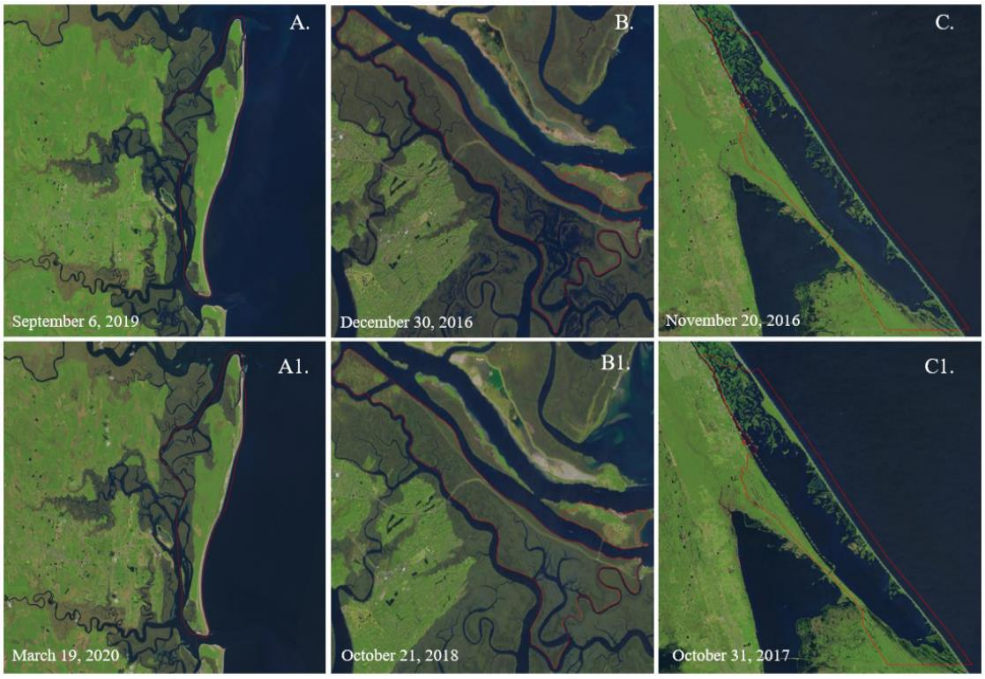

Figure 3-2. Sentinel-2-derived site locations: Cumberland Island NS (A, A1.), Fort Pulaski NM (B, B1.), and Canaveral NS (C, C1.). Top panel (A-C) represents the initial Sentinel-2 image collected to compare with the bottom panel (A1., B1. And C1.) of the changes that occurred in a different year.

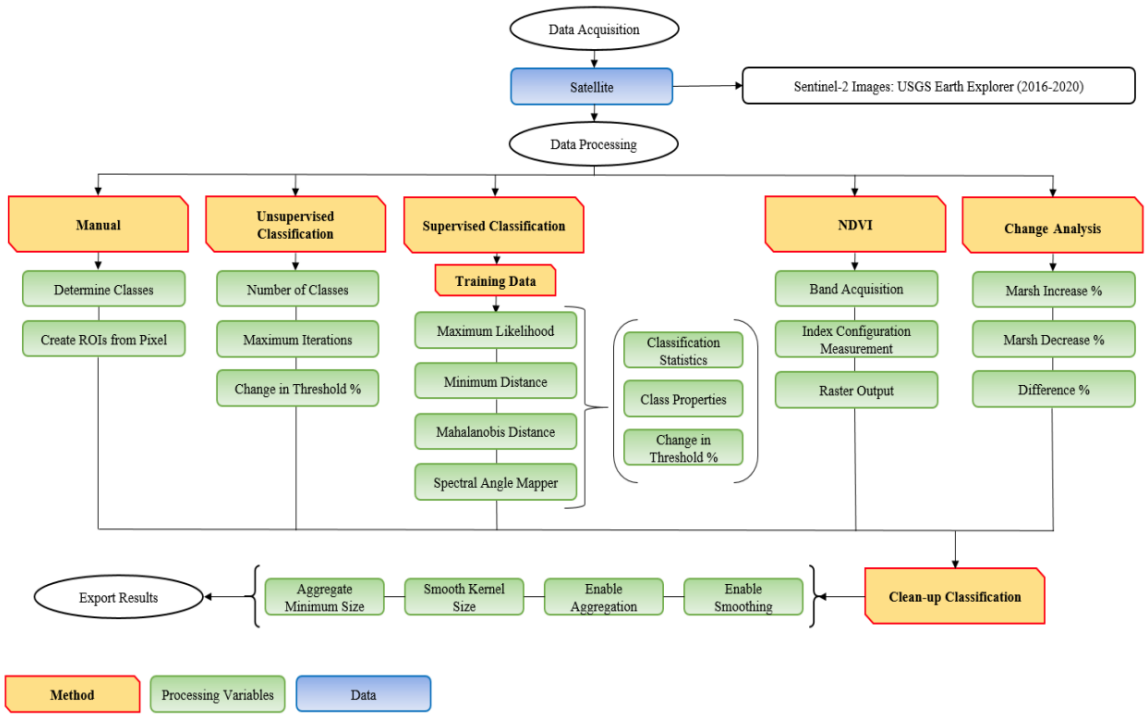

Figure 3-3. Processing procedure representing data acquisition, data processing, and final output. Each processing method was used to characterize salt marshes spatially and temporally.

Data Processing

To perform this analysis, a classification workflow was created in ENVI 5.3-NV5 Geospatial to categorize the pixels in an image into different classes using supervised and unsupervised classification schemes. The unsupervised classification schemes (K-means and IsoData) were performed using no training data, while the supervised classification schemes (maximum likelihood, minimum distance, Mahalanobis distance, and spectral angle mapper) trained the algorithm using manual data input from existing region-of-interest (ROI) and field-based data. These classification schemes have been used in coastal vegetative environments to better predict and understand the changes that are occurring [*Aslan et al., 2016; Giri et al., 2007; Yagoub and Kolan, 2006*]. Additionally, the NDVI was used to quantify the vegetation biomass by measuring the difference between near-infrared and red light. This index identifies vegetation

reflection and absorption for assessing vegetation density. These procedures resulted in a change analysis to identify and quantify how the salt marsh changed between two time periods. The results were then validated to confirm reliable outputs.

Unsupervised Classification

The unsupervised classification schemes used were K-means and IsoData. These schemes served as a pre-processing procedure to identify the effectiveness of using an unsupervised classification based solely on statistics. Each of these schemes focused on calculating statistics for each class. The IsoData unsupervised classification calculated class means that were distributed evenly throughout the image, while the remaining unselected pixels were grouped by their minimum value [*NV5 Geospatial, 2022*]. Through this repeated analysis, the means were recalculated, and the pixels were reclassified with respect to the new iteration of means [*NV5 Geospatial, 2022*]. This process continued until the number of pixels in each class changed by less than the selected pixel probability change threshold (0.8000) or the maximum number of iterations was reached (Figure 3-4).

K-Means unsupervised classification calculated the original class means evenly throughout the image and then grouped the pixels to the nearest class using its minimum value calculated [*NV5 Geospatial, 2022*]. All pixels were classified to the nearest class using a probability threshold of 0.8000 (Figure 3-4). This process continued until the maximum number of classes was reached or the number of pixels in each class changed by less than the established threshold.

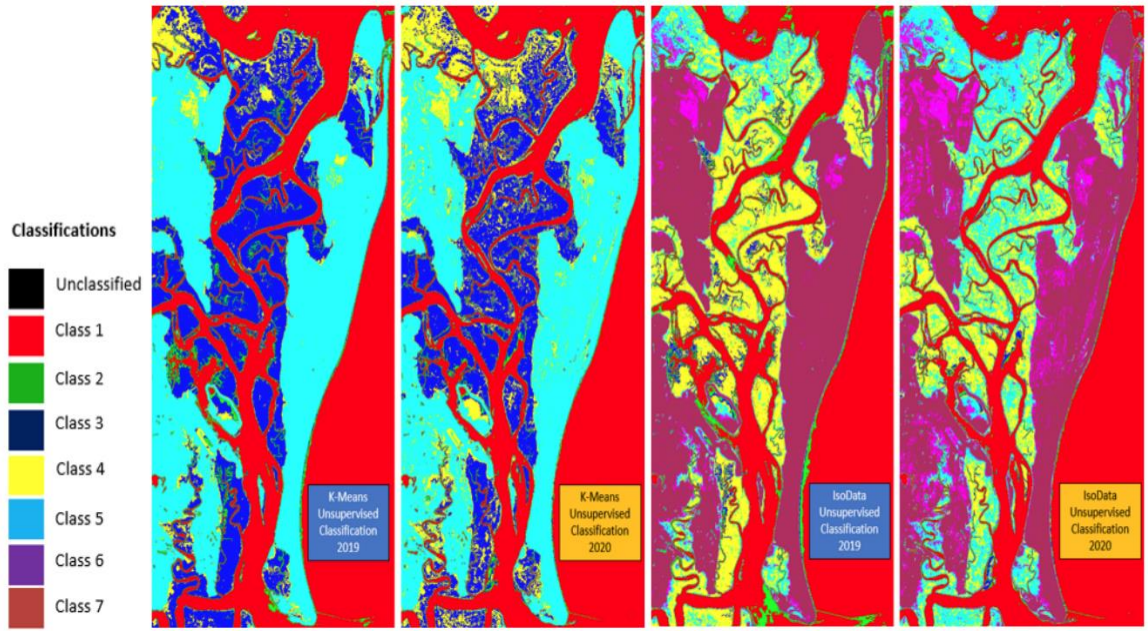

Figure 3-4. Unsupervised classification using IsoData and K-means at Cumberland Island NS from 2019 to 2020.

Supervised Classification

The supervised classification schemes clustered select pixels in the dataset on the basis of manual ROIs and field-based training data (Figure 3-5). The ROIs and training data were used to select each pixel that was representative of the determined features (water and marsh). The field-based training data incorporated 133 GPS points to identify salt marsh areas. These GPS points were added and matched to the pixel-based ROIs selected. Pixel-based ROIs were selected one at a time (1 × 1), or up to an area of 5 × 5 pixels on the raster layer was selected. Each selection or grouping of pixels was selected repeatedly to determine each class. The classification schemes used were maximum likelihood, minimum distance, Mahalanobis distance, and spectral angle mapper. The maximum likelihood classification assumes that the statistical values for each class in each specified band are distributed evenly and calculates the probability that a given pixel belongs to the specified pre-determined class [*NV5 Geospatial, 2022*]. The probability threshold

was a single value at 0.8000 for all classes. The data scale factor (default 255.00) was used as a division factor to convert integer scaled reflectance and radiance data into floating-point values. The no output rule image was applied.

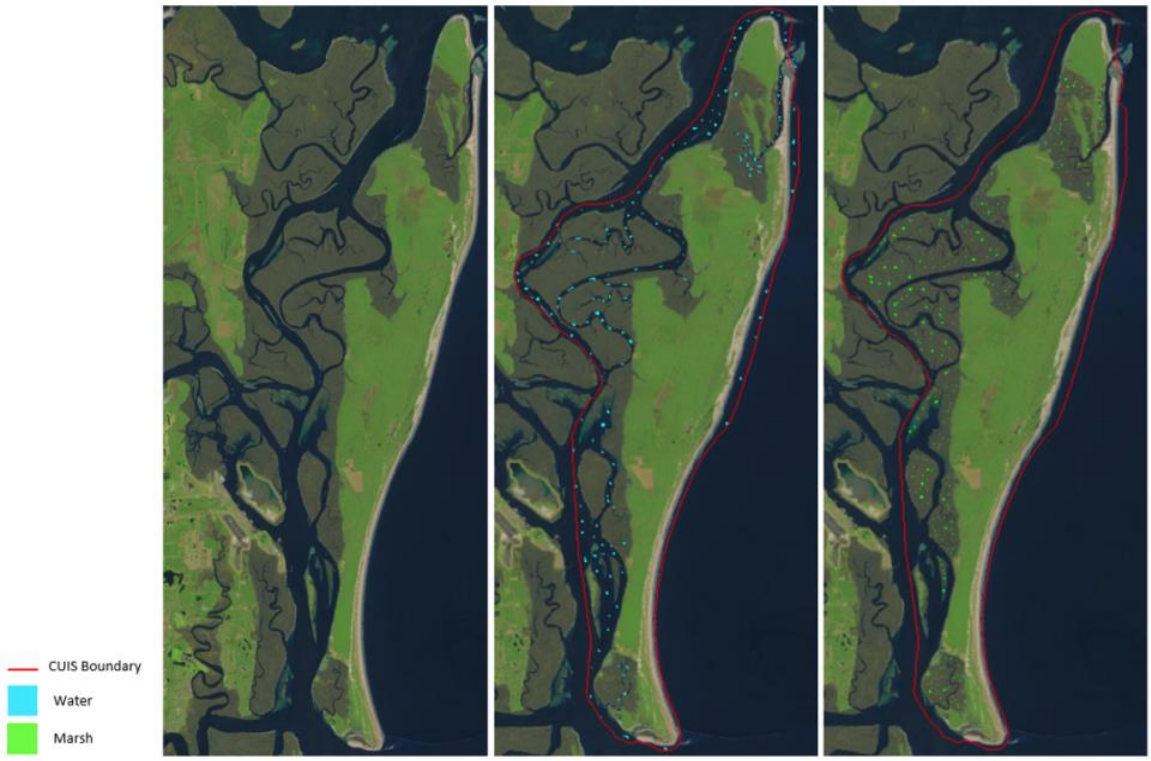

Figure 3-5. Manual ROIs and field-based training data of pixel selection to determine water and marsh areas.

Normalized Difference Vegetation Index (NDVI)

The NDVI was used to quantify the vegetation biomass to understand the vegetation density in the select sites. The NDVI is a ratio calculated between red light (RED) and near-infrared (NIR) values (formula below). The NDVI range is −1 <= X <= 1 (Figure 3-6). Negative values represent water, values close to zero (−0.1 < X < 0.1) represent bare soil/unconsolidated material, less positive values (0.1 < X < 0.4) represent sparse to intermediate vegetation, and values approaching 1 (X <= 1) are categorized as dense vegetation [*Jones and Vaughan, 2010; Korchagina et al., 2020; Huang et al., 2021; Nardin et al., 2021*].

NDVI Formula: NDVI = (NIR – RED) / (NIR + RED)

Vegetation Classification and NDVI Index Values				
Different Land Areas	**Water**	**Bare Soil/ Unconsolidated Material**	**Sparse to Intermediate Vegetation**	**Dense Vegetation**
NDVI Values	Negative Values	Values close to Zero	Low Positive Values	Values Approaching 1
NDVI Scale				
NDVI Values (X)	$X < 0$	$-0.1 < X < 0.1$	$0.1 < X < 0.4$	$X > 1$

Figure 3-6. NDVI vegetation classification and scale values.

Change Detection Analysis

The resulting change detection maps from the maximum likelihood classification scheme were used to identify increases/decreases in salt marsh area temporally. Band 3 (the green band) was selected to identify these changes by calculating the difference between the initial image and the final image during the specified period. Images were geometrically aligned with the same viewing geometry and coordinate system. To identify the increases and decreases in salt marsh area, the Otsu thresholding method was applied. This algorithm assumes that the image contains two classes of pixels and then calculates the optimum threshold separating the two classes [*NV5 Geospatial, 2022*]. The optimal threshold (or set of thresholds) is selected automatically; it is not based on differentiation but on the integration of the zeroth to first-order cumulative moments of the gray-level histogram [*Otsu, 1979*]. The Otsu thresholding algorithm is a nonparametric approach for automatic threshold identification and has been widely used in coastal wetland analysis [*Xu et al., 2020; Jia et al., 2021; Liu et al., 2015; Kuleli et al., 2021*].

Validation

The validation process was an evaluation of the processed data to confirm that the technique produced reliable outputs characterizing the spatial and temporal analysis of salt marshes. This approach incorporates validating a single classification (maximum likelihood) using the change detection analysis. The methods used to validate the results were (1) threshold output, (2) selection of ROIs, (3) identification of known open water sources, and (4) extraction of values to points. Each of the validation processes was operated through this classification to characterize the areas of under- and over-predictions for each site. These methods incorporated the manual ROIs, field-based training data, and probability threshold values to identify accuracy. The field-based training data consisted of 133 GPS points locating salt marsh areas. These points were used to validate that the areas classified as salt marsh were accurate.

To perform the threshold output validation technique, the established ROIs were processed under different probability thresholds to assess the maximum likelihood classification accuracy. The probability threshold value was used to identify the accuracy of the processed results under 0.80, 0.90, and 0.995. These threshold values were determined to ensure that the pixel was actually representative of the feature class. A probability threshold of 0.80 or better is stricter than a lower threshold value in allowing a pixel in a class. Each year was processed under all thresholds to select the pixels assigned to the class that had the highest probability according to the probability threshold set. If the highest probability is smaller than the specified threshold, the pixel remains unclassified.

ROI selection is a validation process of selecting 30% and 70% of the recorded ROIs to determine the difference in the output produced. The ROIs selected are random and do not follow a particular pattern. Each ROI was selected in both water and marsh areas.

The open water source validation process involves identifying how accurately the bodies of water are classified. This process is used to validate that all the areas mapped as water are in fact designated water sources. The purpose of using water body detection is to (1) identify how each classification scheme performed in identifying pixels of a different feature class, (2) how the water body results differ from salt marsh detection, (3) how the selection of water ROIs changes when they have neighboring salt marsh ROIs, and (4) whether the classification scheme can identify the changes occurring with the water bodies that ultimately impact the salt marshes.

The extraction of values to points was used to identify the accuracy of the classification scheme on the training data and ROIs created to identify the marsh areas and water sources. This process extracts the cell values of a raster on the basis of the set of point features and then records the values in the attribute table of an output feature class. The input raster is not resampled in the environment. Instead, the cell values are extracted from the input raster in its original resolution and spatial reference by projecting the input locations to the raster's reference from the values extracted.

3.4. Results

The results present the salt marsh change detection and NDVI outputs for the selected NPS sites (Cumberland Island NS, Fort Pulaski NM, and Canaveral NS) from 2016 to 2020. Areas designated as salt marsh increases/decreases feature the salt marsh area changes. They demonstrate how vulnerable salt marshes are along the southeastern US and highlight the effectiveness of this remote sensing technique to enhance coastal natural resource conservation.

Cumberland Island National Seashore

Cumberland Island NS was analyzed from 2019 to 2020, as this period exhibited no cloud cover over this specified region (Figure 3-7). The marsh areas, tributaries, channels, tidal inlets,

and bodies of water were mapped effectively by the maximum likelihood classification scheme to capture changes occurring at this site.

The change detection analysis displayed shifts in tidal inlets and channels and along the coastline. There was a decrease of 1.8% in salt marsh, with a large portion of this decrease along channel inlets on the most westward areas of the site boundary (Figure 3-7). Areas detected as increases in salt marsh were identified in the western, northern, and southern regions of the site by 1.4% (Figure 3-7).

The NDVI results supported the maximum likelihood classification and change detection analysis. Increases and decreases in salt marsh were analogous in areas where water, bare soil, and sparse–intermediate vegetation was present. The NDVI values in the 2019 image ranged from −0.52 to 0.83, and those in the 2020 image ranged from −0.48 to 0.78 (Figure 3-7). The vegetation index indicated bare soil/unconsolidated material around the entire site boundary. In the tidal inlets and channels, the NDVI values categorized the tidal inlets and channels as water and bare soil/unconsolidated material. Approaching the eastern region of the site from the west, the vegetation index indicated a transition from sparse–intermediate vegetation to dense vegetation. The areas categorized as marsh land ranged from bare soil/unconsolidated material to sparse–intermediate vegetation, while the most eastern region appeared to have small locations of dense vegetation.

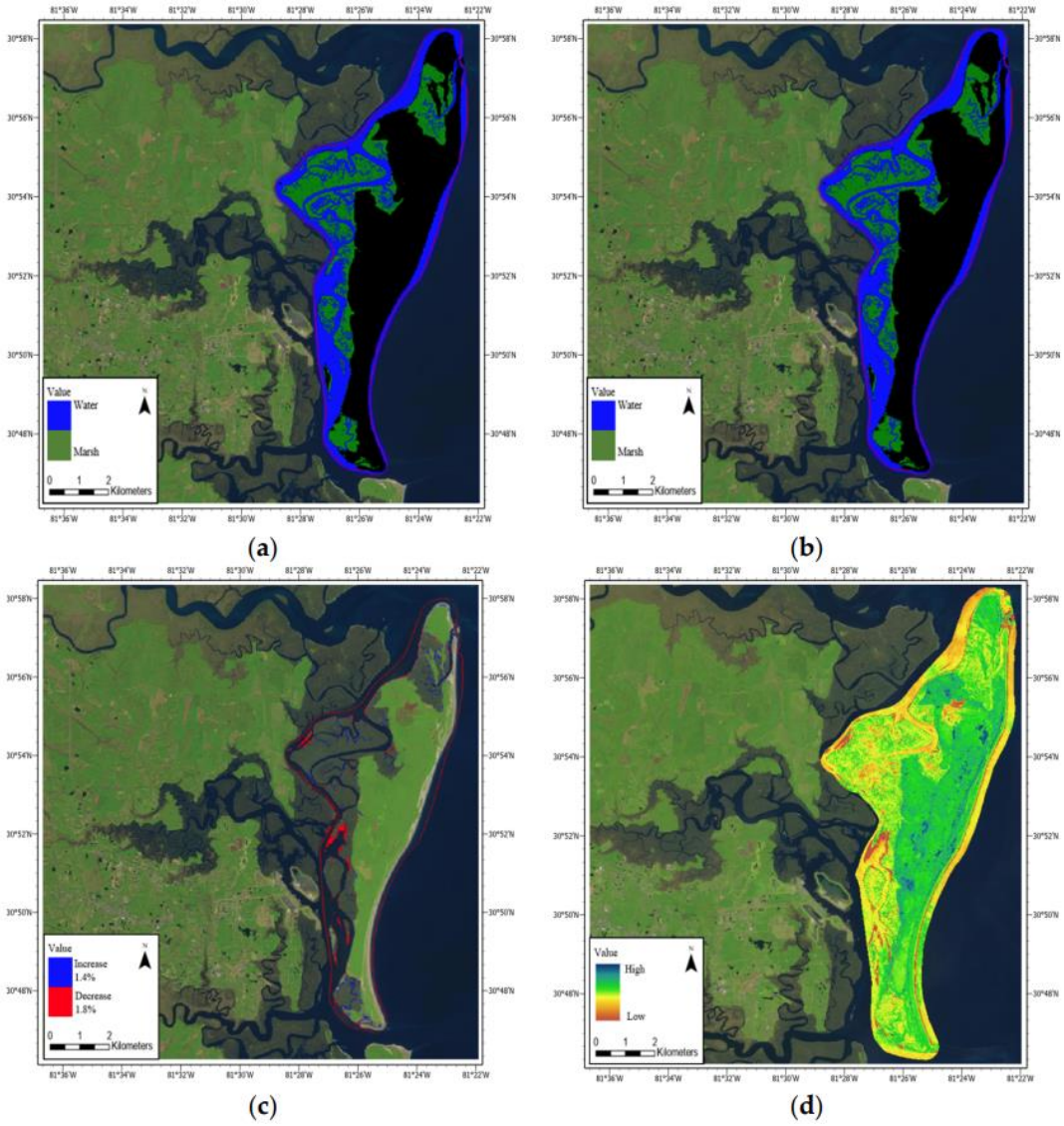

Figure 3-7. Maximum likelihood classification of Cumberland Island National Seashore from 2019 (a) to 2020 (b). (c) Change detection analysis of marsh land. (d) NDVI salt marsh assessment determining differential reflection of the vegetation density and relative growth using spectral reflectivity of solar radiation from 2019 to 2020.

Canaveral National Seashore

Canaveral NS was assessed from 2016 to 2017 through the maximum likelihood classification scheme (Figure 3-8). Through this scheme, some marshes were able to be identified; however, the water bodies were identified best. The black areas are areas that were not identified

by the classification process. The change detection process was able to identify some of the classified salt marsh changes (Figure 3-9). Marsh areas in the southernmost region of the site had the largest decreases, while areas of marsh increase were represented in areas along the western and eastern boundaries of the site. The majority of changes identified were in the channels and tidal inlets; however, notable increases were present inland along the western site boundary.

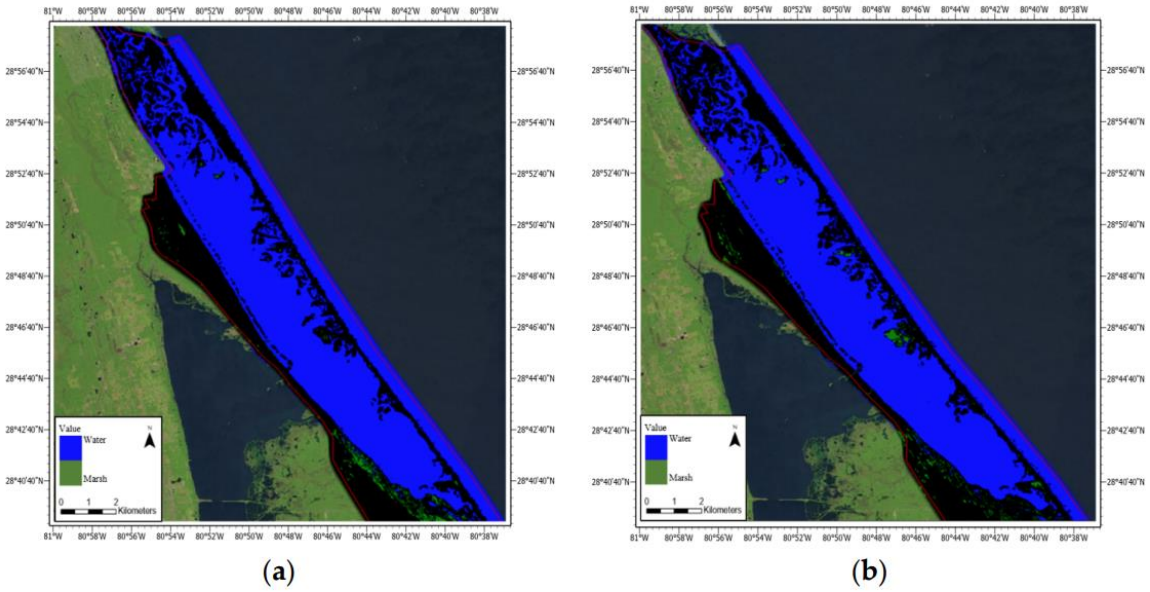

Figure 3-8. Supervised maximum likelihood classification of Canaveral National Seashore from 2016 to 2017. Image (a): 2016; image (b): 2017.

The NDVI results paired well with the change detection analysis (Figure 3-10). In this site, the vegetation index values for the 2016 image were −0.55 to 0.78 and −0.64 to 0.82 for 2017. The spectral signatures of the marshes along the eastern border of the site were considered to be water, bare soil/unconsolidated material, and sparse to intermediate vegetation.

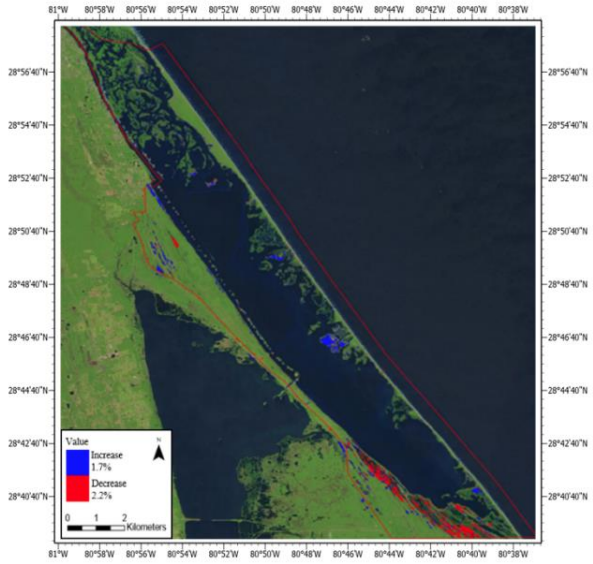

Figure 3-9. Canaveral National Seashore change detection analysis of marsh land from 2016 to 2017.

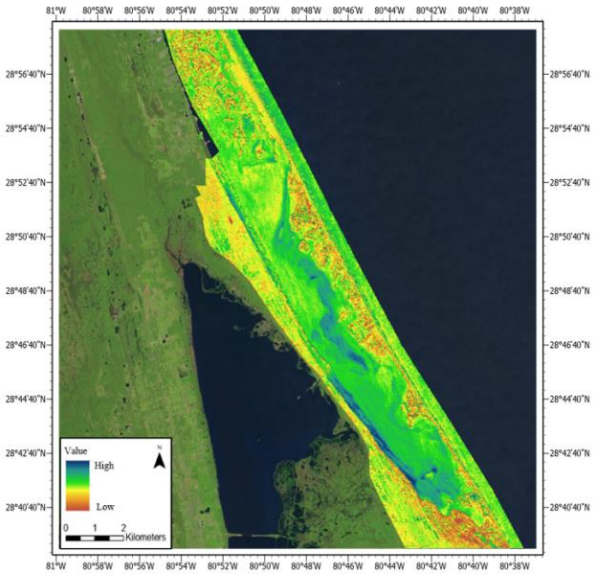

Figure 3-10. NDVI salt marsh assessment of Canaveral National Seashore displaying differential reflection of the vegetation density and relative growth using spectral reflectivity of solar radiation from 2016 to 2017.

Supervised Classification Accuracy

Supervised classification schemes, i.e., maximum likelihood, Mahalanobis distance, spectral angle mapper, and minimum distance, were used to assess the productivity of each method and its accuracy (Figure 3-11). The maximum likelihood produced the most accurate result, with 90% of the marsh pixels and 99% of the water pixels mapped accurately (Table 3-1)

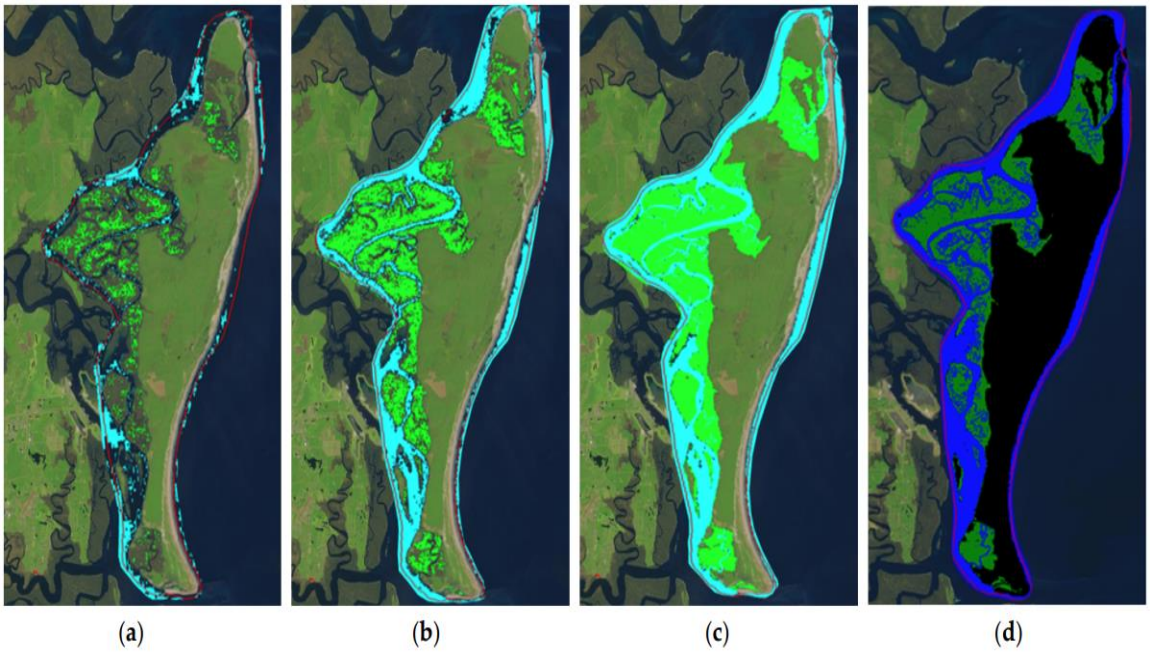

Figure 3-11. Supervised classification schemes: Mahalanobis distance (a), spectral angle mapper (b), minimum distance (c), and maximum likelihood classification (d).

Table 3-1. Supervised classification scheme accuracy of all ROIs inputted at Cumberland Island National Seashore.

	Supervised Classification Scheme Accuracy %			
Classifications	**MarshPixels(270)**	**MarshAccuracy %**	**WaterPixels(207)**	**WaterAccuracy %**
Maximum Likelihood	243	90%	207	99%
Minimum Distance	239	89%	197	95%
Spectral Angle Mapper	234	87%	168	81%
Mahalanobis Distance	62	23%	8	43%

Tidal Influence

Fort Pulaski NM highlights the importance of considering the tidal influence in diurnal environments (Figure 3-12). On 30 December 2016 and 21 October 2018, the tidal influence was 1.8–2.7 m. In conducting the supervised classification during this time, the results displayed the impact of seasonality on this environment. Due to the tidal stage, the marshes present were submerged, not removed.

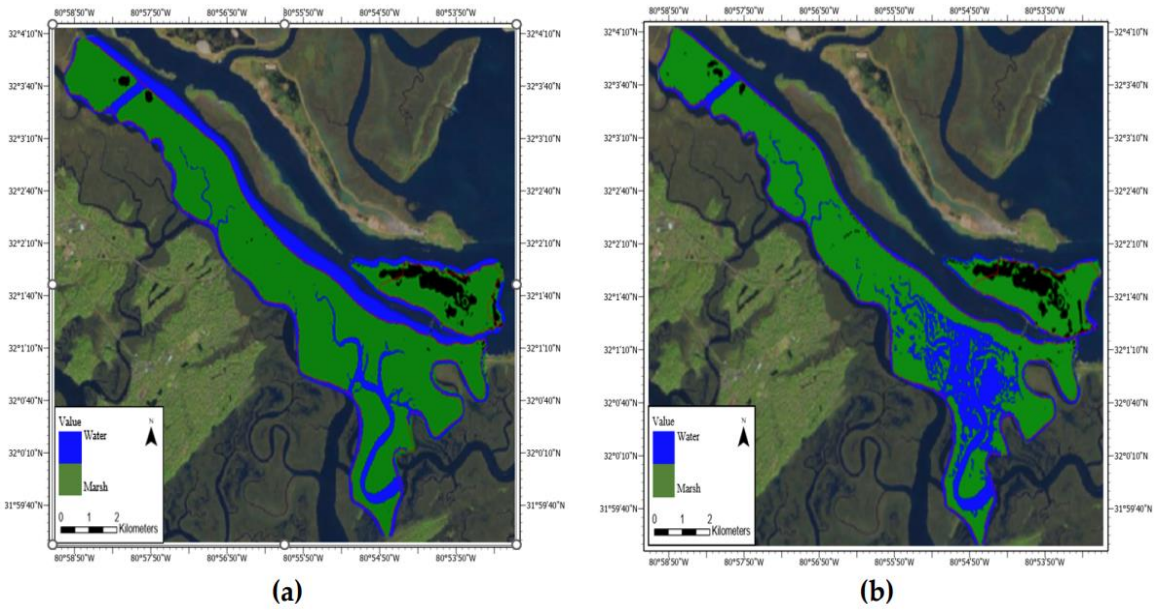

Figure 3-12. Supervised maximum classification of Fort Pulaski National Monument from 2016 to 2018. Image (a): 2016; image (b): 2018.

In this assessment, the change detection analysis was identifying areas where the marsh was submerged due to the tidal influence. These marsh areas were submerged in the tidal inlets and the southeast region of the site boundary. As these marsh environments are representative of dynamic processes, validating the maximum likelihood accuracy is a must (Table 3-2). The maximum likelihood classification validation results displayed the accuracy of this approach.

Table 3-2. Validation accuracy assessment from the maximum likelihood classification scheme for each site.

Validation Accuracy %			
Features	**Input Points (ROIs)**	**Conferred Points**	**Accuracy %**
Cumberland Island National Seashore			
Salt Marsh	270	242	90%
Water	207	205	99%
Canaveral National Seashore			
Salt Marsh	12	9	75%
Water	102	100	98%
Fort Pulaski National Monument			
Salt Marsh	240	226	94%
Water	71	70	99%

3.5. Discussion

In the southeastern US, salt marshes represent some of the most vulnerable wetlands. This research outlined the feasibility of using remote sensing-based classification methods for assessing salt marsh changes. Variations of this technique are widely known and have been applied to understand coastal vegetative changes; however, this methodology has not been utilized in this region, nor has it been assessed [*Calzadilla Perez et al., 2002; Ogburn and Alber, 2006; Stagg and Mendelssohn, 2010*]. Before the supervised classification process was implemented, the unsupervised classification scheme was performed. The unsupervised classification produced seven classes that were determined from the statistical routine (i.e., clustering) on the basis of their shared spectral signatures. This is an important step because the classification categorizes unknown similarities and difference in the data by grouping similar features.

Although the identification of distinct features was determined, the algorithm generated multiple classes that represented a single feature (Figure 3-4). This is due to not having a training sample and/or an ROI to define each feature class accurately. Using the results of the unsupervised

classification improved the supervised classification by selecting the necessary ROIs representative of the select features by the spectral signatures clustered. To enhance this automation process, the unsupervised classification can improve the number of classes determined, as too many classes can saturate the classification results, yielding inaccurate assumptions of the area analyzed. Improving the range of clustering from the spectral signatures of each pixel will provide better interpretation when training data are limited. The unsupervised classification serves its purpose when no training data exist, but it has to be coupled with a supervised classification scheme to ensure accurate results. According to these results, spectral angle mapper, minimum distance, and Mahalanobis distance were each selected to determine the best method from the supervised classification methods; however, the maximum likelihood classification results showed the most promise in accurately assessing marsh changes (Figure 3-11). Each NPS site was assessed through this scheme to determine whether this classification would produce an accurate interpretation of the environment. Each site was mapped appropriately through the manual input ROIs and field-based training data. The pixels selected captured similarly vegetated marsh areas in Canaveral NS and Cumberland Island NS (Figures 3-7 and 3-8). The channels and tidal inlets, where most of the changes occurred, also produced viable results. In selecting pixel-based ROIs, details matter, and in order to provide the most accurate interpretation, each individual pixel was selected randomly throughout the Sentinel-2 image. Pixels that neighbored another class or bordered a new feature class were not selected to prevent the over-estimation of another class feature. When all ROIs were combined, the maximum likelihood classification yielded the highest accuracy percentage (Table 3-1). Table 3-1 displays the number of marsh and water pixels that accurately represent these features. Subsequentially, the input of all ROIs improved the performance of minimum distance and spectral angle mapper.

The NDVI provided a supportive source displaying the differential reflection of the vegetation biomass presence. This assessment supported the maximum likelihood classification and change detection analysis, displaying that the majority of the marsh areas in these sites were from bare/soil unconsolidated material to sparse–intermediate vegetation (Figures 3-7 and 3-10). In the areas where the results indicated salt marsh decreases, the NDVI values were less than zero, displaying no vegetation. By utilizing this vegetative index, spatial change relationships were captured, the distribution was quantified, and the accuracy of mapping was classified.

To further our interpretation of the salt marsh changes occurring, a change detection analysis was performed on each NPS site to determine the exact location of such changes. The results indicated that salt marshes were largely decreasing during the study period; however, there were areas of increase (Figures 3-7 and 3-9). Notably, the largest salt marsh decrease occurred in or around the channels, coastline, and tidal inlets. Studies have shown that the majority of the cases of diebacks, submergence, and/or removal have occurred within these geomorphological features [*Stagg and Mendelssohn, 2010; Fagherazzi et al., 2012; Fagherazzi et al., 2008; Leung and Prasad, 2008; Pham et al., 2019*]. As a result, these processes alter channelization, contributing to hydrologic and hydrogeological changes. In Fort Pulaski NM, we highlighted the influence of high/low tide in these environments (Figures 3-12 and 3-13). As a result of tidal influence, decreases in salt marshes are representative of salt marshes being submerged, not removed [*Leung and Prasad, 2019; Pham et al., 2019*]. Hurricanes are common in the coastal southeastern US, causing rapid sea level rise and the submergence of salt marsh areas [*Michener et al., 1997*]. In understanding how rapidly these coastal areas change, it is important to note that in collecting data in these regions, the data must be tidally synced. In Figures 3-12 and 3-13, we demonstrate how data can be misinterpreted due to the data not being under the same tidal influence. Using this

method to classify vegetative changes is efficient, but pre-data collection must be suitable to provide viable results in identifying areas of concern and areas where changes are occurring.

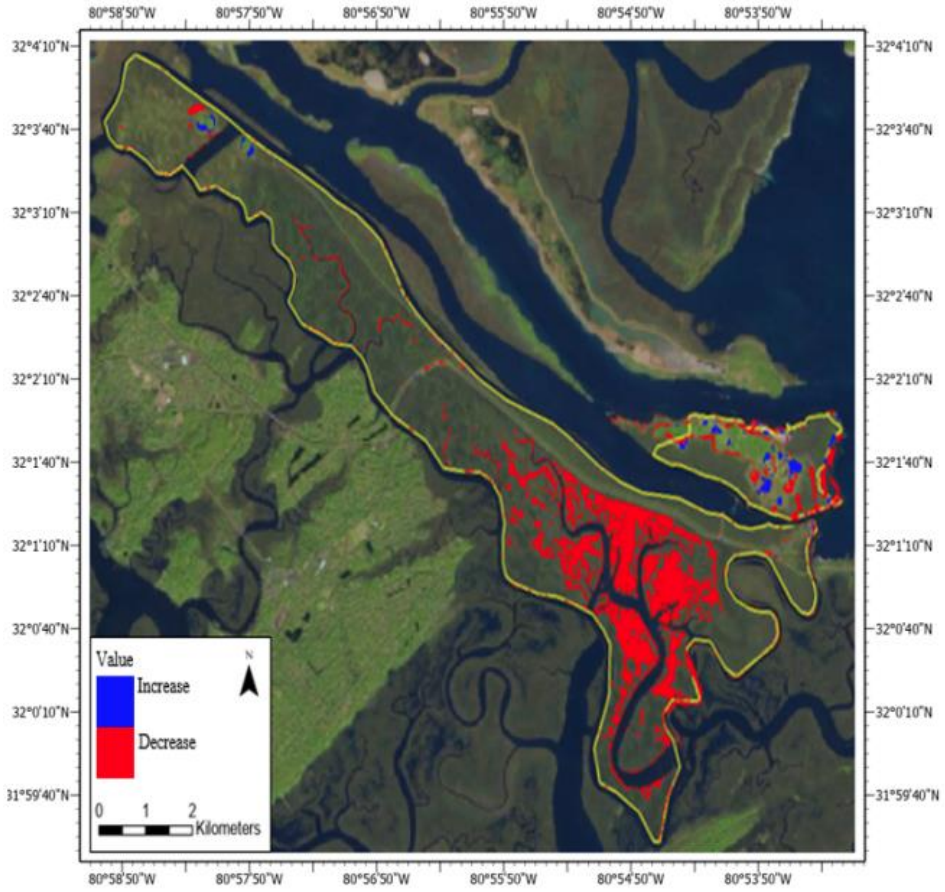

Figure 3-13. Fort Pulaski National Monument change detection analysis of marsh land from 2016 to 2018.

This study provides a detailed methodology that focuses on the establishment of a remote sensing-based procedure to classify salt marshes and detect changes in the marsh extent; however, some limitations are apparent. First, data availability and field-based data collection at each site would have increased the overall accuracy of the classification scheme used at Cumberland Island NS and Canaveral NS, as field-based training data were only applied to Fort Pulaski NM. Coupling field-based data to support this technique would have resulted in more precise results from the manually selected ROIs. Second, in completing this type of analysis, the spatial extent of the salt

marshes must be considered. In areas where the extent of salt marshes is prominent, the maximum likelihood classification is efficient. Alternatively, if the areal extent of the salt marshes is relatively small, this procedure is not as effective in salt marsh monitoring. Third, the period in which data is collected must be considered. These datasets were collected because of their clarity due to lack of cloud cover and the areal cover over the sites; however, due to differences in seasons, the amount of salt marsh present was impacted by diurnal variations. In the case of salt marsh studies, the tidal influence must be considered to alleviate misinterpretation. Fort Pulaski NM was not collected at approximately the same tidal level relative to a particular datum; however, even with this limitation, this method still highlighted areas of concern and showed how the salt marsh areas responded after being submerged. Lastly, the number of ROIs used when classifying each image must be taken into consideration. Overall, this classification scheme works best when there are more pixels selected in respect to its pixel value to provide a better interpretation. The more statistics collected for each band distributed spatially throughout the image, the higher probability that a given pixel or set of pixels belongs to a specific class feature. However, due to the classification scheme calculating each pixel, some results may yield an over- or underestimation of each feature class. This occurred while processing Canaveral NS, and therefore, the method was adjusted to capture an output that closely resembled the designated features. Fewer ROIs (12) were used to produce a more accurate result. Because Canaveral NS had a small areal extent of salt marsh presence, the maximum likelihood classification performed better with fewer ROIs selected. At this particular site, a higher number of ROIs produced an overestimation of salt marshes. Some of the pixel's representative of salt marshes neighborhood other features not representative of salt marshes in close proximity that yielded false results. Even after considering these limitations, this

multi-phased methodology was shown to be reliable in that it offers a high degree of performance and accuracy.

Studies have demonstrated that this method produces an overall accuracy ranging from 79% to over 88% [*Byrd and Kelly, 2006; Giri et al., 41; Leung and Prasad, 2019; Pham et al., 2019*]. In this study, we produced an overall accuracy ranging from 75% to 99% (Table 3-2). At each of the sites, the water bodies were mapped with 99% accuracy. In the marsh areas, the range was from 75% to 94% accuracy. The percentage of errors was likely due to the salt marshes' spatial extent, the inclusion of field-based data collection, and the variability of satellite imagery noise due to differences in the stage of tides. Due to the large spatial extent of the salt marshes at Fort Pulaski NM and Cumberland Island NS, the conferred points of the selected input ROIs yielded >90% accuracy. The maximum likelihood classification was able to better capture salt marsh features, as there were more pixels of identifiable marsh locations. Additionally, Fort Pulaski NM produced the most accurate results due to the combination of manual input ROIs and field-based data collection to yield more precise results.

3.6. Conclusion

Coastal salt marsh ecosystems are continually threatened by climatic effects and anthropogenic activity. As these ecosystems continue to experience these stressors and changes, analyzing changes in these environments will inevitably become more difficult due to their inaccessible locations and rapid transformation. The use of remote sensingbased techniques with high spatial resolutions offers a valuable tool to provide proper management and an understanding of these shifting ecosystems. Furthermore, coupling remote sensing-based techniques with field-based data collection can provide more accurate results in understanding the nature of the processes occurring in these environments.

In this study, we provided a detailed methodology that analyzed salt marshes in Cumberland Island NS, Fort Pulaski NM, and Canaveral NS. Through this approach, salt marshes were identified, changes in area were detected, and the NDVI was used to quantify the vegetation biomass to understand vegetation density changes. This study did not show a permanent loss, and changes in increases/decreases can be attributed to short-term changes between two periods. According to these results, repeatable assessments are warranted to identify long-term trends. Through this process, we learned the critical state of these marsh environments as well as the value of applying these techniques. This advanced methodology has improved our understanding of the salt marsh changes occurring at these NPS sites while highlighting the disadvantages that exist in some scenarios.

This multi-phased technique furthers our understanding of the fundamental practices in analyzing coastal salt marshes through remote sensing-based approaches. As these detection techniques focused on salt marshes in this study, this application has the ability to be replicated under different environments and vegetation types. This developed framework enhances the reliability of change detection image processing due to the validated overall accuracy. As salt marshes continue to evolve, this approach offers the flexibility to capture ongoing changes. In a future study, deep learning, artificial neural networks, and support vector machine methods will have great potential for improving the classification of salt marshes.

To further characterize how vegetation is impacted by the effects of climate change, this study offers a monitoring tool that can be applied to improve coastal natural resource management. A field-based and remote sensing method is imperative in an uncertain climate and ever-changing ecomorphodynamic system, and utilizing this approach will ensure that salt marshes continue to serve as a pivotal resource in these aquatic environments.

References

Alber, M.; Swenson, E.M.; Adamowicz, S.C.; Mendelssohn, I.A. Salt marsh dieback: An overview of recent events in the US. Estuar. Coast. Shelf Sci. 2008, 80, 1–11.

Aslan, A.; Rahman, A.F.; Warren, M.W.; Robeson, S.M. Mapping spatial distribution and biomass of coastal wetland vegetation in Indonesian Papua by combining active and passive remotely sensed data. Remote Sens. Environ. 2016, 183, 65–81.

Barbier, E.B.; Hacker, S.D.; Kennedy, C.; Koch, E.W.; Stier, A.C.; Silliman, B.R. The value of estuarine and coastal ecosystem services. Ecol. Monogr. 2011, 81, 169–193.

Belluco, E.; Camuffo, M.; Ferrari, S.; Modenese, L.; Silvestri, S.; Marani, A.; Marani, M. Mapping salt-marsh vegetation by multispectral and hyperspectral remote sensing. Remote Sens. Environ. 2006, 105, 54–67.

Berger, M.; Moreno, J.; Johannessen, J.A.; Levelt, P.F.; Hanssen, R.F. ESA's sentinel missions in support of Earth system science. Remote Sens. Environ. 2012, 120, 84–90.

Byrd, K.B.; Kelly, M. Salt marsh vegetation response to edaphic and topographic changes from upland sedimentation in a Pacific estuary. Wetlands 2006, 26, 813–829.

Calzadilla Pérez, A.; Damen, M.C.J.; Geneletti, D.; Hobma, T.W. Monitoring a recent delta formation in a tropical coastal wetland using remote sensing and GIS. Case study: Guapo River delta, Laguna de Tacarigua, Venezuela. Environ. Dev. Sustain. 2002, 4, 201–219.

Campbell, A.D.; Fatoyinbo, L.; Goldberg, L.; Lagomasino, D. Global hotspots of salt marsh change and carbon emissions. Nature 2022, 612, 701–706.

Campbell, A.; Wang, Y. High spatial resolution remote sensing for salt marsh mapping and

change analysis at Fire Island National Seashore. Remote Sens. 2019, 11, 1107. Remote Sens. 2024, 16, 2 18 of 19

Campbell, A.D.; Wang, Y. Salt marsh monitoring along the mid-Atlantic coast by Google Earth Engine enabled time series. PLoS ONE 2020, 15, e0229605.

Cotton, D.L.; Adams, B.P.; O'Hare, N.K.; Bernardes, S.; Jordan, T.R.; Madden, M. Vegetation Mapping at Canaveral National Seashore: Photointerpretation Key and Final Vegetation Map; Natural Resource Report NPS/SECN/NRR—2020/2084; National Park Service: Fort Collins, CO, USA, 2020.

Craft, C.B.; Seneca, E.D.; Broome, S.W. Vertical accretion in microtidal regularly and irregularly flooded estuarine marshes. Estuar. Coast. Shelf Sci. 1993, 37, 371–386.

Crooks, S.; Herr, D.; Tamelander, J.; Laffoley, D.; Vandever, J. Mitigating Climate Change through Restoration and Management of Coastal Wetlands and Near-Shore Marine Ecosystems: Challenges and Opportunities; The World Bank: Washington, DC, USA, 2011.

Crosby, S.C.; Sax, D.F.; Palmer, M.E.; Booth, H.S.; Deegan, L.A.; Bertness, M.D.; Leslie, H.M. Salt marsh persistence is threatened by predicted sea-level rise. Estuar. Coast. Shelf Sci. 2016, 181, 93–99.

Dale, J.; Burnside, N.G.; Hill-Butler, C.; Berg, M.J.; Strong, C.J.; Burgess, H.M. The use of unmanned aerial vehicles to determine differences in vegetation cover: A tool for monitoring coastal wetland restoration schemes. Remote Sens. 2020, 12, 4022.

Davey, C.A.; Redmond, K.T.; Simeral, D.B. Weather and Climate Inventory, National Park Service, Southeast Coast Network; Natural Resource Technical Report NPS/SECN/NRTR—2007/010; National Park Service: Fort Collins, CO, USA, 2007.

Day, J.W.; Christian, R.R.; Boesch, D.M.; Yáñez-Arancibia, A.; Morris, J.; Twilley, R.R.; Naylor, L.; Schaffner, L.; Stevenson, C. Consequences of climate change on the ecogeomorphology of coastal wetlands. Estuaries Coasts 2008, 31, 477–491.

DiGiacomo, A.E.; Bird, C.N.; Pan, V.G.; Dobroski, K.; Atkins-Davis, C.; Johnston, D.W.; Ridge, J.T. Modeling salt marsh vegetation height using unoccupied aircraft systems and structure from motion. Remote Sens. 2020, 12, 2333.

Duarte, C.M.; Dennison, W.C.; Orth, R.J.; Carruthers, T.J. The charisma of coastal ecosystems: Addressing the imbalance. Estuaries Coasts 2008, 31, 233–238.

European Space Agency-Sentinel. 2022. Sentinel User Guides Product Type. Available online: https://sentinels.copernicus.eu/ web/sentinel/user-guides/sentinel-2-msi/product-types/level-1c (accessed on 21 July 2023).

Fagherazzi, S.; Hannion, M.; D'Odorico, P. Geomorphic structure of tidal hydrodynamics in salt marsh creeks. Water Resour. Res. 2008, 44.

Fagherazzi, S.; Kirwan, M.L.; Mudd, S.M.; Guntenspergen, G.R.; Temmerman, S.; D'Alpaos, A.; Van De Koppel, J.; Rybczyk, J.M.; Reyes, E.; Craft, C.; et al. Numerical models of salt marsh evolution: Ecological, geomorphic, and climatic factors. Rev. Geophys. 2012, 50.

Fagherazzi, S.; Marani, M.; Blum, L.K. The Ecogeomorphology of Tidal Marshes; American Geophysical Union: Washington, DC, USA, 2004.

Farris, A.S.; Defne, Z.; Ganju, N.K. Identifying salt marsh shorelines from remotely sensed elevation data and imagery. Remote Sens. 2019, 11, 1795.

Fretwell, S.; Wagner, A.; Lee, A. "A Million Acres of 'Priceless' Marshes Protect NC, SC,

GA. Will They Perish in Rising Tides?" The News and Observer. 2021. Available online: https://pulitzercenter.org/stories/million-acres-priceless-marshes-protect-ncsc-ga-will-they-perish-rising-tides (accessed on 18 June 2023).

Giri, C.; Ochieng, E.; Tieszen, L.L.; Zhu, Z.; Singh, A.; Loveland, T.; Masek, J.; Duke, N. Status and distribution of mangrove forests of the world using earth observation satellite data. Glob. Ecol. Biogeogr. 2011, 20, 154–159.

Giri, C.; Pengra, B.; Zhu, Z.; Singh, A.; Tieszen, L.L. Monitoring mangrove forest dynamics of the Sundarbans in Bangladesh and India using multi-temporal satellite data from 1973 to 2000. Estuar. Coast. Shelf Sci. 2007, 73, 91–100.

Gorelick, N.; Hancher, M.; Dixon, M.; Ilyushchenko, S.; Thau, D.; Moore, R. Google Earth Engine: Planetary-scale geospatial analysis for everyone. Remote Sens. Environ. 2017, 202, 18–27.

Guimond, J.; Tamborski, J. Salt marsh hydrogeology: A review. Water 2021, 13, 543.

Halpern, B.S.; Walbridge, S.; Selkoe, K.A.; Kappel, C.V.; Micheli, F.; d'Agrosa, C.; Bruno, J.F.; Casey, K.S.; Ebert, C.; Fox, H.E.; et al. A global map of human impact on marine ecosystems. Science 2008, 319, 948–952.

Hartig, E.K.; Gornitz, V.; Kolker, A.; Mushacke, F.; Fallon, D. Anthropogenic and climate-change impacts on salt marshes of Jamaica Bay, New York City. Wetlands 2002, 22, 71–89.

Huang, S.; Tang, L.; Hupy, J.P.; Wang, Y.; Shao, G. A commentary review on the use of normalized difference vegetation index (NDVI) in the era of popular remote sensing. J. For. Res. 2021, 32, 1–6.

Hughes, A.L.; Wilson, A.M.; Morris, J.T. Hydrologic variability in a salt marsh: Assessing

the links between drought and acute marsh dieback. Estuar. Coast. Shelf Sci. 2012, 111, 95–106.

IPBES (Intergov. Sci. Policy Platf. Biodivers. Ecosyst. Serv.). The Assessment Report on Land Degradation and Restoration. Rep., IPBES, Bonn, Ger, 2018. Available online: http://www.ipbes.net (accessed on 18 June 2023).

Jia, M.; Wang, Z.; Mao, D.; Ren, C.; Wang, C.; Wang, Y. Rapid, robust, and automated mapping of tidal flats in China using time series Sentinel-2 images and Google Earth Engine. Remote Sens. Environ. 2021, 255, 112285.

Jones, H.G.; Vaughan, R.A. Remote Sensing of Vegetation: Principles, Techniques, and Applications; Oxford University Press: Oxford, UK, 2010.

Kennish, M.J. Coastal salt marsh systems in the US: A review of anthropogenic impacts. J. Coast. Res. 2001, 17, 731–748.

Kirwan, M.L.; Mudd, S.M. Response of salt-marsh carbon accumulation to climate change. Nature 2012, 489, 550–553.

Korchagina, I.A.; Goleva, O.G.; Savchenko, Y.Y.; Bozhikov, T.S. The use of geographic information systems for forest monitoring. In Journal of Physics: Conference Series; IOP Publishing: Bristol, UK, 2020; Volume 1515, p. 032077.

Kuleli, T.; Guneroglu, A.; Karsli, F.; Dihkan, M. Automatic detection of shoreline change on coastal Ramsar wetlands of Turkey. Ocean. Eng. 2021, 38, 1141–1149.

Leung, L.Y.; Prasad, R. Potential Impacts of Accelerated Climate Change: Third Annual Report of Work (No. PNNL-27452-Rev. 1); Pacific Northwest National Lab (PNNL): Richland, WA, USA, 2019.

Liu, Y.; Zhou, M.; Zhao, S.; Zhan, W.; Yang, K.; Li, M. Automated extraction of tidal

creeks from airborne laser altimetry data. J. Hydrol. 2015, 527, 1006–1020.

Mariotti, G.; Canestrelli, A. Long-term morphodynamics of muddy backbarrier basins: Fill in or empty out? Water Resour. Res. 2017, 53, 7029–7054.

McManamay, R.H.; Curtis, A.C.; Heath, S.C. Vegetation Mapping at Fort Pulaski National Monument; Natural Resource Report NPS/SECN/NRR—2013/718; National Park Service: Fort Collins, CO, USA, 2013.

McManamay, R.H. Vegetation Mapping at Cumberland Island National Seashore; Natural Resource Report NPS/SECN/NRR—2017/1511; National Park Service: Fort Collins, CO, USA, 2017.

Mcowen, C.J.; Weatherdon, L.V.; Van Bochove, J.W.; Sullivan, E.; Blyth, S.; Zockler, C.; Stanwell-Smith, D.; Kingston, N.; Martin, C.S.; Spalding, M.; et al. A global map of saltmarshes. Biodivers. Data J. 2017, 5, e11764.

Michener, W.K.; Blood, E.R.; Bildstein, K.L.; Brinson, M.M.; Gardner, L.R. Climate change, hurricanes and tropical storms, and rising sea level in coastal wetlands. Ecol. Appl. 1997, 7, 770–801.

Mwamba, M.J.; Torres, R. Rainfall effects on marsh sediment redistribution, North Inlet, South Carolina, USA. Mar. Geol. 2002, 189, 267–287.

Nardin, W.; Taddia, Y.; Quitadamo, M.; Vona, I.; Corbau, C.; Franchi, G.; Staver, L.W.; Pellegrinelli, A. Seasonality and characterization mapping of restored tidal marsh by NDVI imageries coupling UAVs and multispectral camera. Remote Sens. 2021, 13, 4207.

NV5 Geospatial. 2022. ENVI Classification. Available online: https://www.nv5geospatialsoftware.com/docs/Classification (accessed on 21 July 2023).

Ogburn, M.B.; Alber, M. An investigation of salt marsh dieback in Georgia using field

transplants. Estuaries Coasts 2006, 29, 54–62.

Orson, R.; Panageotou, W.; Leatherman, S.P. Response of tidal salt marshes of the US Atlantic and Gulf coasts to rising sea levels. J. Coast. Res. 1985, 1, 29–37.

Otsu, N. A threshold selection method from gray-level histograms. IEEE Trans. Syst. Man Cybermetrics 1979, 9, 62–66.

Pham, T.D.; Xia, J.; Ha, N.T.; Bui, D.T.; Le, N.N.; Takeuchi, W. A review of remote sensing approaches for monitoring blue carbon ecosystems: Mangroves, seagrasses and salt marshes during 2010–2018. Sensors 2019, 19, 1933.

Pieschke, R.L. U.S. Geological Survey Distribution of European Space Agency's Sentinel-2 Data: U.S. Geological Survey Fact Sheet 2017–3026; U.S. Geological Survey: Sioux Falls, SD, USA, 2017; 2p. Remote Sens. 2024, 16, 2 19 of 19

Roughgarden, J.; Running, S.W.; Matson, P.A. What does remote sensing do for ecology? Ecology 1991, 72, 1918–1922.

Sanderson, E.W.; Ustin, S.L.; Foin, T.C. The influence of tidal channels on the distribution of salt marsh plant species in Petaluma Marsh, CA, USA. Plant Ecol. 2000, 146, 29–41.

Scavia, D.; Field, J.C.; Boesch, D.F.; Buddemeier, R.W.; Burkett, V.; Cayan, D.R.; Fogarty, M.; Harwell, M.A.; Howarth, R.W.; Mason, C.; et al. Climate change impacts on US coastal and marine ecosystems. Estuaries 2002, 25, 149–164.

Schuerch, M.; Vafeidis, A.; Slawig, T.; Temmerman, S. Modeling the influence of changing storm patterns on the ability of a salt marsh to keep pace with sea level rise. J. Geophys. Res. Earth Surf. 2013, 118, 84–96.

Schwarz, C.; van Rees, F.; Xie, D.; Kleinhans, M.G.; van Maanen, B. Salt marshes create more extensive channel networks than mangroves. Nat. Commun. 2022, 13, 2017.

Silvestri, S.; Marani, M.; Marani, A. Hyperspectral remote sensing of salt marsh vegetation, morphology and soil topography. Phys. Chem. Earth Parts A/B/C 2003, 28, 15–25.

Silvestri, S.; Marani, M. Salt-marsh vegetation and morphology: Basic physiology, modelling and remote sensing observations. Ecogeomorphology Tidal Marshes 2004, 59, 5–25.

Simas, T.; Nunes, J.P.; Ferreira, J.G. Effects of global climate change on coastal salt marshes. Ecol. Model. 2001, 139, 1–15.

South Atlantic Salt Marsh Initiative. Executive Summary: Marsh Forward—A Regional Plan for the Future of the South Atlantic Coast's Million-Acre Salt Marsh Ecosystem. 2023. Available online: https://www.marshforward.org (accessed on 5 August 2023).

Stagg, C.L.; Mendelssohn, I.A. Restoring ecological function to a submerged salt marsh. Restor. Ecol. 2010, 18, 10–17.

Stagg, C.L.; Osland, M.J.; Moon, J.A.; Feher, L.C.; Laurenzano, C.; Lane, T.C.; Jones, W.R.; Hartley, S.B. Extreme precipitation and flooding contribute to sudden vegetation dieback in a coastal salt marsh. Plants 2021, 10, 1841.

Tempest, J.A.; Harvey, G.L.; Spencer, K.L. Modified sediments and subsurface hydrology in natural and recreated salt marshes and implications for delivery of ecosystem services. Hydrol. Process. 2015, 29, 2346–2357.

Valiela, I.; Teal, J.M.; Volkmann, S.; Shafer, D.; Carpenter, E.J. Nutrient and particulate fluxes in a salt marsh ecosystem: Tidal exchanges and inputs by precipitation and groundwater 1. Limnol. Oceanogr. 1978, 23, 798–812.

Vo, Q.T.; Oppelt, N.; Leinenkugel, P.; Kuenzer, C. Remote sensing in mapping mangrove

ecosystems—An object-based approach. Remote Sens. 2013, 5, 183–201.

Wilson, A.M.; Evans, T.; Moore, W.; Schutte, C.A.; Joye, S.B.; Hughes, A.H.; Anderson, J.L. Groundwater controls ecological zonation of salt marsh macrophytes. Ecology 2015, 96, 840–849.

Xu, R.; Zhao, S.; Ke, Y. A simple phenology-based vegetation index for mapping invasive spartina alterniflora using Google Earth engine. IEEE J. Sel. Top. Appl. Earth Obs. Remote Sens. 2020, 14, 190–201.

Yagoub, M.M.; Kolan, G.R. Monitoring coastal zone land use and land cover changes of Abu Dhabi using remote sensing. J. Indian Soc. Remote Sens. 2006, 34, 57–68.

Yeo, S.; Lafon, V.; Alard, D.; Curti, C.; Dehouck, A.; Benot, M.L. Classification and mapping of saltmarsh vegetation combining multispectral images with field data. Estuar. Coast. Shelf Sci. 2020, 236, 106643.

Zhang, M.; Ustin, S.L.; Rejmankova, E.; Sanderson, E.W. Monitoring Pacific coast salt marshes using remote sensing. Ecol. Appl. 1997, 7, 1039–1053.

CHAPTER 4

SOUSS MASSA BASIN SUBSIDENCE ASSESSMENT USING INTERFEROMETRIC SYNTHETIC APERTURE RADAR[3]

[3] Richards, D. F., IV; Milewski, A. M. Submitted to *Water Resources Research*, June 2024

Abstract

The Middle East and North Africa (MENA) region represents the most water scarce area in the world. Due to rapid population growth, climatic regime effects, and increased anthropogenic activity, the water resource demand exceeds the sustainable supply. The Souss-Massa Basin in Morocco has experienced extensive groundwater abstraction causing accelerated subsidence rates. The primary groundwater aquifer, Plio-Quaternary Plain Aquifer, is pumped by over 20,000 wells at a rate of 650 MCM/yr., exceeding the rate of recharge by 260 MCM/year. Synthetic Aperture Radar (SAR) offers the ability to observe landscape changes through archived data. This radar technique provides effective observations for measuring movements (mm to cm) that cover a given area. Using SAR data acquired from the European Space Agency, the Souss-Massa Basin was analyzed to identify how the over-exploitation of groundwater resources influences landscape changes that impact groundwater dynamics. To support this analysis, the approximate amount of water stored in this region was determined by Gravity Recovery and Climate Experiment (GRACE). Results suggest there is a correlation between groundwater storage changes and land deformation in the Souss Massa basin. Total water storage and groundwater storage decreased to -10cm between 2016-2021, while the SAR analysis displayed land deformation from 2016-2021. In addition, this study provides applicability to other MENA regions facing similar water resource demands to provide the opportunity for better water resource management. As the demand for water resources is expected to increase, this coupled remote sensing approach will enhance our understanding of the landscape changes that are occurring to better meet such water resource demand.

4.1. Introduction

Global water resources pose an eminent threat to the sustainability and functionality of the world. Many parts of the developing world, specifically arid and semiarid environments, will experience large increases in relative water demand [*Vorosmarty et al., 2000*]. Groundwater abstraction and water depletion will continue to increase with the pace of water demand (Figure 4-1) [*Wada et al., 2010*]. Water use in Africa is set to increase substantially over the next few decades because of population growth and irrigation for agriculture [*Vorosmarty et al., 2005*]. Water is scarce in the North African region. Population growth and water usage, particularly for irrigation, have contributed to water stress through withdrawals of more than annual renewable supplies [*Milewski et al., 2020*]. Though all North African countries experienced declines in groundwater storage except for Morocco, the Souss Massa Basin in Morocco has experienced the effects of anthropogenic demand and groundwater depletion [*Hssaisoune et al., 2016, Lezzaik and Milewski, 2017*]. The Souss Massa Basin faces extreme water resource demand resulting in the over-abstraction of its aquifers. This anthropogenic activity contributes to coastal subsidence influencing groundwater and total water storage changes. Due to the Souss Massa Basin's current state, this examination focused on identifying a correlation between surface displacement and groundwater storage changes. Understanding the available groundwater resources and how they are impacted from over-abstraction will not only better characterize this coastal dryland but also allow for informed decision-making in meeting the water resource demand.

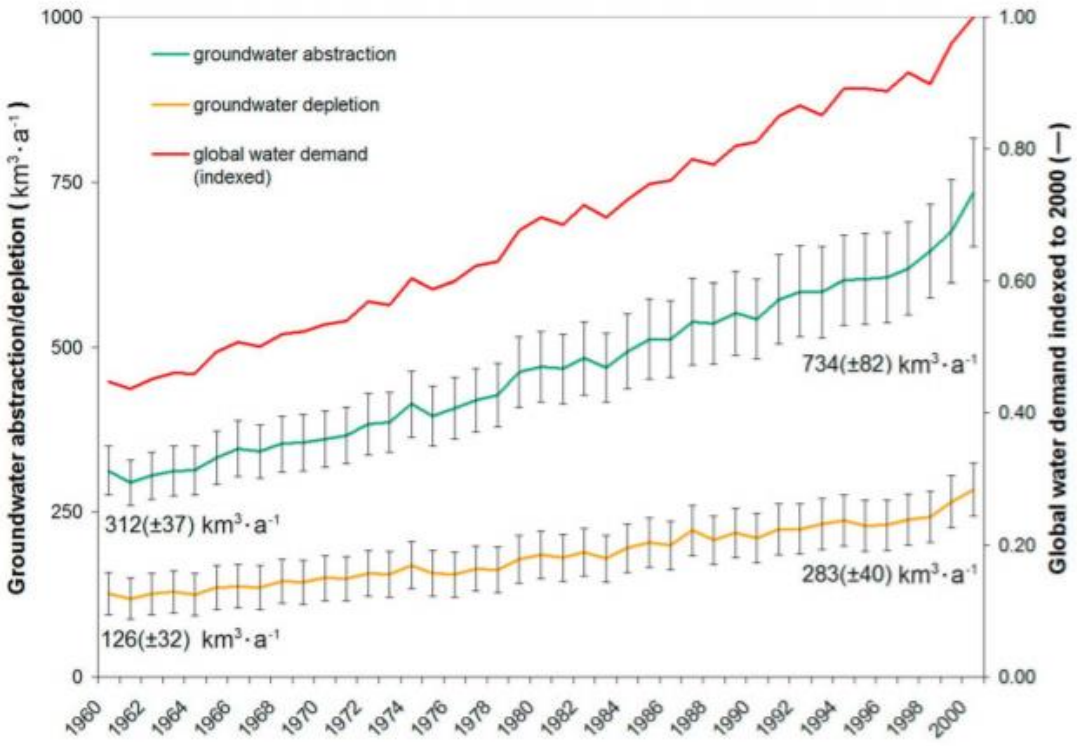

Figure 4-1. Global groundwater abstraction, depletion and demand indexed between 1960-2000 [*Wada et al., 2010*].

In the Souss Massa Basin, the volume of water used amounts to approximately 1,100 million m^3, 68% of this volume is pumped from groundwater. The volume of water allocated to agriculture amounts to almost 1,050 million m^3 for irrigation and around 50 million m^3 to drinking and industrial water [*Hssaisoune et al., 2016*]. According to the Hydraulic Agency of Souss-Massa-Draa Basin, the demand for drinking and industrial water has grown from 52 mm^3 in 2005 to 70 mm^3 in 2020. The increase in water demand irrigation from the hydro-agricultural development is estimated to grow from 149,000 ha in 2003 to nearly 150,000 ha in 2020 [*Hssaisoune et al., 2016*]. Consequently, recurring, and extended periods of drought have increased water scarcity, resulting in the over-abstraction of groundwater sources [*Bouchaou et al., 2011; Bouchaou et al., 2008; Tagma et al., 2009*]. Local agencies estimate the total water abstraction is 650 million cubic meters per year. This exceeds groundwater recharge by an

estimated 260 million cubic meters annually. The recurring groundwater abstraction has led to a decrease in the water table levels in a range of 0.5-2.5 m/year in the last four decades (Figure 4-2) [*Souss-Massa-Draa Hydraulic Basin Agency, 2007*].

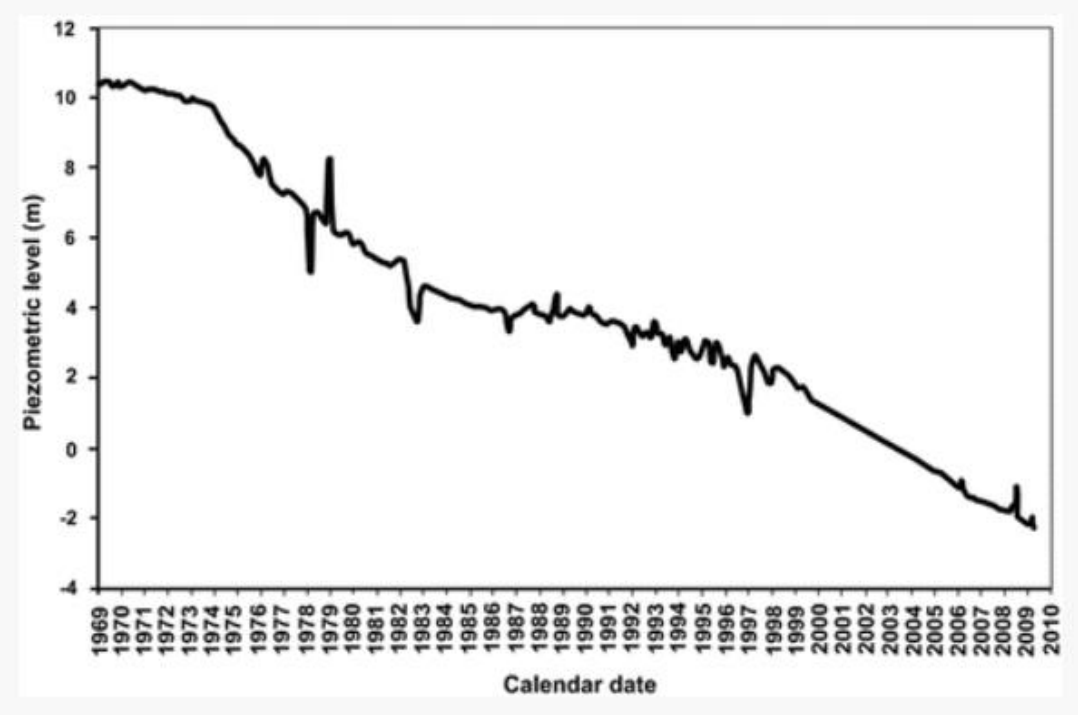

Figure 4-2. Water table decreases during the past 4 decades (1969-2010) [*Hssaisoune et al., 2016*].

The water balance and water levels of the Souss-Mass Basin indicate an overall decrease in water resources due to the combination of the natural decreased recharge and extent of abstraction. From 1972 to 2007 the water balance of shallow aquifers displayed a decreasing trend of infiltration from rain and surface runoff in the Souss and Massa-Chtouka aquifer system, except for a spike in 1996 (Table 4-1). The reduction of the water table of the Souss and Massa-Chtouka aquifer is due to the decrease of infiltration from soil compaction and vegetation, less/variable rainfall, and over-abstraction of groundwater resources. The decreasing water deficit varies between both shallow aquifer systems, which are variable in time and space, quantity of recharge and inflow to groundwater systems, the amount of groundwater abstraction, and the distribution

and intensity of the selected pumping wells. The demand for water in the Souss Massa Basin exceeds the sustainable supply, but what is important to note is the effect climate regimes have on recharge in this region. It is evident that recurring droughts will further deplete the available water resources [*Hssaisoune et al., 2016*].

Table 4-1. Water balance of the shallow aquifer of Massa-Chtouka (million cubic meters) [*Hssaisoune et al., 2016*].

Shallow aquifer	**1976**	**1979**	**1985**	**1994**	**1996**	**1998**	**2003**	**2007**
Recharge								
Infiltration from rain and surface runoff	66.2	62.8	57.8	31.3	105	29.7	39.6	31
Valley bank infiltration	88.7	208.5	50.2	17.3	490	31	199	160
Irrigation water return	14.3	13.7	8	10.2	80	17.4	15.8	4.5
Artificial recharge	–	–	–					9
Upward flow from deep groundwater	3	3	3	3	3	3	3	3
Contribution from exposed aquifers	48	48.8	43.7	46.2	192	174.9	65	60
Total recharge	220	337	163	108	870	256	323	268
Discharge								
Groundwater flow	22	19.9	15	19	142	16.4	4	4
Upward by Souss River	8.2	60.5	0	0	0	0	0	0
Pumping for irrigation by traditional farmers	116	73.7	11.1	65.4	33.8	67.6	519	521
Pumping for irrigation for public and private sectors	250	278.1	365.4	375	431	488		
Pumping for drinking and industrial water	8.1	9.8	16.6	18.6	30	41.9	28.7	26
Total discharge	405	442	408	478	637	614	551	555
Balance	−185	−105	−246	−370	233	−358	−228	−283

Climatic changes in the Souss Massa Basin have not only impacted groundwater resources, but has collectively, with the abstraction of groundwater, exploited this region. Monitoring water resources in an arid region is difficult, as reliability and availability of datasets are not common [*Milewski et al., 2009; Ritzema et al., 2010; Milewski et al., 2009; Ireson et al., 2006; Lezzaik et al., 2018; Milewski et al., 2015*]. Numerous studies on precipitation and/or temperature have characterized this basin and climate variables on temporal and spatial scales [*Tramblay et al., 2013; Bouchaou et al., 2011; N'da et al., 2016; Filahi et al., 2016; Hssaisoune et al., 2017*].

However, climate and hydrogeological data must be interpreted to understand the hydrogeological impacts on groundwater resources. Milewski et al., 2020, recognized the lack of available datasets to characterize this region, thus, the development of an integrated model of satellite remote sensing (e.g., Gravity Recovery and Climate Experiment (GRACE), Tropical Rainfall Measuring Mission (TRMM)), Soil Water Assessment Tool (SWAT), and climate projections model was created [*Milewski et al., 2020*]. This model evaluated Morocco and the Souss Massa Basin on a regional scale.

The integrated model predicts an overall decrease in projected precipitation, -5.1% in 2020 to -10.6% by 2050, which in turn will lead to decreases in the amount of runoff (2020: -6.8%, 2050: -13.8%) and potential groundwater recharge (2020: -8.8%, 2050: -17.6%). As a result, the impact of climate change is expected to affect the groundwater more than surface water runoff [*Milewski et al., 2020*]. The areas are expected to receive low precipitation and higher temperatures where the majority is lost to evapotranspiration [*Milewski et al., 2020*]. Through remote sensing techniques, the determination of climate change in precipitation and total water storage was identified, examination of current and projected impacts on surface/groundwater resources was assessed, and the relation of climate regime effects on groundwater resources was investigated.

This study is not only critical in understanding the effects of climate regimes in the Souss Massa Basin hydrogeological system, but it also creates an approach to better understand groundwater resources in coastal drylands. Due to the climate regime effects occurring in the Souss Massa Basin resulting in the decrease of groundwater resources, land subsidence can take place. From the over-abstraction of groundwater resources, groundwater levels will decline causing aquifer compaction contributing to a decrease of total groundwater storage [*Ingebritsen and*

Galloway, 2014; Galloway and Sneed, 2014; Tolman and Poland, 1940; Poland and Davis, 1969; Poland, 1984; Sneed, 2008; Sneed and Galloway, 2000; Poland and Davis, 1969; Pavelko 2003].

In this process, groundwater levels drop in the aquifer causing a reduction of upward pressure by the fluid. If the downward pressure by the confining unit remains constant, an increase in effective stress by the aquifer can occur. As a result of over-abstraction, the effective stress acting on the aquifer will increase, causing the aquifer to consolidate. The hydraulic head will drop in the aquifer, eventually resulting in the same amount of head drop in the confining layer [*Sun et al., 1999*]. The fine-grained unconsolidated sediments that were originally deposited in random orientations are rearranged and compacted when groundwater levels decline. The result is stacked sediments have less occupancy space and less space between them. This could potentially cause the volume of the groundwater removed to be equal to the volume of subsidence [*Jacob, 1939; Narasimhan et al., 1984; Parker and Springfield, 1950*].

In identifying the correlation between surface displacement and groundwater storage changes, Interferometric Synthetic Aperture Radar (InSAR) and GRACE data was applied. InSAR is a heavily used platform that has been applied for decades to analyze land deformation associated with different phenomena [*Galloway and Hoffmann, 2007; Amelung et al., 1999; Chaussard et al., 2014; Li et al., 2017; Motagh et al., 2017; Norman and Heggy, 2015; Minderhoud et al., 2017*]. GRACE datasets have been proven to provide various hydrological interpretations including groundwater and total water storage anomalies [*Rodell et al., 2006; Yeh et al., 2006; Rodell and Famigletti, 2002; Feng et al., 2013; Voss et al., 2013; Rodell et al., 2009*]. Utilizing InSAR techniques in conjunction with GRACE data provides the opportunity to make informed assessments of the relative landscape changes influencing groundwater storage changes.

Integrating GRACE data with surface level changes to characterize terrain models has been proven to enhance monitoring capabilities [*Houborg et al., 2012; Long et al., 2013; Yirdaw et al., 2008*].

The Souss Massa Basin is a region that is highly dependent on the functionality of its aquifer systems, thus, better groundwater management practices need to be established. Combining the results from the InSAR data collection processing with the GRACE dataset is not routinely incorporated, however, this examination has proven to be beneficial in providing insight to the changes occurring. Through its capabilities the final output displayed its usefulness in interpreting how landscape changes impact groundwater resources.

4.2. Study Area

The Souss-Massa Basin is considered one of the most important agriculture areas in Morocco, producing more than half of Morocco's citrus and vegetables [*Choukr-Allah et al., 2014*]. This basin is located in the middle western region of Morocco, totaling 27,000 km^2 of occupying surface area with about 21,300 km^2 of the area representing mountainous terrain with the remaining plains covering 5,700 km^2 [*Hssaisoune et al., 2016*]. The plains contain the groundwater reservoir for this region. The Souss-Massa Basin is bounded by the Anti-Atlas Mountains in the south, the High Atlas Mountains in the north, the Siroua massif in the east, and the Atlantic Ocean in the west (Figure 4-3). The elevations in this basin range from 0 m, the Atlantic Ocean, to 4,168 m, the Toubkal summit in the High Atlas Mountains [*Hssaisoune et al., 2016*].

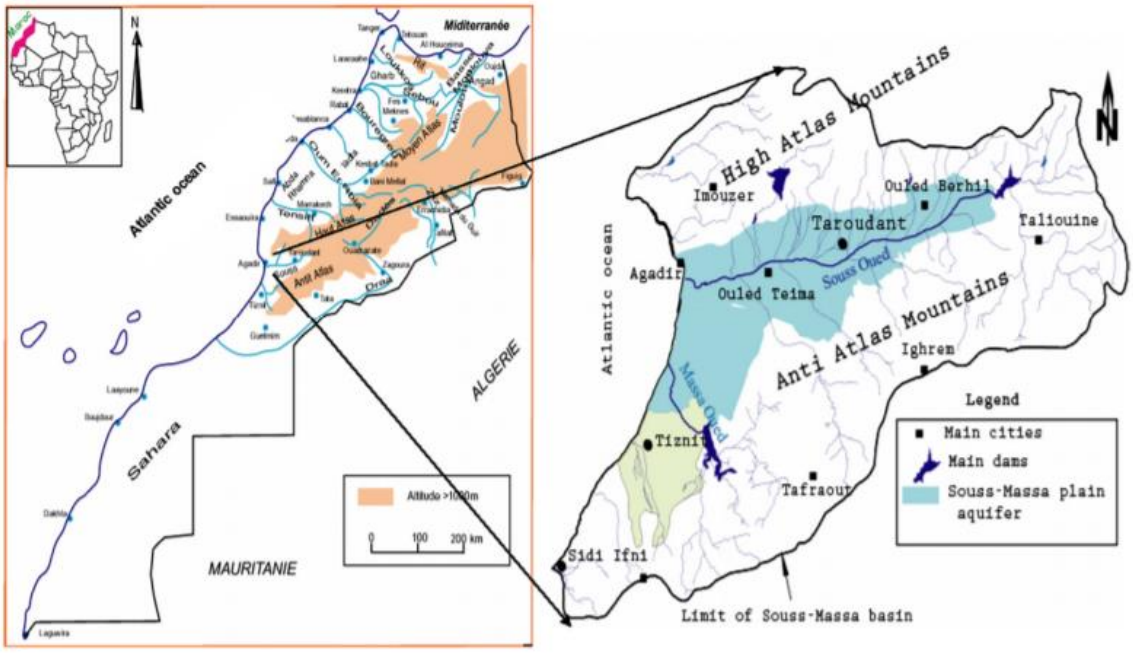

Figure 4-3. Geographical map of the Souss-Massa basin in the western region of Morocco [*Bouchaou et al., 2008*].

The geology of the Souss-Massa Basin formations range in age from Paleozoic to Quaternary [*Hssaisoune et al., 2016*]. This basin is composed of Plio-Quaternary sediments such as sands, gravels, and lacustrine limestone, covering the north of the basin and a Paleozoic schist basement in the south. The geomorphology of the Souss-Massa Basin is described as a plain that resembles the shape of a gutter that is characterized by the Atlas Mountain foothills following the Souss River [*Hssaisoune et al., 2016*]. The elevation of the plains ranges from 700 to 0 m over a distance of 150 km [*Saidi, 1995*]. As there are many geomorphological processes occurring, this basin is affected by spatial channel erosion occurring both laterally and vertically, alluvial processes resulting in colluvium deposition of sediments, and braided channels that are widening. Aeolian processes also occur, creating ripples and dunes. Winds may erode, transport and deposit sedimentary materials depending on the local climatic regime.

The Souss Massa basin is a part of the pre-African trench, which is characterized as a narrow zone of sedimentary deposits embedded between the High Atlas in the north and the Anti-Atlas in the south. Beneath the Souss Valley are detritic formations and calcareous marls of Plio-Quaternary deposits that overlie a Cretaceous-Eocene syncline [Dijon, 1969]. The northern flank of the syncline appears on the side of the High Atlas Mountains and the southern flank is located on the hills in the middle of the valley.

The age of the geological formations ranges from Paleozoic to Quaternary. The plain is composed of Plio-Quaternary sediments, which cover a Cretaceous syncline in the north of the basin and a Paleozoic schistose basement in the south [*Hssaisoune et al., 2016*]. The Plio-Quaternary strata in the plain are locally heterogeneous both in vertical and lateral directions. The syncline axis is oriented in the east-west direction. The northern flank outcrops vertically in the High Atlas and marks a vertical fault, known as the South Atlas fault [*Hssaisoune et al., 2016*]. The basin is often characterized as a tertiary synclinorium structure [*Hssaisoune et al., 2016*]. The plain is an E-W oriented depression separated from the Ouarzazate basin by the Siroua high plateau.

The subsurface structure of the Souss Massa plain has discontinuities corresponding to faults of the basement of the plain that are divided into NE-SW, WSW-ENE, and N-S. The orientation of the NE-SW discontinuity corresponds to the El Klea fault. This fault extends towards the ocean, separating the coastal area of the Souss downstream of the western plain of Chtouka and middle of the Souss Massa plain [*Hssaisoune et al., 2016*]. The discontinuity oriented ENE-WSW is of Cretaceous outcrops toward the Anti-Atlas and High Atlas [*Hssaisoune et al., 2016*]. The discontinuity oriented N-S passes through Oulad Berhil. These faults have divided the Souss Massa plain into four underground compartments: (1) a collapsed area between the El Klea fault

crossing the Atlantic coast forming the coastal aquifer of the Souss Massa basin, (2) a depression in the south by Cretaceous hills in the plain and to the north by the South Atlas foothills, (3) an area between the Cretaceous outcrop in the center of the Souss Valley and Paleozoic outcrop of the Anti-Atlas, and (4) a compartment between Oulad Berhil and Aoulouz in the Souss upstream [*Hssaisoune et al., 2016*].

The climate of the Souss-Massa Basin is semiarid to arid with rainfall varying annually. The mean annual temperatures estimated during 1981-2010 display the lowest temperatures of 10-11°C in the eastern mountainous areas, while the highest temperatures of 18-19°C occur in the southwestern region of the basin. The annual evaporation varies from 1,400 mm in the mountains and near the Atlantic coast to 2,000 mm in the plains [*Ait Brahim et al., 2016*].

The lithology of the Souss Massa basin has a complex lithology. The three dominant facies are: (1) lacustrine, clayey limestone, and calcareous marls overlain by (2) fluviolacustrine facies of sandy clayey material in the lower part, and (3) solidified conglomerates that are near the foothills of the High Atlas region [*Hssaisoune et al., 2016*]. The Souss formation transmissivity ranges from 7×10^{-3} and 8×10^{-4} m^2/s. The thickness ranges from 200 to 400 m zones (Figure 4-4) [*Hssaisoune et al., 2016*]. In the fossil bed of the Souss Valley there are sands, sandstones and gravels from alluvium material dating from the Quaternary. The transmissivity is in the range of 50×10^{-2} m^2/s with a storage coefficient ranging between 5×10^{-2} and 1×10^{-1}. The thickness of this fossil bed is from 20 to 40 m and can reach 50 m upstream (Figure 4-4) [*Hssaisoune et al., 2016*]. South of Agadir are conglomerates, sandstones, and shaly limestones form the Pliocene Agadir marine (Figure 4-4). The transmissivity in the Agadir marine ranges between 2×10^{-3} and 20×10^{-3} m^2/s [*Hssaisoune et al., 2016*]. The Cretaceous outcrops in the plain are located in the center of the plain at the hillf of the Cretaceous syncline. This outcrop flanks the Turonian outcrops

and interacts laterally with the Plio-Quaternary aquifer [*Hssaisoune et al., 2016*]. The karstified area has a transmissivity ranging from 5 x 10^{-2} and 20 x 10^{-2} m^2/s. The deep karst is representative of lower transmissivity values of 2.5 x 10^{-4} m^2/s [*Hssaisoune et al., 2016*]. This facies ranges from 10 to 30 m thick (Figure 4-5).

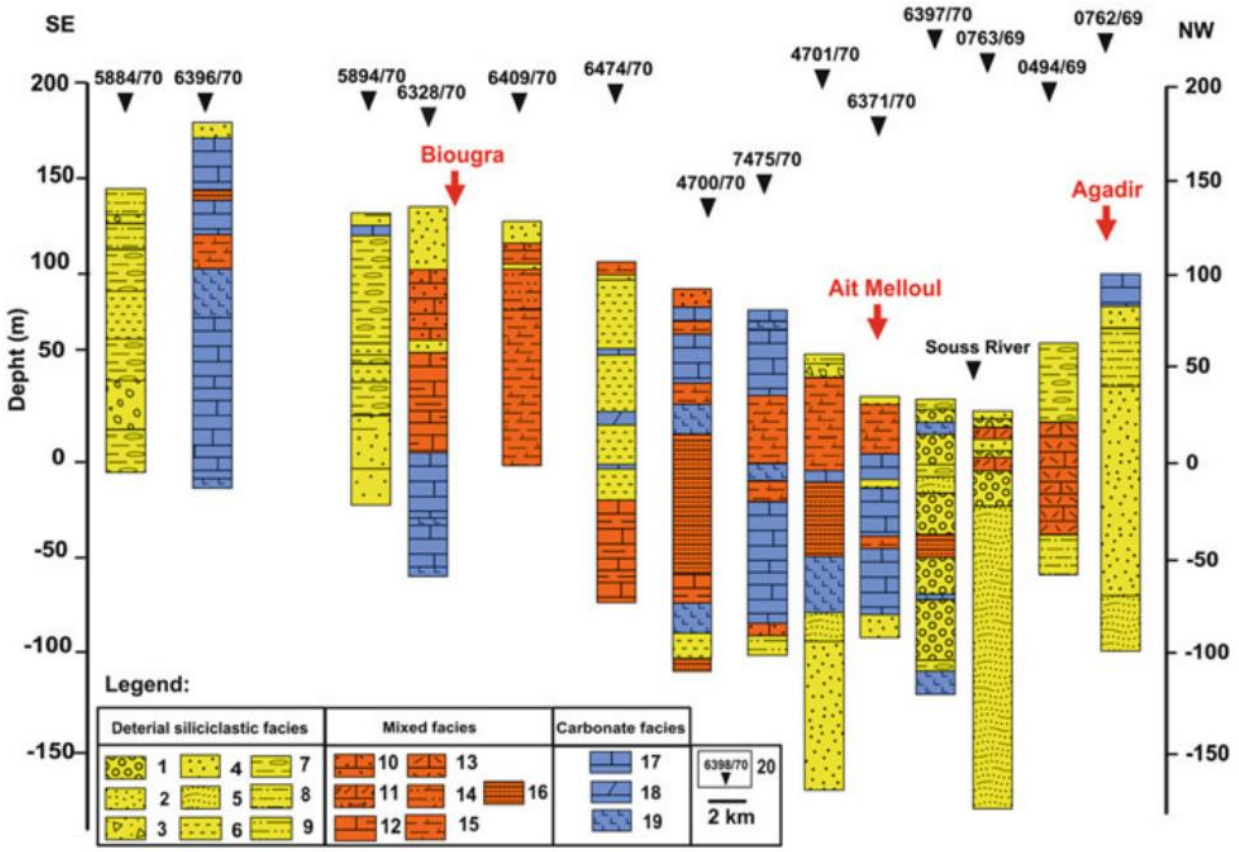

Figure 4-4. Geological cross section established after hydrogeologic borehole data in the Souss displaying lithology. (1) pebbles; (2) sand; (3) alluvium; (4) sandstone; (5) marls with pebbles; (6) clay; (7) clay and pebbles; (8) sandy clay; (9) clayey sand; (10) sandy limestone; (11) shelly limestone; (12) clayey limestone; (13) calcareous marls; (14) sandy maarl; (15) alternance marl and calcareous marls; (16) clay and marl; (17) limestone; (18) dolomite; (19) marl; (20) borehole code [*Hssaisoune et al., 2016*].

The hydrology of this region is dominated by the Souss and the Massa Rivers, creating two hydrographic regions that have their independent topographic and drainage systems. The Atlas Mountain tributaries combine, forming the Souss Valley. This valley flows into the plains extending east to west toward the Atlantic Ocean. The flow of the Souss River and its tributaries are seasonal with irregular and sometimes high floods between October and February. The hydrogeology of the Souss-Massa Basin represents a shallow and deep aquifer system that is directly influenced by the dry seasons, thus impacting the groundwater availability. In the shallow aquifer, groundwater flows through sedimentary material such as sandy marl, sandstone, conglomerates, calcareous marl, limestone, sandstone, silt, and alluvium across the plain. Conglomerate formations are mainly from alluvial fans on the mountainous foothills [*Bouchaou et al., 2008*]. Further towards the south there are Neogene and Quaternary orogenic phases lacustrine formations composed of calcareous clay, interbedded clay, and sandstone with conglomerates [*Ambroggi, 1952; Dijon, 1969*]. The deep confined aquifer in the northern part of the region is recharged from lateral water flow from the foothills of the High Atlas Mountains [*Hssaisoune, 2016*]. Some recharge also occurs from infiltration from the rivers in the foothills [*Boutaleb, 2000*]. The deep aquifer is composed of Cenomanian-Turonian limestone and dolomite [*Boutaleb, 2000*]. The groundwater tables are affected by annual rainfall and soil permeability.

4.3. Methodology

To achieve our objectives, we applied a Sentinel-1 InSAR data processing procedure using GRACE satellite mission to determine total water storage/groundwater storage of the basin. Sentinel 1-A Single Look Complex (SLC) data (2016-2021) were acquired from the United States Geological Survey (USGS) Earth Explorer and the European Space Agency (ESA) [*European Space Agency-Sentinel, 2022*]. Twelve Sentinel-1 images were acquired to capture surface

subsidence across the basin. The data presented includes three time periods: 21 December 2016 to 28 December 2017, 23 December 2018 to 30 December 2019, and 21 December 2016 to 31 December 2021. The Sentinel Application Platform (SNAP) was used as the integrated processing framework to identify the surface subsidence occurring. A three-step process was utilized to quantify the displacement measurements. The first step was InSAR processing, where phase measurements were determined from interferograms, topography, deformation, and coherence image estimation from Sentinel 1-A SLC data. Next, Differential Interferometric Synthetic Aperture Radar (DInSAR) was used to produce the differential interferogram to determine the extent of deformation. Finally, a phase unwrapping technique was applied to display the displacement measurements. Geocoding was then used to produce a terrain corrected product of relative changes. GRACE's satellite mission provided the opportunity to determine groundwater changes by observing changes in the Earth's gravity field to approximate changes in the amount of water stored in the basin.

In InSAR analysis the two common sources of error are decorrelation, both temporal and geometric, and phase errors. These are introduced by the spatially and temporally random variations of the refractive index of the atmosphere and ionosphere [Simons and Rosen, 2015]. Decorrelation leads to difficulty in interpreting the geodetic measurements because the repeat period of the orbital satellites is in the order of weeks and temporal sampling is poor. Though these errors were addressed and corrected in this study, to further mitigate this issue and provide a more accurate measurement, global positioning system (GPS) coordinates can be used. GPS measurements have the advantage of frequency measurements for ionospheric correction and continuous temporal sampling while observing multiple satellites.

GRACE datasets are useful; however, the limitations must be known. These datasets have approximately a resolution of 1 degree latitude by 1 degree longitude representing a 100 x 100 km square area. With the low resolutions, decisions based on a single cell comes with high uncertainty. However, numerous studies have displayed that the same mass concentrated over small areas are still proven to be useful [*Longuevergne et al., 2013; Tourian et al., 2015; Huang et al., 2015*].

Even with these limitations and challenges, this examination has provided insights on the usefulness of remote sensing techniques in an arid water scarce region, while also completing the examination's purpose of (1) identifying the surface displacement occurring and (2) making a correlation between the surface displacement and groundwater storage. This first-order approach is valuable in advancing our understanding of the changes occurring in the region and the advancement of remote sensing-based approaches in water resource management.

Interferometric Synthetic Aperture Radar (InSAR)

InSAR directly measures the phase change between two coherent phase images (interferograms) of the same ground pixel on Earth's surface. If the distance between the ground and satellite changes between the two acquisitions due to surface movement, a phase shift will occur. This technique is used for mapping ground deformation from Synthetic Aperture Radar (SAR) images of the Earth's surface that is collected from orbiting satellites (i.e., Sentinel-1, ERS-1, ERS-2, ENVISAT, ALOS PALSAR, TerraSAR-X, COSMO-SkyMed, RADARSAT-2 [*Ferretti, 2014*]. The measurement of three-dimensional surface displacements, with some spatial continuity from natural and human-induced phenomena, details a time series from data archived images. The radar waves penetrate most weather clouds providing its own illumination so SARs can image any time of day under most conditions.

This technique involves acquiring raw image data from the transmission of a series of coded pulses from the designated flight track or azimuth direction and imaging the designated terrain through radar side points (Figure 4-5). Through the duration of the flight track, an echo is recorded from each pulse between transmission events to detail the amplitude and phase shift. The amplitude is the strength of the return signal, influenced by the surface physical properties. The phase is the measurement in units of radar wavelength detailing the changes in distance between the time of the two radar images. These pulses effectively return the integrated backscatter over the pulse and azimuth beam extent. When the two signals are combined, the interferometric phase difference between the received signals is formed for each image point. Each image is resolved into range-azimuth coordinates. The phase difference is then determined, resulting in an interferogram. The interferogram is the geometric path length difference to the image point (Figure 4-6). This representation depends on the changes in surface topography, and through this representation, the phase difference can be converted into an altitude for each image point. The flight track travels at constant azimuth across the landscape. The range resolution of radar has backscattered energy from all surface scatterers within the range resolution that contributes to the radar return over the given area [*Simons and Rosen, 2015*]. The accuracy of the InSAR measurement is typically several millimeters to centimeters, being a fraction of the SAR wavelength, whereas the stereoscopic accuracy is in the order of several meters [*Simons and Rosen, 2015*].

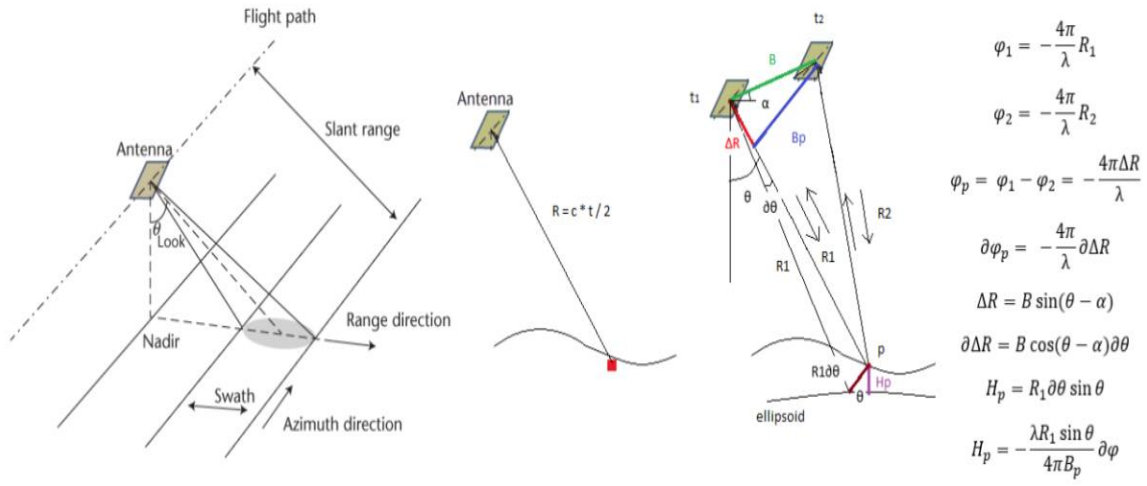

Figure 4-5. SAR imaging geometry (left image), Determination of slant range (distance between radar and target) as R = c*t/2 (middle image) and InSAR geometry (right image) based on which the height of point P (Hp: topographic height) is determined, B is the baseline (orbit distance), Bp is the perpendicular baseline (projection of perpendicular baseline to the slant range), θ is the look angle of the satellite [*Simons and Rosen, 2015*].

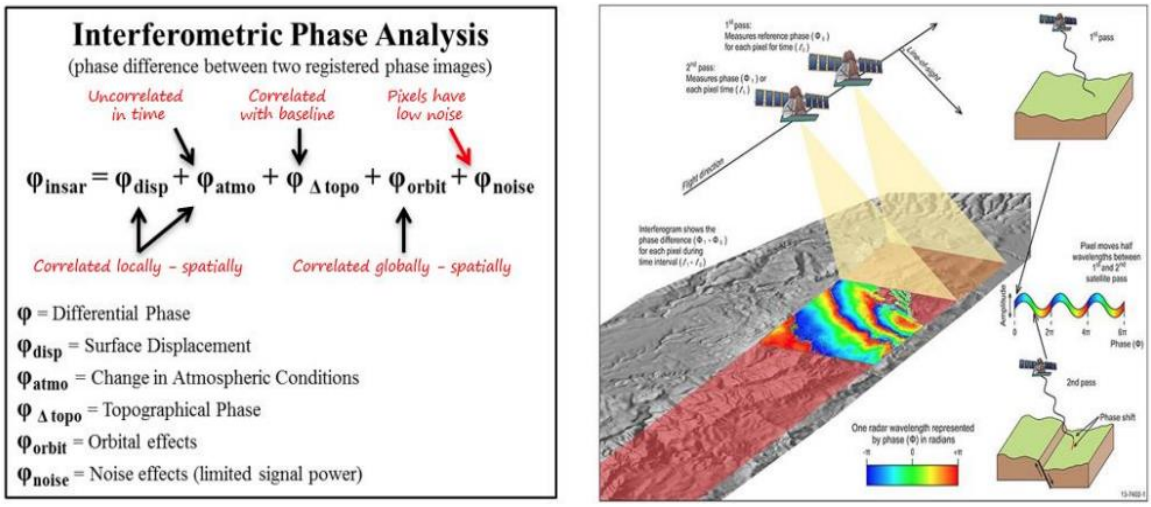

Figure 4-6. Two SAR images of the same area are acquired at different times. If the surface moves between the two acquisitions a phase shift is recorded. An interferogram maps this phase shift spatially [*Geoscience Australia, 2019*].

Data Acquisition

Sentinel 1-A SLC datasets were collected from 2016 to 2021 over the Souss Massa basin. The Sentinel-1 mission includes twin satellites with synthetic aperture radars (SAR) and together provide all-weather, day-and-night imagery of Earth's surface. The Sentinel-1 A data product was acquired in Interferometric Wide Swath (IW) mode and distributed as a Level-1 product in a Single Look Complex (SLC) product type [*European Space Agency-Sentinel, 2022*]. This product was chosen as it represents images in the slant range by azimuth imaging plane, in the image plane of satellite data acquisition. Each of the image pixels contain the magnitude value (amplitude and phase data) and are georeferenced using orbit data from the satellite. The satellite provides global coverage with a center frequency of C-band at 5.405 GHz. In using the IW sub-swath, the polarization chosen was Vertical Transmit-Vertical Receive (VV) Single Polarization, due to its sensitivity of providing polarized signal returns over flat surfaces [*European Space Agency-Sentinel, 2022*]. The Spatial Resolution is 5 x 20 m and a swath width of 250 km [*European Space Agency-Sentinel, 2022*]. The Off-Nadir Angle, the angle between the local nadir vector and the local magnetic field vector pointing towards the magnetic north, is 29.1° to 46.0° [*European Space Agency-Sentinel, 2022*].

GRACE time series data was acquired from 2003 to 2021. The time series data provided estimates of total water storage (cm) and groundwater storage (cm) anomalies. The raw GRACE data was processed using NASA's Global Land Data Assimilation System (GLDAS) model to compute the surface water component [*NASA GLDAS, 2004*]. To compute total water storage (TWSa), the sum of the components of the GLDAS models that represent surface water storage is subtracted by the total of the GRACE dataset to estimate a groundwater storage anomaly (GWa) [*McStraw et al., 2022*]. To compute the GWa, the canopy storage dataset (CANa), snow water

equivalent (SWEa) and the soil moisture (SMa) of the GLDAS model are converted by subtracting the mean of the values and averaging them across the three GLDAS model to produce a component anomaly dataset [*McStraw et al., 2022*]. A standard deviation from the GLDAS models is used to estimate uncertainty and error range. Using this mass balance approach, the groundwater anomaly is produced [*McStraw et al., 2022*]. Detailing the difference between the TWSa and the sum of the surface water component anomalies. Please see below:

$$GWa = TWSa - (SWEa + CANa + SMa)$$

The uncertainty and error range of the groundwater storage component from both GRACE and GLDAS is estimated by computing the square root of the sum of the squares of the uncertainty of the individual components (i.e., TWSa, SWEa, CANa, SMa) as measured by standard deviations [*McStraw et al., 2022*]. Please see below:

$$GWa = \sqrt{((\sigma TWSa)^2 - (\sigma SWEa)^2 - (\sigma CANa)^2 - (\sigma SMa)^2)}$$

Data Processing

To perform this analysis, model builder workflow was created in SNAP 9.0.0 64-Bit. In the Sentinel toolbox, two sub-swath images are selected for the specified years to identify the subsidence that occurred. The pre-processed sub-swath images are split between 2 to 5 bursts of the total 8 bursts of radar echoes that are representative of this image series (Figure 4-7). The bursts are retracted to images on the specific area of study (i.e., Souss Massa basin). The parameters used to process the split images in Sentinel-1 Tops Split include selecting the IW sub-swath and VV polarization. The output product is the split image displaying demarcation lines defining the bursts. This process is repeated for the second selected image.

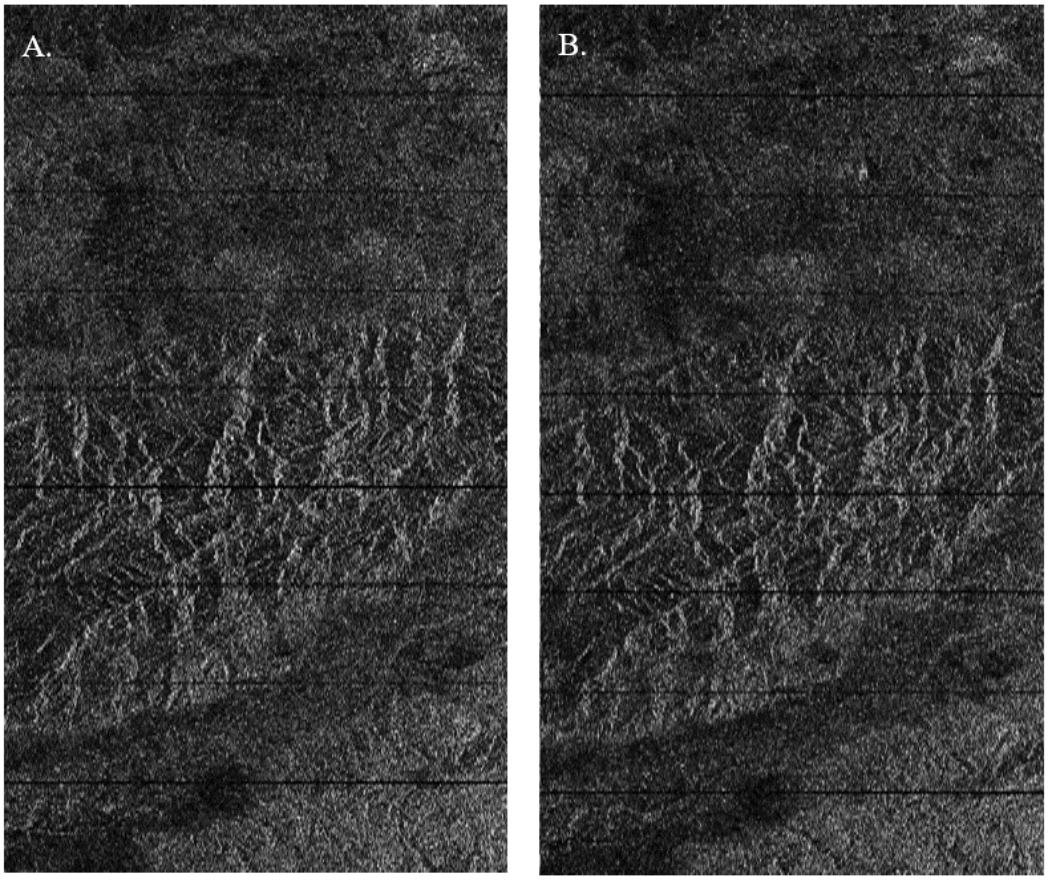

Figure 4-7. Sentinel 1-A SLC sub-swath images of the 8 bursts representative of the time series. Image (A.) 2020 sub-swath, Image (B). 2021 sub-swath

The orbital file for the selected images is defined as the 3rd polynomial. This file provides accurate satellite position and velocity data for the images captured. The Sentinel images are co-registered from a Shuttle Radar Topography Mission (SRTM) 3 Arc-Second Digital Elevation Model (DEM) using a BICUBIC interpretation DEM re-sampling method to ensure each ground target corresponds to the same pixel in range azimuth of both images. To refine the images, the Enhance Spectral Diversity (ESD) is added to the model to exploit the data. The ESD performs range and azimuth correction for every burst and overlapped area. ESD outputs an interferogram and coherence image estimation from the co-registered images (Figure 4-9). Due to the images

consisting of a series of bursts, TOPSAR Deburst is incorporated in the model to de-burst the image so that it has a continuous coverage of the ground surface (Figure 4-8).

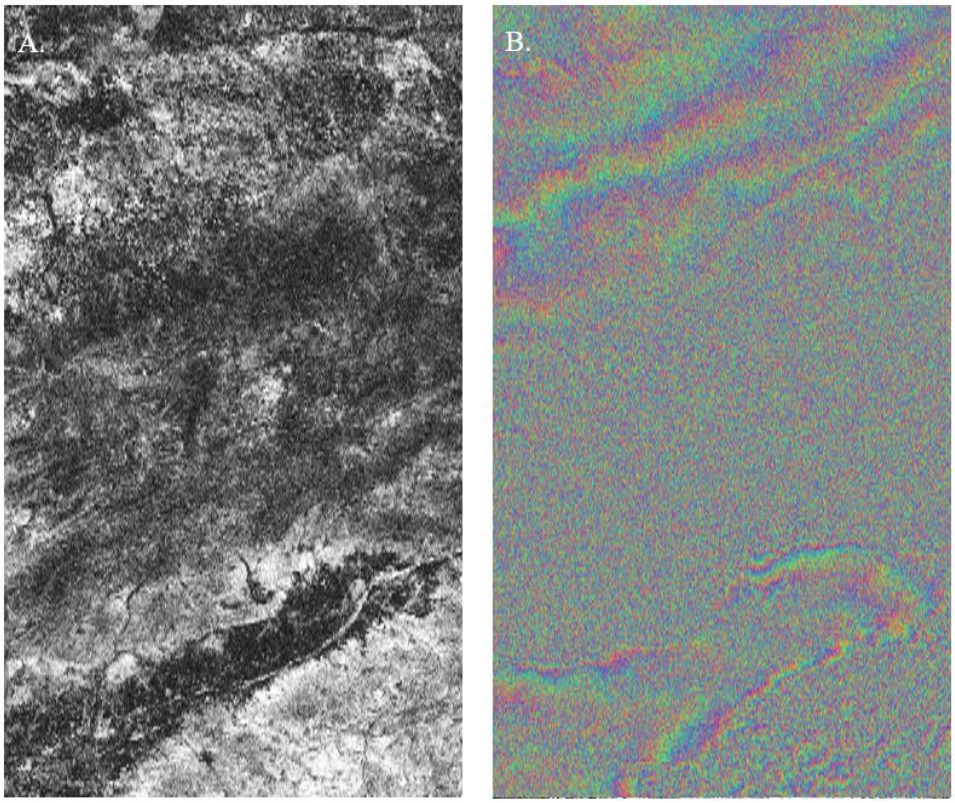

Figure 4-8. Coherence image estimation from the ESD output (Image A). De-bursted interferogram of ground surface (Image B).

Differential Interferometric Synthetic Aperture Radar (DInSAR)

DInSAR is a technique used to exploit multiple SAR images acquired over the same area and appropriate the data processing and analysis procedures to separate the phase displacement from the other phase components to estimate the images (Table 4-2).

Table 4-2. DInSAR technique to identify phase difference between two images.

DInSAR principle of first image *(Phase M)*:	$\varphi_M = \varphi_{geom\text{-}M} + \varphi_{scatt\text{-}M} = \frac{4 \cdot \pi \cdot MP}{\lambda} + \varphi_{scatt\text{-}M}$
DInSAR principle of second image *(Phase S)*:	$\varphi_S = \varphi_{geom\text{-}S} + \varphi_{scatt\text{-}S} = \frac{4 \cdot \pi \cdot SP}{\lambda} + \varphi_{scatt\text{-}S}$
InSAR technique exploits the phase difference *(Phase S- Phase M)*:	$\Delta\varphi_{Int} = \varphi_S - \varphi_M = \frac{SP - MP}{\frac{\lambda}{4\pi}} + \varphi_{scatt\text{-}S} - \varphi_{scatt\text{-}M}$

To output the deformation occurring in the Souss Massa basin, a multi-step approach is used in the model development. To emphasize the phase signatures related to deformation, topographical phase contributions are removed using the referenced SRTM 3 Arc-Sec DEM. TopoPhase Removal is selected to simulate an interferogram and subtract it from the processed interferogram. This step will correct the interferogram and produce a non-topographically influenced differential interferogram in the form of fringes. To improve image interpretability, multi-look processing is applied to reduce the speckled noise, geometric decorrelation, volume scattering, and temporal decorrelation of the original InSAR image. Phase Filtering is applied to further smooth the interferogram by reducing the phase noise. To reduce the pixel size and improve spatial resolution, there are four range looks and two azimuth looks, resulting in a mean square pixel value of 27.3 m. The resulting product of the DInSAR image corresponding to the deformation differs from the coherence image (Figure 4-9). The areas of low coherence (black areas) and high coherence (white areas) do not correspond to the phase measurements. To provide accurate phase measurements, Phase Unwrapping must be applied.

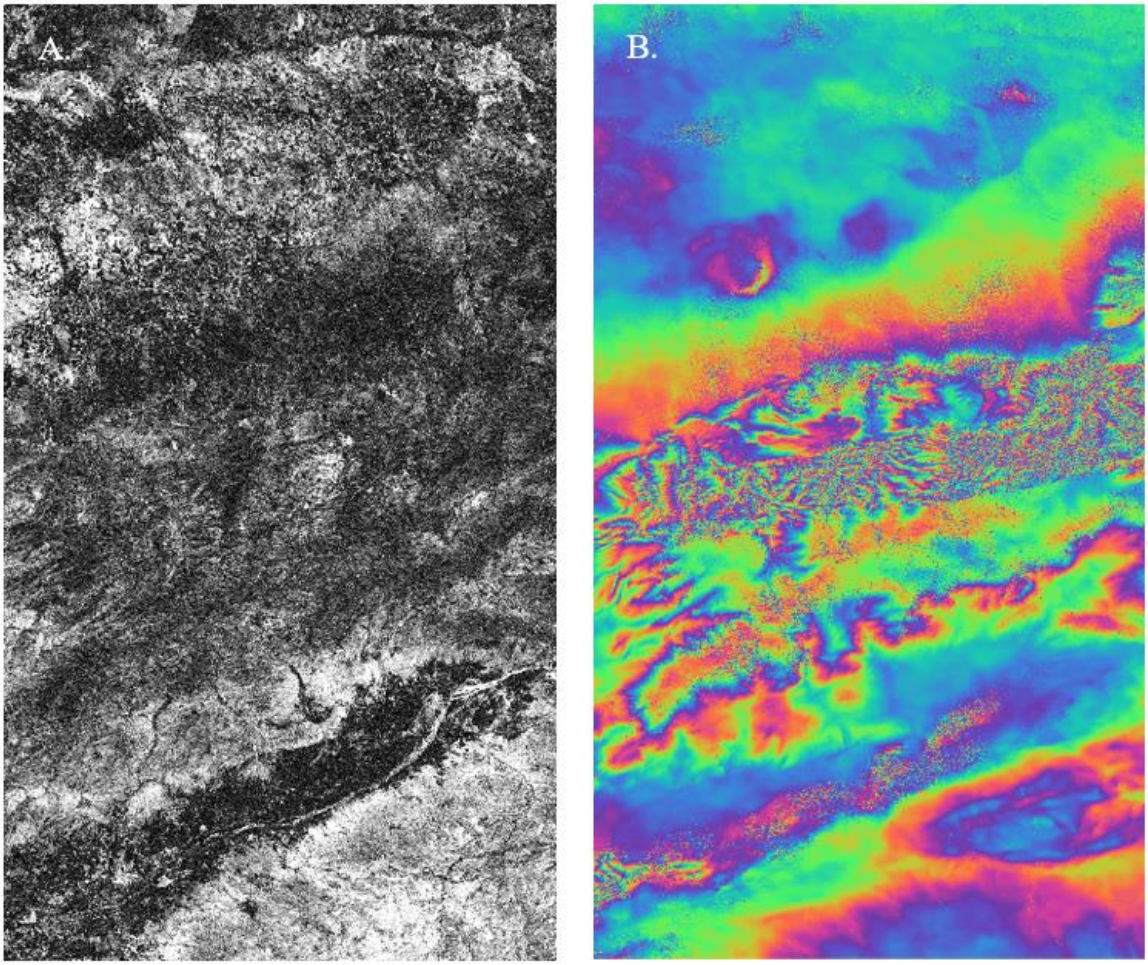

Figure 4-9. Coherence image after Phase Filtering is applied (Image A). DInSAR deformation image displaying fringes (Image B).

Phase Unwrapping involves correcting the ambiguity of the integrated phase difference between neighboring pixels. The interferometric phase is ambiguous and only known within 2π. To relate the interferometric phase to the topographic height, this unwrapping phase must occur. The altitude of ambiguity h_a is characterized as the altitude difference that generates an interferometric phase change of 2π after interferogram flattening. Once the integer values that are equivalent to an integer number of 2π phase cycles are deleted, the phase variation between two points on the flattened interferogram will provide a measurement of the actual altitude variation. To perform this important step, the Statistical-Cost, Network-Flow Algorithm for Phase

Unwrapping (SNAPHU) algorithm must be implemented. This algorithm computes the maximum likely unwrapped solution given from the observed input data [*Chen and Zebker, 2000; Chen and Zebker, 2001; Chen and Zebker, 2002*]. SNAPHU incorporates built-in statistical models specifically for topography, deformation, and smoothing data. SNAPHU completes the Phase Unwrapping process by outputting the phase displacement over the given area, however, the unwrapped product must be terrain corrected. SNAPHU does not correct for areas with no-elevation data, it assumes data is present. Due to this, geocoding is applied to correct for the terrain features. The Range-Doppler Terrain Correction is applied to mask areas without elevation. To complete this process, the SRTM 3 Arc-Sec DEM is used in the bi-linear interpolation of the DEM resampling and image resampling. From these process parameters the output image is orthorectified. The final output displays a geocoded masked and unwrapped interferogram characterizing the displacement of the area (Figure 4-10). The negative values of the phase displacement image display the surface subsidence, while the positive values display heaves.

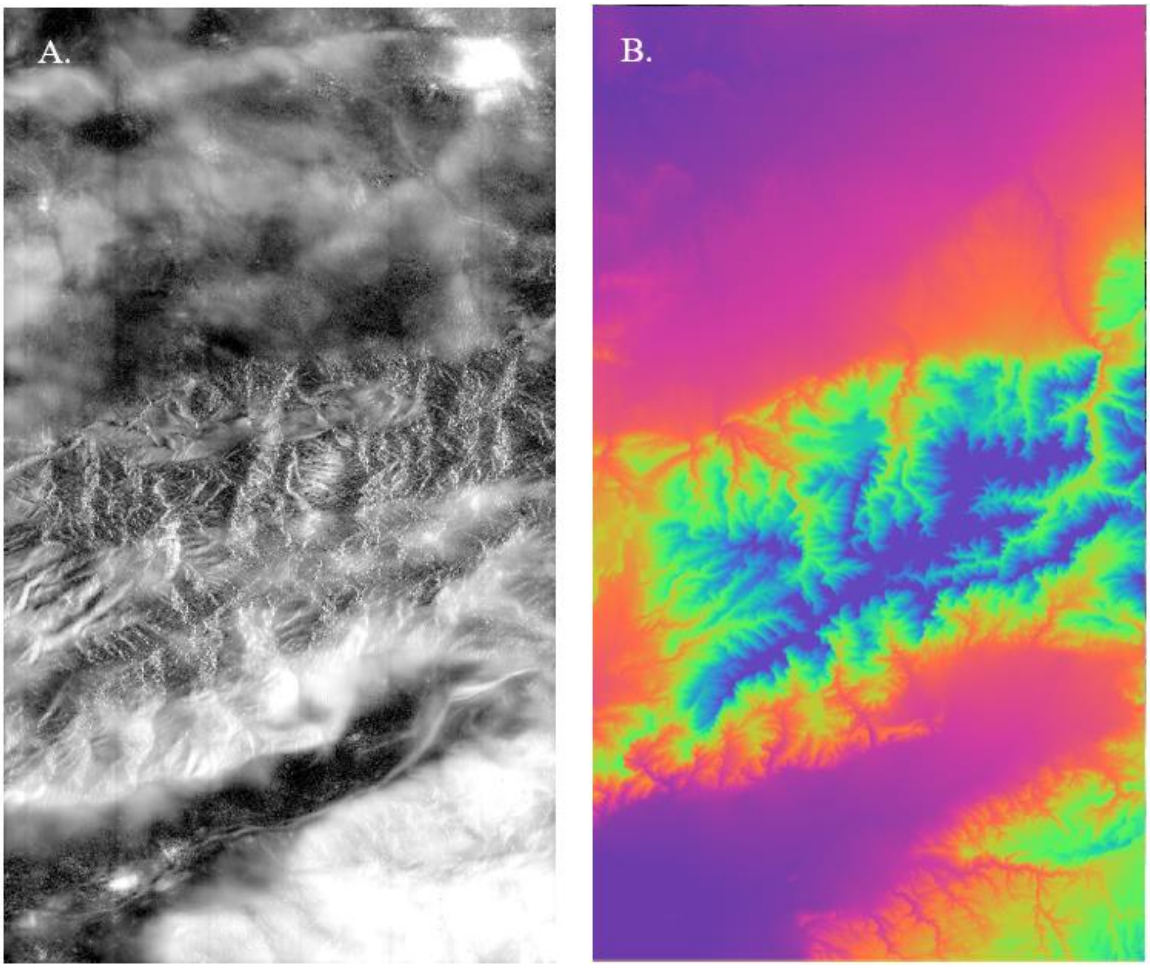

Figure 4-10. Phase unwrapped image processed using SNAPHU (Image A). Geocoded masked and unwrapped interferogram characterizing displacement of the area (Image B).

4.4. Results

The results show the amount of surface deformation that has occurred from 2016-2021 in the Souss Massa basin both temporally and spatially. Areas designated as red highlight the largest amount of deformation occurring. Overall, the extent of deformation spanned from -2cm to 2cm. Through InSAR, this analysis demonstrates how vulnerable this basin is to surface deformation/subsidence, while also demonstrating the correlation between groundwater storage changes and surface deformation in the basin. This examination offers the opportunity to display the correlation between landscapes changes and groundwater dynamics. In exploring how the

overexploitation of groundwater resources influences landscape changes that impact groundwater dynamics, this remote sensing approach can provide better understanding in coastal water resource management.

In 2016-2017, the results indicate the basin did not experience relative changes from the coastline to the center of the basin around the Imintanoute region. However, deformation was prominent in the Marakesh and Ourika valley region with up to 2cm of subsidence occurring (Figure 4-11). Across the northern region of the basin, from Essaouira to the border of Marrakesh, deformation was approximately 1cm. Throughout the southern region of the basin, deformation was not detected.

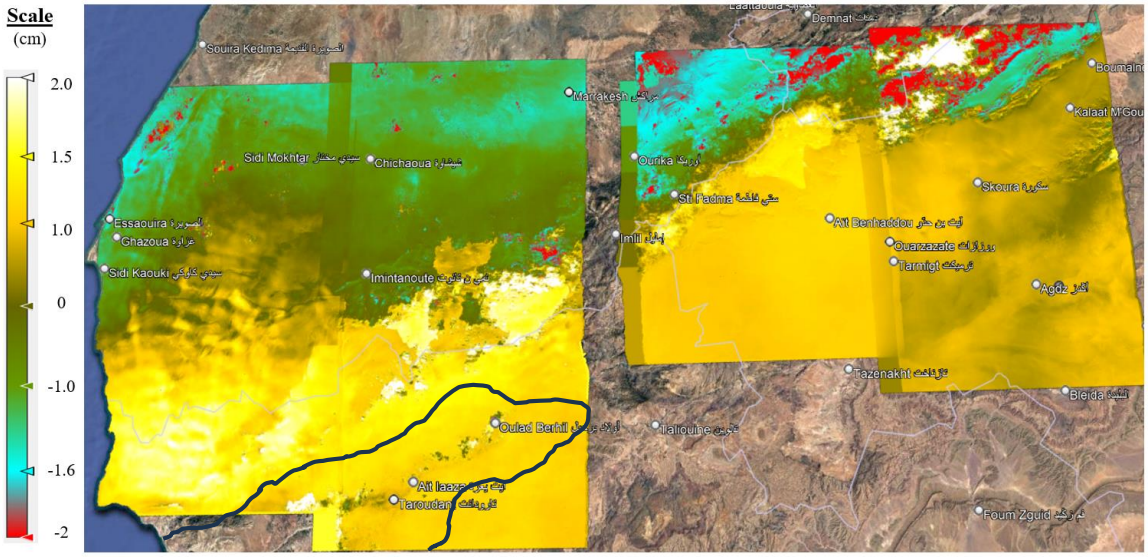

Figure 4-11. InSAR surface displacement assessment of relative changes from 2016-2017 in the Sous Massa basin.

In 2018-2019, the results indicate that land deformation became more prominent throughout the region. Surface deformation was detected in both the northern and southern regions of the basin. Deformation became more prominent in the center of the basin spanning from parts of the Sidi Kaouki region to the Oulad Berhil and Imlil regions. During this timeline, surface

deformation is identified as increasing towards the coastline (Figure 4-12). In addition, it has increased in the Ait Benhaddou, Ouarzazate, Tarmigt, Bleida, and Agdz regions as well.

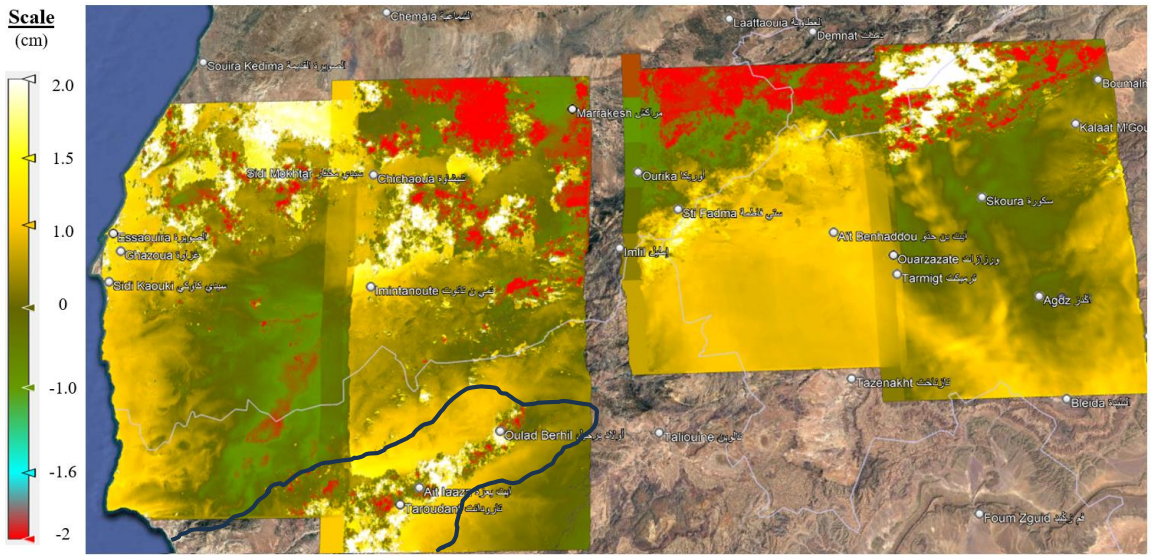

Figure 4-12. InSAR surface displacement assessment of relative changes from 2018-2019 in the Souss Massa basin.

In this examination, 2016-2019 were chosen as they represented areas where prominent surface displacement occurred. To provide an overall assessment of these relative changes, the years 2016-2021 were analyzed (Figure 4-13). Temporally and spatially, displacement is observed trending a southwest transect throughout the basin. Displacement is prominent up to 2cm along the coastline near Agadir, and towards the center of the basin in Oulad Berhil and regions around Imintanoute. In the observed regions towards the north, approximately 2cm of displacement is observed in the Ourika valley area, Imlil and Sti Fadma.

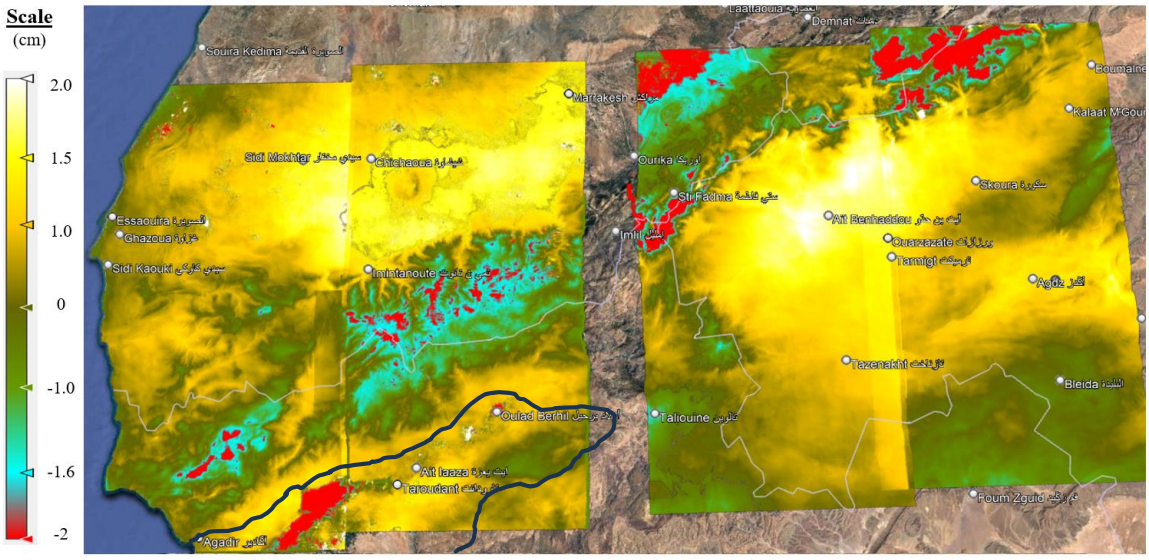

Figure 4-13. InSAR surface displacement assessment of relative changes from 2016-2021 in the Souss Massa basin.

To correlate the relative landscape changes to groundwater and total water storage changes, GRACE mission datasets were used. GRACE data provided the opportunity to determine groundwater changes by observing changes in the Earth's gravity field to approximate changes in the amount of water stored in a region. The total water storage is defined as the sum of all above and below surface water storages, including canopy water, rivers and lakes, soil moisture, and groundwater. It represents a synthetic proxy of the dynamic of slow-responding hydrological quantities, specifically the monitorization of long-term hydrological drought [*Tapley et al., 2004; Cammalleri et al., 2019; Landerer and Swenson, 2012; Wahr et al., 2004*].The total groundwater storage is computed from the change in total water storage deduced from the total of soil moisture storage, surface water storage and snow water storage changes using land surface models [*Famiglietti et al., 2011; Rodell et al., 2009; Famiglietti and Rodell, 2013; Rickey et al., 2015; Shamsudduha et al., 2012*].

GRACE data indicates that the total water and groundwater storage decreased to 10cm between 2016-2021. The total water storage displayed a steady decline from 2016 to 2021 (Table 4-3). There were occurrences where the total water storage increased, specifically at the beginning of 2018, however, those increases were limited as the overall storage volume was in a decreasing trend. The observed increase of total water storage was due to increased precipitation events that occurred during that particular year. Those increased precipitation events are considered anomalies under the dry climate conditions.

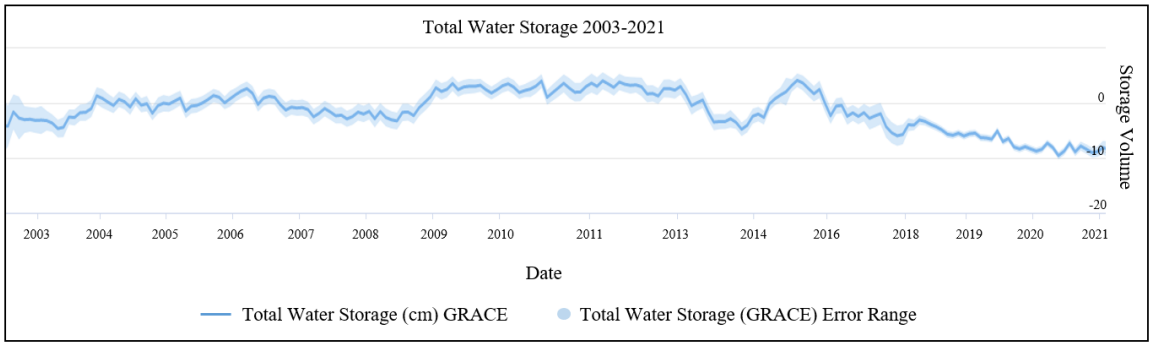

Table 4-3. GRACE total water storage anomaly assessment in the Souss Massa basin from 2003-2021.

The groundwater storage assessment from 2016-2021 details the storage volume fluctuations from 2016 to 2019 displaying periods of when recharging is occurring and when it is not. (Table 4-4). Though the volume is steadily following a decreasing trend, the groundwater storage decreased heavily in 2017 but recovered by the beginning of 2018. This cycle was repeated in 2019, but in the first half of 2020 the groundwater storage remained relatively constant with no sharp increases or decreases. Towards the end of 2020, the groundwater storage assessment details the largest decrease of groundwater storage since monitorization from GRACE's satellite mission beginning in 2003.

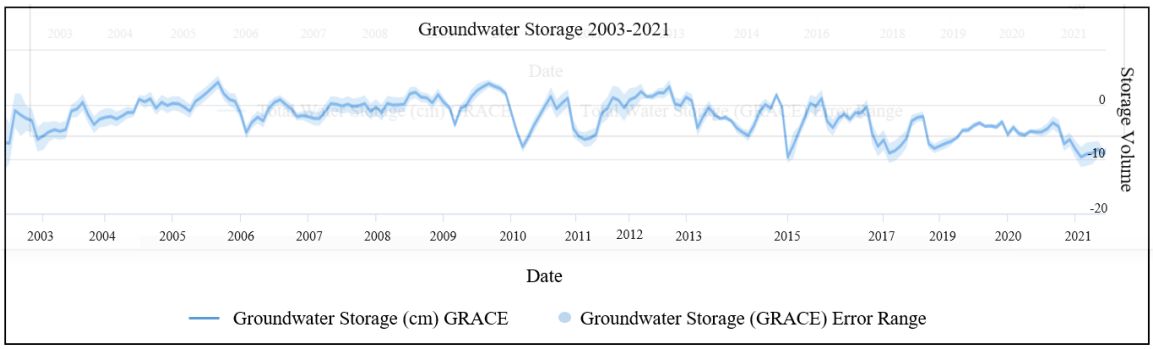

Table 4-4. GRACE groundwater storage anomaly assessment in the Souss Massa basin from 2003-2021.

4.5. Discussion

In the Souss Massa basin of Morocco, the occurrences of coastal subsidence have become a potentially dangerous phenomenon that is impacting this region while exposing its vulnerability to geomorphological changes that affect critical water resources. The influences of climate change and increased anthropogenic activity have contributed to the land displacement within this basin. The research presented here examines how remote sensing-based techniques can be used analyze subsidence and water storage within a region. With InSAR's capabilities and GRACES's satellite data, surface deformation and groundwater storage changes have been examined. These remote sensing techniques are widely known and have been applied in numerous coastal water scarce regions [*Castellazzi et al., 2016; Castellazzi et al., 2016; Zheng et al., 2018; Yu et al., 2021; Ojha et al., 2020; Liu et al., 2019*].

Limitations and Challenges

This study provided an examination of the monitorization of relative changes in surface displacement, additional analysis will be needed to provide absolute change and further evidence of the theory that inelastic deformation is occurring. To provide absolute change, persistent scatterer interferometry (PSI) must be applied. PSI is based on the use of a single master image

and the selection of stable and highly coherent scatterers in a time series [*Ferretti et al., 200; Crosetto et al., 2016*]. The PSI method will identify the overall land deformation, and the distribution of standard deviation of the velocity of deformation occurring temporally and spatially. The temporal data will provide a constant rate throughout the time series. To provide evidence of inelastic deformation, a combined InSAR and modeling package could be used to further our understanding as to what extent the downward displacement of land causes irreversible inelastic deformation in aquifer systems. The combined modeling package will simulate the compaction of compressible fine-grained beds with the aquifer system. To identify the extent of the aquifer's inelasticity, the effective stress must be determined. When deformation occurs, there are pore-pressure changes resulting in changes in effective stress. Depending on the rate and extent of subsidence that is occurring in some areas of the Souss Massa Basin, the effective stress is greater than the pre-consolidation stress, resulting in inelastic deformation. The modeling package will simulate the interbeds of the aquifer system because it assumes that water is either released from and/or directed into storage with changes in the head of the aquifer within a single model time stamp. Additionally, time-dependent drainage and compaction of the interbeds in the confined units will be accounted for. They will account for the delayed changes in storage, while the package will calculate net compaction, elastic expansion of interbeds, and changes in vertical position of land surface in individual model layers [*Hoffman et al., 2003*].

4.6. Conclusion

The Souss Massa basin in Morocco is continually being threatened by climatic regime effects and anthropogenic activity. This examination of landscape changes highlights how rapidly the effects of climate change are occurring. Using InSAR and GRACE remote sensing-based tools, surface displacement was identified, and those results were correlating to changes in total water

storage and groundwater storage depletion in this region. This examination provides a perspective of the imminent concern as these coastal drylands are extremely vulnerable to landscape changes that impact groundwater resources. Many populations are experiencing water stress due to the global water demand and the impact of changes on the water supply in coastal drylands. The Souss-Massa basin is representative of an over-populated region where there are limited water resources and extensive groundwater abstraction [*Bouchaou et al., 2008; Bouchaou et al., 2011; Sowers et al., 2011; d'Oleire-Oltmanns et al., 2011*]. To better reach the water resource demand, remote sensing-based approaches similar to these are needed.

As this study provided a first-order assessment of how landscape changes influence groundwater dynamics, the relative changes detected can assist in further interpretation of evaluating the impacts of coastal geomorphological changes under different spatial distributions from environmental processes across a range of scales. This integrated perspective of understanding how each of these processes have contributed to the evolution of coastal drylands is essential in furthering our understanding of groundwater dynamics.

References

Ait Brahim, Y; Seif-Ennsair, M; Malki, M; N'da, B; Choukrallah, R; El Morjani, ZEA; Sifeddine, A; Abahous, H and Bouchaou, L. 2016. Assessment of Climate and Land Use Changes: impacts on groundwater Resources in the Souss-Massa River Basin. The Souss-Massa River basin, Morocco. The handbook of Environmental Chemistry. (53) pp121-142

Ambroggi, R. 1952. Souss Valley, hydrogeology of Morocco; Notes and mem. Serv. Geol., Morocco No. 97: 269-284.

Amelung, F., Galloway, D. L., Bell, J. W., Zebker, H. A., & Laczniak, R. J. 1999. Sensing the ups and downs of Las Vegas: InSAR reveals structural control of land subsidence and aquifer-system deformation. Geology, 27(6), 483-486.

Bouchaou, L; Michelot, J; Vengosh, A; Hsissou, Y, Qurtobi, M; Gaye, C; Bullen, T; Zuppi, G. 2008. Application of multiple isotopic and geochemical tracers for investigation of recharge, salinization, and residence time of water in the Souss-Massa aquifer, southwest of Morocco. *J. Hydrol.* 352, 267-287.

Bouchaou, L; Tagma, T; Boutaleb, S; Hssaisoune, M and El Morjani, ZEA. 2011. Climate change and its impacts on groundwater resources in Morocco: The case of the Souss-Massa basin. In Climate Change Effects on Groundwater Resources: A Global Synthesis of Findings and Recommendations; Taylor & Francis Group: Albingdon, UK

Boutaleb, S. 2000. Impact of the geology and climate of watersheds on the water quality of a large alluvial aquifer in a semi-arid climate. Application to the hydrological relations between the Western High Atlas and the Souss plain. National doctoral thesis, Univ. Ibn Zohr, Fac. Sci. Agadir, p. 189.

Cammalleri, C., Barbosa, P., Vogt, J.V. (2019). Analyzing the Relationship between

Multiple Timescale SPI and GRACE Terrestrial Water Storage in the Framework of Drought Monitoring. Water 11(8), 1672. https://doi.org/10.3390/w11081672.

Castellazzi, P., Martel, R., Galloway, D. L., Longuevergne, L., & Rivera, A. 2016. Assessing groundwater depletion and dynamics using GRACE and InSAR: Potential and limitations. *Groundwater*, *54*(6), 768-780.

Castellazzi, P., Martel, R., Rivera, A., Huang, J., Pavlic, G., Calderhead, A.I., Chaussard, E., Garfias, J. and Salas, J., 2016. Groundwater depletion in Central Mexico: Use of GRACE and InSAR to support water resources management. Water resources research, 52(8), pp.5985-6003.

Chaussard, E; Wdowinski, S; Cabral-Cano, Enrique and Amelung, Falk. 2014. Remote Sensing of Environment 140, 94-106.

Chen, C. W., & Zebker, H. A. (2000). Network approaches to two-dimensional phase unwrapping: intractability and two new algorithms. *JOSA A*, *17*(3), 401-414.

Chen, C. W., & Zebker, H. A. (2002). Phase unwrapping for large SAR interferograms: Statistical segmentation and generalized network models. *IEEE Transactions on Geoscience and Remote Sensing*, *40*(8), 1709-1719.

Chen, C. W., & Zebker, H. A. (2001). Two-dimensional phase unwrapping with use of statistical models for cost functions in nonlinear optimization. *JOSA A*, *18*(2), 338-351.

Chouker-Allah, R; Hirich, A and Nrhira, A. 2014. Assessment of global change impacts on groundwater resources in Souss-Massa basin. In: Final SCARCE international conference, Tarragona, Spain, 20-21

Crosetto, M; Monserrat, O; Cuevas-Gonzalez, M; Devanthery, N and Crippa, B. 2016.

Persistent scatterer interferometry: A review. ISPRS J. Photogramm. Remote Sens. 115, 78-89.

D'Oleire-Oltmanns, S; Marzolff, I; Peter, KD; Ries, JB and Ait Hssaine, A. 2011. Monitoring soil erosion in the Souss Basin, Morocco, with a multiscale object-based remote sensing approach using UAV and satellite data. In *Proceedings of the 1st World Sustainability Forum*; Sciforum Electronic Conference Series; MDPI: Basel, Switzerland.

European Space Agency-Sentinel. 2022. Sentinel User Guides Product Type. Available online: https://sentinels.copernicus.eu/ web/sentinel/user-guides/sentinel-2-msi/product-types/level-1c (accessed on 05 August 2022).

Ferretti, A. (2014). Satellite InSAR Data: reservoir monitoring from space (EET 9). Earthdoc.

Feng, W., Zhong, M., Lemoine, J. M., Biancale, R., Hsu, H. T., & Xia, J. (2013). Evaluation of groundwater depletion in North China using the Gravity Recovery and Climate Experiment (GRACE) data and ground-based measurements. Water Resources Research, 49(4), 2110-2118.

Famiglietti, J. S., Lo, M., Ho, S. L., Bethune, J., Anderson, K. J., Syed, T. H., Swenson, S. C., Linage, C. R. d., and Rodell, M. 2011. Satellites measure recent rates of groundwater depletion in California's Central Valley, Geophys. Res. Lett., 38, L03403, https://doi.org/10.1029/2010GL046442.

Famiglietti, J. S. and Rodell, M. 2013. Water in the Balance, Science, 340, 1300–1301, https://doi.org/10.1126/science.1236460.

Ferretti, A; Prati, C and Rocca, F. 2001. Permanent scatterers in SAR interferometry. IEEE. Trans. Geosci. Remote Sens. 39, 8-20.

Filahi, S; Tanarhte, M; Mouhir, L; El Morhit, M and Tramblay, Y. 2016. Trends in indices of daily temperature and precipitations extremes in Morocco. *Theor. Appl. Climatol.* 124, 959-972.

Filahi, S; Tanarhte, M; Mouhir, L; El Morhit, M and Tramblay, Y. 2016. Trends in indices of daily temperature and precipitations extremes in Morocco. *Theor. Appl. Climatol.* 124, 959-972.

Galloway, DL and Hoffman, J. 2007. The application of satellite differential SAR interferometry-derived ground displacements in hydrogeology *Hydrogeology Journal* 15, 133-154

Galloway, DL and Sneed, M. 2014. Analysis and simulation of regional subsidence accompanying groundwater abstraction and compaction of susceptible aquifer systems in the USA. Boletin de la Sociedad Geologica Mexicana, Vol. 65, No. 1, Numero especial Geoquimica Ambiental, pp. 123-136.

Hoffman, J; Leake, SA; Galloway, DL and Wilson, AM. 2003. MODFLOW-2000 groundwater model- User guide to the Subsidence and Aquifer-System Compaction (SUB) Package: U.S. Geological Survey Open-File Report 03-233, 46 p.

Houborg, R., Rodell, M., Li, B., Reichle, R., & Zaitchik, B. F. (2012). Drought indicators based on model-assimilated Gravity Recovery and Climate Experiment (GRACE) terrestrial water storage observations. Water Resources Research, 48(7).

Hssaissoune, M; Boutaleb, S; Benssaou, M and Bouchaou, L. 2016. Physical geography, geology, and water resource availability of the Souss-Massa River Basin. In: Choukr-Allah, R; Ragab, r; Bouchaou, L; Barcelo, D (eds) The Souss-Massa River Basin, Morocco. Springer, Switzerland, pp 27-56.

Huang, Z., Y. Pan, H. Gong, P.J.F. Yeh, X. Li, D. Zhou, andW. Zhao. 2015. Subregional-scale groundwater depletion detected by GRACE for both shallow and deep aquifers in North China plain. Geophysical Research Letters42, no. 6:1791–1799.

Ingebritsen, SE and Galloway, DL. 2014. Coastal subsidence and relative sea level rise. *Environ. Res. Lett.* 9, 091002, 4pp.

Ireson, A; Makropoulos, C and Maksimovic, C. 2006. Water resources modelling under data scarcity: coupling: Mike Basin and ASM groundwater model. Water Resour.Manag. 20, 567-590.

Jacob, CE. 1939. Fluctuations in artesian pressure produced by passing railroad trains as shown in a well on Long Island, New York. Trans Am Geophys Union 20:666-674

Landerer, F.W., Swenson, S.C. 2012. Accuracy of scaled GRACE terrestrial water storage estimates. Water Resour. Res., 48, W04531.

Lezzaik, K and Milewski, A. 2017. A quantitative assessment of groundwater resources in the Middle East and North Africa region. Hydrogeol. J. 26, p. 251.

Lezzaik, K; Milewski, A and Mullen, J. 2018. The groundwater risk index: development and application in the Middle East and North Africa region. Sci Total Environ 628-629:1149-1164.

Li, L; Zhang, M and Katzenstein, K. 2017. Calibration of a Land Subsidence Model Using InSAR Data via the Ensemble Kalman Filter. Groundwater. 55, (6), pp.871-878

Long, D., Scanlon, B. R., Longuevergne, L., Sun, A. Y., Fernando, D. N., & Save, H. (2013). GRACE satellite monitoring of large depletion in water storage in response to the 2011 drought in Texas. Geophysical Research Letters, 40(13), 3395-3401.

Liu, Z., Liu, P.W., Massoud, E., Farr, T.G., Lundgren, P. and Famiglietti, J.S., 2019.

Monitoring groundwater change in California's central valley using sentinel-1 and grace observations. Geosciences, 9(10), p.436.

McStraw, T. C., Pulla, S. T., Jones, N. L., Williams, G. P., David, C. H., Nelson, J. E., & Ames, D. P. (2022). An Open-Source Web Application for Regional Analysis of GRACE Groundwater Data and Engaging Stakeholders in Groundwater Management. *JAWRA Journal of the American Water Resources Association*, *58*(6), 1002-1016.

Milewski, A; Elkadiri, R and Durham, M. 2015. Assessment and comparison of TMPA Satellite Precipitation Products in Varying Climatic and Topographic Regimes in Morocco. *Remote Sens.*7, 5697-5717.

Milewski, A; Lezzaik, K and Rotz, R. 2020. Sensitivity analysis of the groundwater risk index in the Middle East and North Africa region. *Environ Process* 7:53-71. Doi:10.1007/s40710-019-00421-7.

Milewski, A; Seyoum, WM; Elkadiri, R and Durham, M. 2020. Multi-scale hydrologic sensitivity to climatic and anthropogenic changes in Northern Morocco. *Geosciences* 10 (1), 13. Doi:10.3390/geosciences10010013.

Milewski, A; Sultan, M; Jayapraksh, SM; Balekai, R and Becker, R. 2009. RESDEM, a tool for integrating temporal remote sensing data for use in hydrogeologic investigations. *Comput. Geosci.* 35, 2001-2010.

Milewski, A; Sultan, M; Yan, E; Becker, R; Abdeldayem, A; Soliman, F and Gelil, KA. 2009. A remote sensing solution for estimating runoff and recharge in arid environments. J. Hydrogeol. 373, pp. 1-14.

Longuevergne, L., C.R. Wilson, B.R. Scanlon, and J.F. Cr´etaux.2013. GRACE water

storage estimates for the Middle East and other regions with significant reservoir and lake storage, Hydrology and Earth System Sciences17, no. 12:4817–4830

Minderhoud, PSJ; Erkens, G; Pham, VH; Bui, VT; Erban, L; Kooi, H and Stouthamer, E. 2017. Impacts of 25 years of groundwater extraction on subsidence in the Mekong delta, Vietnam. *Environ. Res. Lett.*12, 064006

Motagh, M; Shamshiri, R; Haghighi, MH; Wetzel, HU; Akbari, B; Nahavandchi, H; Roessner, Sigrid and Arabi, S. 2017. Quantifying groundwater exploitation induced subsidence in the Rafsanjan plain, southeastern Iran, using InSAR time-series and in situ measurements. Engineering Geology, 218, pp.134-151

Narasimhan, TN; Kanehiro, BY and Witherspoon, A. 1984. Interpretation of earth tides response to three deep, confined aquifers. J Geophys res 89 B3:1913-1924

NASA Global Land Data Assimilation System (GLDAS). 2022. GLDAS: Project Goals. Available online: https://ldas.gsfc.nasa.gov/gldas (accessed on 01 October 2022)

N'da, AB; Bouchaou, L; Reichert, B; Hanich, L; Brahim, YA; Chehbouni, A; Beraaouz, EH and Michelot, JL. 2016. Isotopic signatures for the assessment of snow water resources in the Moroccan High Atlas Mountains: Contribution to surface and groundwater recharge. Environ. Earth Sci. 75, 755.

Normand, JCL and Heggy, E. 2015. InSAR Assessment of Surface Deformations in Urban Coastal Terrains Associated with Groundwater Dynamics. IEEE Transactions on Geoscience and remote Sensing, 53, (12), pp.6356-6371

Ojha, C., Werth, S. and Shirzaei, M., 2020. Recovery of aquifer-systems in Southwest US following 2012–2015 drought: Evidence from InSAR, GRACE and groundwater level data. Journal of Hydrology, 587, p.124943.

Parker, GG and Springfield, VT. 1950. Effects of earthquakes, rains, tides, winds, and atmospheric pressure changes on the water in geological information of southern Florida. Econ Geol 45:441-460

Pavelko, MT. 2003. Estimates of hydraulic properties from a one-dimensional numerical model of vertical aquifer-system deformation, Lorenzi Site, Las Vegas, Nevada: Carson City, Nevada, U.S. United States Geological Survey, Water-Resources InvestigationsReport03-4083, 36 p.http://pubs.usgs.gov/wri/wri034083/index.html

Poland, JF. 1984. Guidebook to the studies of land subsidence due to groundwater withdrawal: Paris, UNESCO, Studies and reports in hydrology 40, http://wwwrcamnl.wr.usgs.gov/ rgws/Unesco/,

Poland, JF and Davis, GH. 1969. Land subsidence due to withdrawal of fluids, in Varnes, DJ, Kiersch, G. (eds.): Reviews in Engineering Geology, 2, 187-269.

Richey, A. S., Thomas, B. F., Lo, M.-H., Reager, J. T., Famiglietti, J. S., Voss, K., Swenson, S., and Rodell, M. 2015. Quantifying renewable groundwater stress with GRACE, Water Resour. Res., 51, 5217–5238, https://doi.org/10.1002/2015WR017349.

Ritzema, H; Froebrich, J; Raju, R; Sreenivas, C and Kselik, R. 2010. Using participatory modeling to compensate for data scarcity in environmental planning: A case study from India. *Environ. Model. Softw.* 25, 1450-1458.

Rodell, M., Chen, J., Kato, H., Famiglietti, J. S., Nigro, J., & Wilson, C. R. 2007. Estimating groundwater storage changes in the Mississippi River basin (USA) using GRACE. Hydrogeology Journal, 15, 159-166.

Rodell, M., and Famiglietti, J. S. 2001. An analysis of terrestrial water storage variations

in Illinois with implications for the Gravity Recovery and Climate Experiment (GRACE). Water Resources Research, 37(5), 1327-1339.

Rodell, M., & Famiglietti, J. S. 1999. Detectability of variations in continental water storage from satellite observations of the time dependent gravity field. Water resources research, 35(9), 2705-2723.

Rodell, M., Velicogna, I., & Famiglietti, J. S. 2009. Satellite-based estimates of groundwater depletion in India. Nature, 460(7258), 999-1002.

Saidi, ME. 1995. Contribution to the deep and superficial hydrology of the Souss basin. (Morocco. Thesis. Doct. Univ. Paris IV, p210.

Shamsudduha, M., Taylor, R. G., and Longuevergne, L. 2012. Monitoring groundwater storage changes in the highly seasonal humid tropics: validation of GRACE measurements in the Bengal Basin, Water Resour. Res., 48, W02508, https://doi.org/10.1029/2011WR010993.

Simons, M and Rosen, P. 2015. Interferometric Synthetic Aperture Radar Geodesy. In: Gerald Schubert Treatise on Geophysics, 2nd edition, Vol 3. Oxford: Elsevier. P. 339-385.

Sneed, M. 2008. Aquifer-system compaction and land subsidence data and simulations, the Holly Site, Edwards Air Force Base, California: sacramento, California, California State University-Sacramento, M.S. thesis, 40 p.

Sneed, M., & Galloway, D. L. (2000). Aquifer-system compaction and land subsidence: measurements, analyses, and simulations: the Holly site, Edwards Air Force Base, Antelope Valley, California (No. 4015). US Department of the Interior, US Geological Survey.

Souss-Massa-Draa Hydraulic Basin Agency. 2007. Review of the Integrated Water

Resources Development Master Plan (PDAIRE) for the Souss-Massa basins. Final report of Agence du Bassin Hydraulique Souss-Massa-Draa

Sowers, J; Vengosh, A and Weinthal. 2011. Climate change, water resources, and the politics of adaptation the Middle East and North Africa. *Clim Chang.* 104, 599-627.

Sun, H; Grandstaff, D and Shagam, R. 1999. Land subsidence due to groundwater withdrawal: potential damage of subsidence and sea level rise in southern New Jersey, USA. Environmental Geology, 37, (4)

Tagma, T; Hsissou, Y; Bouchaou, L; Bouragba, L and Boutaleb, S. 2009. Groundwater nitrate pollution in Souss Mass basin southwest Morocco. Afr J Environ Sci Technol 310:301-309.

Tapley, B.D.; Bettadpur, S.; Ries, J.C.; Thompson, P.F., Watkins, M.M. 2004. GRACE measurements of mass variability in the Earth System. Science 2004, 305, 503-505.

Tolman, CF and Poland JF. 1940. Groundwater, saltwater infiltration, and ground surface recession in Santa Clara Valley, Santa Clara County, California: *Transactions, American Geophysical Union,* 1, 23-35.

Tourian, M.J., O. Elmi, Q. Chen, B. Devaraju, S. Roohi, and N. Sneeuw. 2015. A spaceborne multi sensor approach to monitor the desiccation of Lake Urmia in Iran. Remote Sensing of Environment156: 349–360

Tramblay, Y; Ruelland, D; Somot, S; Bouaicha, R and Servat, E. 2013. High-resolution Med-CORDEX regional climate model simulations for hydrological impact studies: A first evaluation of the ALADIN-Climate model in Morocco. *Hydrol. Earth Syst. Sci*. 17, 3721-3739.

Vorosmarty, C; Douglas, EM; Green PA and Revenga, C. 2005. Geospatial indicators of

emerging water stress: an application to Africa *Ambio* 34 230-6

Vorosmarty, C; Green, P; Salisbury, J and Lammers, RB. 2000.Global water resources: Vulnerability from climate change and population growth. Science 289, 284-288.

Voss, K. A., Famiglietti, J. S., Lo, M., De Linage, C., Rodell, M., & Swenson, S. C. (2013). Groundwater depletion in the Middle East from GRACE with implications for transboundary water management in the Tigris-Euphrates-Western Iran region. Water resources research, 49(2), 904-914.

Wada, Y; van Beek, LPH; van Kempen, CM; Reckman, JWTM; Vasak, S and Bierkens, MFP. 2010. Global depletion of groundwater resources. Geophys. Res. Lett., 37, L20402.

Wahr, J.; Swenson, S.; Zlontnicki, V.; Velicogna, I. 2004. Time-variable gravity from GRACE: First results. Geophys. Res. Lett., 31, L11501.

Yeh, P. J. F., Swenson, S. C., Famiglietti, J. S., & Rodell, M. (2006). Remote sensing of groundwater storage changes in Illinois using the Gravity Recovery and Climate Experiment (GRACE). Water Resources Research, 42(12).

Yu, W., Gong, H., Chen, B., Zhou, C. and Zhang, Q., 2021. Combined GRACE and MT-InSAR to Assess the Relationship between Groundwater Storage Change and Land Subsidence in the Beijing-Tianjin-Hebei Region. Remote Sensing, 13(18), p.3773.

Yirdaw, S. Z., Snelgrove, K. R., & Agboma, C. O. 2008. GRACE satellite observations of terrestrial moisture changes for drought characterization in the Canadian Prairie. Journal of Hydrology, 356(1-2), 84-92.

Zheng, M., Deng, K., Fan, H., & Du, S. (2018). Monitoring and analysis of surface deformation in mining area based on InSAR and GRACE. *Remote Sensing*, *10*(9), 1392.

CHAPTER 5

SUMMARY AND CONCLUSIONS

In this research, the use of remote sensing-based techniques was used to understand how coastal landscape changes influence hydrogeological resources along coastal systems. The coastal southeastern US and the Souss Massa basin located in North Africa, were chosen because each region distinctively characterized some of the most prominent processes that impact and control coastal environments (i.e., erosional activity, vegetation density and anthropogenic activity). Understanding the impact of coastal landscape changes on these coastal systems at various sites across a range of scales in different regions is vital given the multiplicities and complex processes. Furthermore, the presented studies offer insight into how the implementation of known and new remote sensing-based techniques can be used to provide further understanding of these dynamic processes.

The LiDAR analysis presents its use in characterizing the spatial and temporal changes of the coastal southeast US, and quantification of changes at select National Park sites. More specifically, this study identified the temporal changes in elevation, and quantification of the spatial volumetric changes, of unconsolidated sedimentary material in the SECN of the NPS. The following conclusions were observed:

1. The LiDAR data applied in this analysis identified the temporal changes in elevation, and quantified the spatial volumetric changes of unconsolidated sedimentary material at the 95^{th} percentile confidence level as a function of the RMSE. This LiDAR assessment offered 95% accuracy, with the possibility of 5% error.

2. Elevation changes can occur rapidly or over extended periods of time. For example, Fort Matanzas NM elevation increased from 2010 to 2013 but decreased from 2016 to 2017 along the coastline, displaying a 1-meter decrease in elevation from 2006 to 2017.
3. Volumetric spatial change of sedimentary material in the coastal sediment budget responded in conjunction with the elevation but the changes were inconsistent. In areas where there was a net gain/net loss of returned sedimentary material, the elevation increased. In areas where there was a net loss/net gain displaying erosional activity, the elevation decreased. For example, from 2009 to 2010 erosional activity in Fort Pulaski NM decreased by 10% but increased by 9% in 2016. These volumetric changes infer the climatic regimes of the southeast US expose these coastal zones to instability.
4. Due to these coastal zones being exposed to fluctuating climate regimes, the quasi-cyclic phenomenon was observed. As a result, there are erosional processes and longshore sediment transport affecting the coastal hydrogeological and geomorphological dynamic.

Salt marshes along the southeastern coast were analyzed to better understand the influence of vegetation changes. The salt marsh analysis explored methods to identify and quantify how salt marshes are changing along the southeastern coast of the US and how they can provide valuable data for coastal natural resource management. The following conclusions were observed:

1. The unsupervised classification improved the supervised classification by selecting the necessary ROIs representative of the select features by the spectral signatures clustered. The unsupervised classification can improve the number of classes determined, however, too many classes can saturate the classification results, yielding inaccurate assumptions of the area analyzed.

2. The maximum likelihood classification results showed the most promise in accurately assessing marsh changes. Each site was mapped appropriately through the manual input ROIs and field-based training data. The pixels selected captured similarly vegetated marsh areas in Canaveral NS and Cumberland Island NS. The channels and tidal inlets, where most of the changes occurred, also produced viable results.
3. When all ROIs were combined, the maximum likelihood classification yielded the highest accuracy percentage. Subsequentially, the input of all ROIs improved the performance of minimum distance and spectral angle mapper.
4. The NDVI provided a supportive source displaying the differential reflection of the vegetation biomass presence. This assessment supported the maximum likelihood classification and change detection analysis, displaying that the majority of the marsh areas in these sites were from bare/soil unconsolidated material to sparse–intermediate vegetation.
5. The change detection analysis indicated that salt marshes were largely decreasing during the study period, along with areas of increase. Notably, the largest salt marsh decrease occurred in or around the channels, coastline, and tidal inlets.
6. In Fort Pulaski NM, we highlighted the influence of high/low tide in these environments. As a result of tidal influence, decreases in salt marshes are representative of salt marshes being submerged, not removed.
7. The results indicated the classification scheme works best when there are more pixels selected in respect to its pixel value to provide a better interpretation. The more statistics collected for each band distributed spatially throughout the image, the higher probability that a given pixel or set of pixels belongs to a specific class feature.

However, due to the classification scheme calculating each pixel, some results may yield an over- or underestimation of each feature class.

8. In this study, the overall accuracy ranged from 75% to 99%. At each of the sites, the water bodies were mapped with 99% accuracy. In the marsh areas, the range was 75% to 94% accuracy. The percentage of errors was likely due to the salt marshes' spatial extent, the inclusion of field-based data collection, and the variability of satellite imagery noise due to differences in the stage of tides.
9. A field-based and remote sensing method is imperative in an uncertain climate and ever-changing ecomorphodynamic system. Utilizing this approach will ensure that salt marshes continue to serve as a pivotal resource in these aquatic environments.

Due to changes in climatic regime effects and increased anthropogenic activity, surface subsidence was assessed. InSAR techniques correlated to GRACE datasets identified how increased anthropogenic activity contributes to surface subsidence and its impacts on groundwater storage in the Souss Massa basin of Morocco. The following major conclusions were observed:

1. Situated between the High Atlas Mountains and Anti Atlas Mountains, the designed approach identified that deformation spanned from the coastline into the inland areas of the Souss Massa basin region.
2. This temporal and spatial change analysis highlighted specific areas in the basin that have experienced the most land deformation. Trending southwest, surface deformation was observed along the coastline near Agadir, and towards the center of the basin in Oulad Berhil and regions around Imintanoute of up to 2cm. Imlil and Sti Fadma located in the northeast region of the basin in the Ourika valley showed approximately 2 cm of deformation as well.

3. GRACE datasets from 2003-2021 were collected, and from 2016-2021 the observed total water storage and groundwater storage decreased to 10 cm.
4. The results suggest the subsidence in this region is intrinsically impacting groundwater storage. Due to the increased anthropogenic activity and demand for water resources in a water scarce region, subsidence has occurred. As surface deformation continues to become a dominant factor in this region, the aquifers can compact resulting in less storage capacity of groundwater resources.

In this research, coastal landscapes were assessed from multiple dimensions to understand the changes occurring and the extent of influence on hydrogeological resources. The presented integrated approaches exhibit the usefulness of remote sensing-based tools to assess landscape changes both spatially and temporally. Understanding coastal processes in relation to water resource management is of imminent concern. These coastal systems are highly susceptible to geomorphological and hydrogeological changes causing impacts to the water supply. This research extends beyond its scientific merit by providing a real-world application of improved monitorization, revised management practices, and innovative approaches to meet the global water and natural resource demand. Furthermore, this research highlights the versatility of remote sensing-based approaches to understand how to implement numerous techniques under different spatial distributions from environmental processes across a range of scales.

As a result of this research, the observations have informed us of how coastal processes impact the hydrogeological dynamic both locally and globally. These select studies offer further insight in providing informed assessments to better understand similar and contrasting environments. This integrated perspective of understanding how each of these different processes

have contributed to the evolution of coastal systems is essential in furthering our understanding of water resource management.